Impact of entrainment, imposed winds and interactive sea surface on the spontaneous organisation of convection

Cycle XXVI

Doctoral School in Environmental and Industrial Fluid Mechanics

Università degli Studi di Trieste

Student: Addisu G. Semie

Advisor: Dr. Adrian Mark Tompkins

Third Year, Cycle XXVIII

Doctoral School in Environmental and Industrial Fluid Mechanics
University of Trieste

April 3, 2016

Acknowledgements

Firstly, I would like to thank my advisor, Dr. Adrian Tompkins, for his unlimited support and guidance that he has given me throughout my PhD research. I am deeply indebted to his constructive criticism as well as his patience to deal with all my inquiries. The passion that he has for his research is motivational for me, which always give me additional energy to work harder.

I would like to thank Dr. Clement Onime for sacrificing his time to give me valuable feedback about my thesis. I feel privileged to witness his kindness and high level of professionalism that allowed me to significantly improve my technical skill. He is always willing to assist me not only with technical problems but also with all kinds of challenges that I may face in my day to day activity. Without his encouragement and support I would not have got the opportunity to start my PhD.

I will forever be thankful for my wife Teguest Berhanu. She has been taking care of all the responsibility of raising our son. I know the last three years were not easy for both of us, it would have been impossible to continue, if she was not strong enough to overcome all the challenges. Thanks to God, the time we will live apart is getting shorter.

I would like to thank ICTP for providing me scholarship for my research. I appreciate the unique research environment of ICTP that allow me to conduct my study without distraction.

The director and instructors of doctoral school in environmental and industrial fluid mechanics of units deserve appreciation for providing a unique opportunity for students with different background.

Thank you, all my friends in the PhD program, especially Marco Santo and Laleh Shabrang, I am grateful for the great time we had together. I would also like to thank my friends, Ambelu Tebabal, Tesfaye Temtime and Ejigu Kebede, who sacrificed their time to read my thesis and give me important comments.

Finally, I would like to thank my family for their love, encouragement and prayers. My junior brother, Messay Gezahegn, I am extremely grateful for all your assistance while I was not there.

Abstract

Spontaneous organisation of convection is investigated using a cloud resolving model with a convection permitting horizontal resolution of 2 km integrated for periods exceeding a month. In the simulations, convection spontaneously organises into clusters occurring in a single moist region surrounded by a dry convection-free region, reproducing the results of previous studies using a range of different models. Energy budget diagnostics are used to confirm the diabatic processes that lead to, or oppose, organisation as the simulations progress. Further analysis on the level of organization is provided using a new organization index that uses the statistics of nearest neighbour cumulative distribution function. The sensitivity of the organised state to the domain setup and imposed winds is investigated.

A range of sensitivity experiments are conducted to document the strength of the organisation to the representation of the sub-grid mixing, which confirm how the entrainment mixing into updraughts is key to the establishment and eventual degree of the organised state. Schemes that produce low entrainment in the lower free-troposphere can prevent the occurrence of organisation. This shows that the entrainment mixing process appears to be a crucial component and a necessary but not sufficient condition for organisation, despite recent emphasis on radiative feedbacks as the main driver for organisation. This also leads to the slightly concerning conclusion that the occurrence and eventual strength of organisation depends on the sub-grid scale turbulence formulation in models, an aspect of the model setup that receives limited attention.

Experiments are conducted using fixed-depth energy balance slab model and the organization structure disappears as a result of negative feedback from shortwave radiation. These preliminary integrations suggest the fixed depth slab ocean have the potential to slow or prevent organization. In contrast, experiments that use a wind-driven evolving mixed layer depth and heat transfer with a deeper 200m layer were still found to display self-organization.

Acronyms

MCSs mesoscale convective systems

SST sea surface temperatures

ITCZ Inter-tropical convergence zone

MJO Madden-Julian Oscillation

RCE radiative convective equilibrium

CRM cloud resolving models

H depth of the convective layer

TOA top of atmosphere

OLR outgoing longwave radiation

CIN convective inhibition energy

h moist static energy

CAPE convection available potential energy

TRMM-LBA Tropical Rainfall Measuring Mission-Large-Scale Biosphere-Atmosphere

LES large eddy simulation

GCMs global general circulation models

WRF Weather Research Forecast

RK Runge-Kutta

PBL planetary boundary layer

N Brunt - Vaisala frequency

TKE Turbulence Kinetic Energy

YSU Yonsei University

RRTMG rapid radiative transfer model for GCMs

LBLRTM line-by-line radiative transfer model

LW Longwave

SW Shortwave

TC tropical cyclone

TCWV total column water vapor

I_{org} organisation index

NND nearest neighbor distance

NNCDF nearest neighbor cumulative density function

LCL lifting condensation level

LNB level of neutral buoyancy

RH relative humidity

TOGA COARE Tropical Ocean Global Atmosphere Coupled Ocean-Atmosphere Response Experiment

xkmh horizontal eddy viscosity term

xkmv vertical eddy viscosity term

c_k TKE eddy coefficient

Contents

1 Introduction **9**

1.1 Cumulus clouds 9

1.2 Deep convection 9

1.3 Organization of convection 11

1.4 Radiative-Convective Equilibrium 13

1.5 Mechanisms 15

1.5.1 Water vapor 16

1.5.2 Cold pools 17

1.5.3 Radiation 20

1.5.4 Surface fluxes 23

1.5.5 Summary of the feedbacks 23

1.6 CRM as a tool to investigate organisation 24

1.7 Objective of the thesis 26

2 Model description, general model setup and diagnostics for organisation **28**

2.1 Model Description 28

2.1.1 Governing equations 28

2.1.2 Miscellaneous technical details 29

2.1.3 Turbulence parametrizations 30

2.1.4 Planetary boundary layer (PBL) schemes 32

2.1.5 Surface layer schemes 33

2.1.6 Microphysics schemes 34

2.1.7 Radiation schemes 37

2.2 General model setup 38

2.2.1 Relaxation of horizontal wind 38
2.2.2 Slab Ocean model 40
2.2.3 Model configuration 41
2.2.4 Summary of default configuration 44
2.3 Diagnostics for organisation 45
2.3.1 OLR 46
2.3.2 TCWV 46
2.3.3 Organization index 47
2.3.4 Summary of diagnostics for organisation 50

3 Convective Organization 51
3.1 Equilibrium state 51
3.2 Vertical profile of the equilibrium state 54
3.2.1 Skew-T 54
3.2.2 Moisture, vertical motion and cloud profiles 57
3.3 Organization process in equilibrium state 58
3.3.1 Evolution to self organisation state 59
3.3.2 Time series of diabatic forces 62
3.3.3 Frozen moist static energy budget 67
3.3.4 Diabatic feedback 69
3.4 Conclusions 76

4 Impact of sub-grid mixing on spontaneous organisation of convection 79
4.1 Introduction 79
4.2 Effects of subgrid Eddy diffusion schemes 82
4.3 Effect of sub grid scale constants on TKE experiments 91
4.4 Conclusions 93

5 Impact of boundary conditions on spontaneous organisation of convection 96
5.1 Sensitivity to horizontal imposed wind 96
5.2 Interactive SST 103
5.2.1 Slab model with fixed mixed layer depth 105
5.2.2 A slab model with varying mixed layer depth 114
5.2.3 Summary 117

6 Conclusions **119**

6.1 Recommendations 125

Chapter 1

Introduction

1.1 Cumulus clouds

Convective cumulus clouds are a predominant in the tropics. Convection is mainly classified as shallow and deep cumulus clouds. Shallow cumulus, with a vertical extent below the 500 hPa level, are short-lived and generate little precipitation, although the radiative impact of the cloud cover they generate is important for climate (Bony and Dufresne, 2005; Medeiros et al., 2008). Deep convection, which reaches close to the tropical tropopause (or on occasion overshoots, penetrating the stratosphere Schmetz et al., 1997; Küpper et al., 2004) is characterized by the presence of strong vertical velocity, intense precipitation, turbulence and higher vertical height (above the 500 hPa level). Deep convection has a significant role in the atmospheric energy cycle by regulating the transport of momentum, water vapor and heat. Deep convective regions are characterized by being more humid on average than subsidence regions and higher upper tropospheric cloud cover associated with the anvils. The fractional area of the tropics covered by convection is critical for the mean tropical climate and its sensitivity (Pierrehumbert, 1995; Lindzen et al., 2001; Emanuel et al., 2014)

1.2 Deep convection

Convection refers to any motion driven by the buoyancy, and in the atmosphere is manifested as vertical motions of air parcels due to atmospheric instability

driven by surface heating and radiative cooling of the atmosphere. The convection motions are referred to as deep when parcels originating in the boundary layer exceed the trade inversion layer, and then generally continue either to the mid-tropospheric levels associated with the melting layer or mostly to the upper troposphere (Johnson et al., 1999). Although the net effect of convection is to dry the atmosphere, deep convection is a local source of water vapor in free troposphere (e.g Betts, 1990). In general, it can be considered as a transport process where boundary layer heat, moisture and momentum are transported upward and redistributed throughout the atmosphere.

The key processes involved in the life cycle of a single cumulus clouds and its interaction with the environment are shown in figure 1.1.

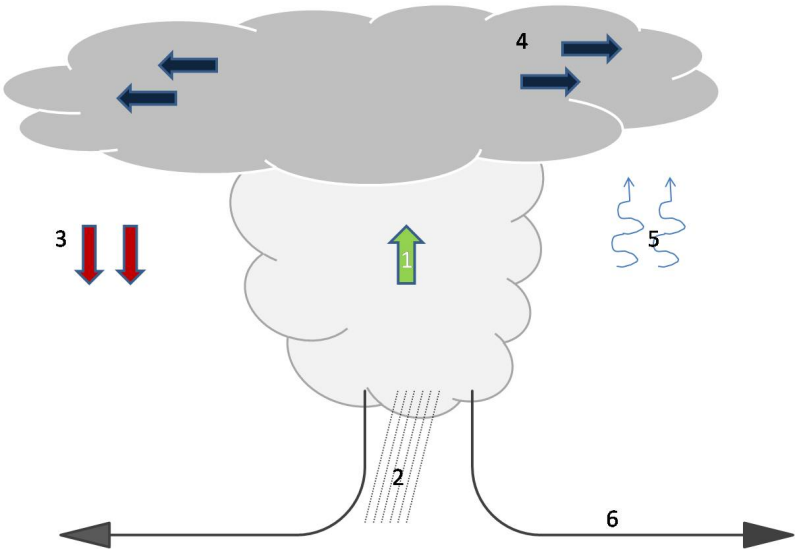

Figure 1.1: Deep convective cumulus cloud and its interaction with environment.

1. When a relatively warmer parcel of air moves upwards in a conditionally unstable atmosphere, it expands and cools as it goes higher and becomes saturated if it is lifted high enough. The latent heating of condensation/freezing provides additional source of energy that enables the parcel of air to reach to level of neutral buoyancy, turbulent mixing occurs with the environment at the edge of the cloud (Houze Jr, 2014).

2. Much of the condensed water falls out of the column as precipitation while a proportion of the vapor is detrained at the level of neutral buoyancy. Precipitation efficiencies are necessarily high for tropospheric-deep parcel motion.

3. Subsidence occurs in the cloud-free environment balancing the upward convective mass flux and warms the air adiabatically as it descends towards the surface.
4. The air arriving at the level of neutral buoyancy is detrained from the cloud, and cooling may occur when the cloud drops/crystals undergo evaporation/sublimation.
5. The cloud anvil impacts the radiation balance by increasing cloud albedo that reduces the radiative heating of the atmosphere below the cloud and the surface. On the other hand, it reduces emittance of infrared radiation which makes the atmosphere warmer.
6. The downdraft from mid-troposphere introduces cool and dry air into the boundary layer and it generates gust fronts at the surface that can trigger new convective events (e.g Tompkins, 2001b).

In the life cycle of a single cumulus cloud, it is observed that deep convection is the result of environmental instability and plays an important role to re-stabilize the system by heating and moistening the free troposphere. One of the key process for the formation of deep convection is the release of latent heat which provides extra energy for air parcels to reach the level of neutral buoyancy (Houze Jr, 2014). Clouds air parcels detrainment can make the upper atmosphere cooler and wetter. Subsidence in the cloud free area balances the upward mass flux and warms the air adiabatically. Mid-troposphere mixing with updraughts can form downdraughts that can bring dry and cool air to the boundary layer. In addition to this, the interaction of the radiation with the cloud anvil is indicated to remarkably affect the heating and cooling of the atmosphere (e.g Ramanathan and Collins, 1991; Chou and Neelin, 1999).

1.3 Organization of convection

Organized or isolated convection is observed for both shallow and deep cumulus clouds with cloud sizes ranging from less than 100 m to tens of kilometers. Larger scale mesoscale organisation and large cloud clusters can occur on scales up to hundreds to even thousands of kilometres (Lilly and Gal-Chen, 2013; Houze Jr, 2014). These large scale phenomena include short-lived aggregation of a few thunderstorms, well-organized squall lines, and long-lived tropical

storms and hurricanes. Organized convection is ubiquitous in the global climate and plays an important role in earth's hydrological cycle (Fritsch and Forbes, 1997). Most extreme events such as heavy rain, flash floods and severe weather are associated with mesoscale convective systems (MCSs) (Fritsch and Forbes, 1997; Mathon et al., 2002).

Deep convection is widely observed in the tropics over regions of warm sea surface temperatures (SST) or high land temperatures. Figure 1.2 shows an infrared image of the Inter-tropical convergence zone (ITCZ) that circles the globe near the equator, indicated by bands of deep cold clouds that are white in the image. This image reveals various levels of convective organisation that extend from clusters of thunderstorms to linearly or nonlinearly organized squall lines and MCSs, and tropical cyclones/hurricanes on the largest scales.

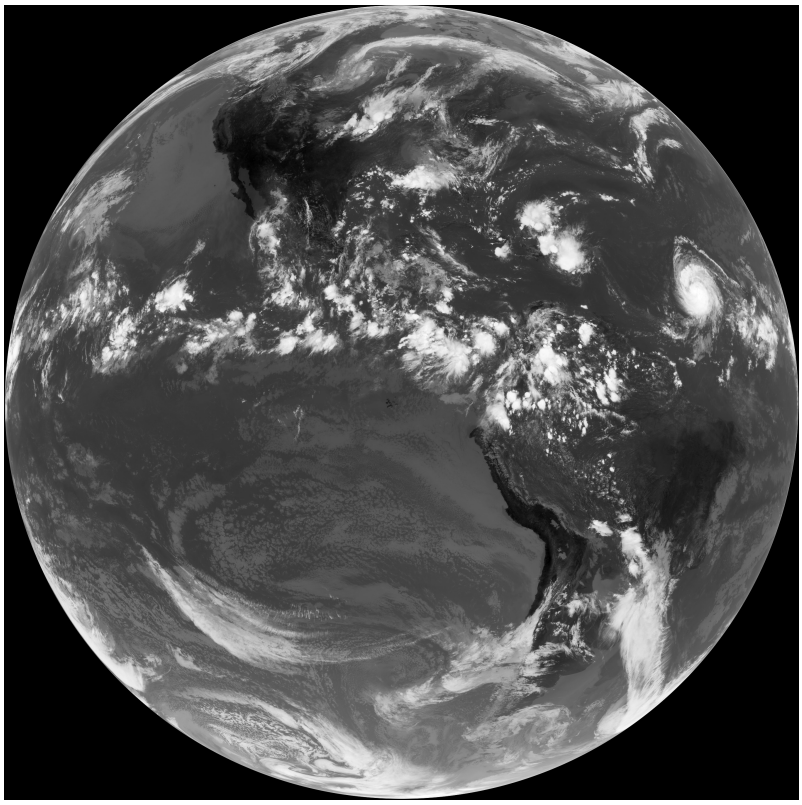

Figure 1.2: Infrared image from GOES 14 showing the inter Tropical convergence zone.(Source https://upload.wikimedia.org/wikipedia/).

Within the ITCZ, convectively coupled equatorial waves are observed to propagate in eastward or westward directions and these waves are identified as important mechanisms for organisation of convection (Kiladis et al., 2009).

Equatorial waves are observed in a wide range of frequencies that vary from a period of one week or more in the case of Rossby and Kelvin waves, to a period of around a day to a few days for higher frequency mixed Rossby gravity and inertio gravity waves (e.g Wheeler and Kiladis, 1999; Wheeler et al., 2000). The peculiar behavior of tropical waves is demonstrated in simulations conducted by Grabowski and Moncrieff (2001) using a two dimensional planetary scale (20,000 km) CRM. They observed the propagation of mesoscale organized systems in westward direction, while the mesoscale organized convective systems propagate in west to east direction. This large scale movement of the convective envelope associated with Kelvin waves, while the propagation of mesoscale organized systems is related to the higher frequency equatorial waves (e.g Grabowski and Moncrieff, 2001; Kiladis et al., 2009).

Beside the convectively coupled equatorial waves, the Madden-Julian Oscillation (MJO) is observed to affect large scale organisation of convection in Tropics Grabowski and Moncrieff (2001). MJO is one of the most striking patterns of convection in the tropics (e.g Madden and Julian, 1971), which is a quasi-periodic convective activity that propagates eastward at around 5 m s^{-1} and dominates the intra-seasonal (30 to 90 day) variability of the atmosphere. Recent studies highlight the need for a better representation of deep convection in global climate models in order to appropriately represent MJO (Grabowski, 2003*a*).

1.4 Radiative-Convective Equilibrium

A single deep convective cumulus cloud has been shown to interact with the environment by transporting heat and moisture in the atmospheric column and modulating the radiation budget through the formation of cloud anvils. This interaction is complicated when the interaction of additional clouds and large scale flow is considered. Therefore, the problem is frequently studied in an idealized framework modelling the state of radiative convective equilibrium (RCE). This has been widely used to understand the fundamental actions of convection without variations in large scale flows (e.g Held et al., 1993; Sui et al., 1994; Tompkins and Craig, 1998a,b; Tompkins and Craig, 1999; Grabowski and Moncrieff, 2001; Robe and Emanuel, 2001; Grabowski and Moncrieff, 2002; Grabowski, 2003*b*; Bretherton et al., 2005; Grabowski, 2006*b*;

Stephens et al., 2008; Muller and Held, 2012; Wing and Emanuel, 2014). In this state the tropical atmosphere compensates the net radiation cooling by subsidence heating in free troposphere which is driven by the convective latent heating, in a mean sense, averaged over the life time of many clouds.

One of the early examples of using RCE to study the tropical atmosphere employed a single column model (Manabe and Strickler, 1964). They introduced a fixed lapse rate constraint to their 1D radiative equilibrium model to approximate the effects of convection. More recently, two dimensional models (e.g Held et al., 1993; Grabowski and Moncrieff, 2001), three dimensional models (Tompkins and Craig, 1998a) including channel-like three dimensional domains (e.g Tompkins, 2001a; Stephens et al., 2008; Wing and Timothy, 2015), have been used with O(1km) convective-permitting resolutions to study RCE, although Tompkins and Craig (1998a); Tompkins (2000a) argued that little numerical advantage was to be gained from the use of 2D models, which had the drawback of modifying the equilbrium mean state by the artificial constraint on the circulation geometry. With the advancement of computational resources, recent cloud resolving models (CRM) use three dimensional domains of many hundreds of kilometres (e.g Bretherton et al., 2005; Muller and Held, 2012; Wing and Emanuel, 2014), now approaching the planetary scale (Bretherton and Khairoutdinov, 2015). RCE simulations can help to understand water vapor interactions and the role of radiative transfer and surface fluxes in mediating these interactions (Bretherton et al., 2005).

The time scale of the experiments required to achieve RCE is determined by radiation (Tompkins and Craig, 1998b). Radiative cooling rates are identified to determine the adjustment time scale through their control of the subsidence velocity in a clear sky environments surrounding the convection (Tompkins and Craig, 1998b), effectively determining the tropospheric-deep mixing time. In the absence of large scale convergence in a state of radiative convective equilibrium, the subsidence velocity is constrained by radiative cooling as indicated by equation 1.1.

$$w_s = \frac{\langle Q_{rad} \rangle}{\overline{\rho} c_p H \frac{d\theta}{dz}} \tag{1.1}$$

where w_s is subsidence velocity, $\langle Q_{rad} \rangle$ is a column integrated radiative cooling per unit area, $\overline{\rho}$ is mean density and $\frac{d\theta}{dz}$ is lapse rate.

The mixing time scale is the time it takes for a theoretical parcel to pass

through the depth of the convective layer (H) with subsidence velocity w_s as given in equation 1.2

$$\tau_{rad} = \frac{w_s}{H} \tag{1.2}$$

where τ_{rad} is the radiative mixing time scale The RCE simulations with a three dimensional CRM conducted by Tompkins and Craig (1998b) to determine the adjustment time scale of tropical atmosphere found the long adjustment time scale to be around 30 days. However, this time scale is much longer in the presence of interactive sea surface temperature (Cronin and Emanuel, 2013).

1.5 Mechanisms

It is known that large scale forcing such as vertical wind shear and SST gradient have significant role in organisation of convection (Rotunno et al., 1988; LeMone et al., 1998; Robe and Emanuel, 2001). However, feedback mechanisms other than large scale forcing can be involved in convective organisation. For instance, convectively enhanced winds could increase local surface fluxes of heat and moisture to facilitate localization of convection (Emanuel, 1987). There are also additional mechanisms such as water vapor (e.g Held et al., 1993; Tompkins, 2001a), cold pools (e.g Tompkins, 2001b; Jeevanjee and Romps, 2013) and radiative feedbacks (e.g Tompkins and Craig, 1998a; Stephens et al., 2008) that can affect the organisation of convection.

Emanuel et al. (2014) have recently suggested that longwave radiative feedbacks could lead to organisation only above a threshold sea surface temperature (SST) in the range observed in the warm pool (30-35^{o}C), posing the intriguing prospect of a potential potent negative climate feedback, whereby convection organisation acts as an iris-like 'safety valve' to prevent excessive surface temperatures (Lindzen et al., 2001; Mauritsen and Stevens, 2015). The correlation between top of atmosphere (TOA), outgoing longwave radiation (OLR) and SST anomalies reverse signs between the west Pacific warm pool area and the central Pacific, hinting at this mechanism Trenberth et al. (2015). Paleo work suggests that the warm pool region was never much warmer than it is today, also indicating a capping mechanism de Garidel-Thoron et al. (2005). An understanding of the factors driving organisation is thus key. Further information regarding these mechanisms is provided in the following sections.

1.5.1 Water vapor

In the tropics, the main sources of free tropospheric water vapor is convective detrainment and evaporation of precipitation falling from convective clouds (e.g Grabowski and Moncrieff, 2004). As a result of this, the observed spatial distribution of free tropospheric humidity is closely tied to convection as initially documented by Gray (1973) and Gray et al. (1975) using low resolution satellite imagery with tropical radiosonde data. At the same time, free tropospheric humidity influences the presence of individual deep clouds (Derbyshire et al., 2004) and occurrence of strong convective systems (e.g Zhang et al., 2003).

In addition to deep convection, there is observational evidence that shows the positive feedback of shallow convection that preconditions the lower troposphere for future deep convection through its moistening effect (e.g Esbensen, 1978; Johnson, 1978; Nicholls and Lemone, 1980). This assists the mesoscale system to form long lasting clusters of convections. In contrast, a dry troposphere which has a tendency to create a stable atmosphere is found to inhibit convection (e.g Numaguti et al., 1995; Yoneyama and Fujitani, 1995; Mapes and Zuidema, 1996). These suggest that water vapor anomalies are dynamically significant through their relationship with convection (Tompkins, 2001a; Grabowski and Moncrieff, 2004). For instance, Grabowski (2003a) demonstrates the suppression of the Madden-Julian oscillation when the interaction of humidity and convection suppressed artificially in simulations.

Observations demonstrate the significant role of mid-tropospheric moisture in organisation of convection. For instance, a strong correlation is observed over tropical oceans between convective precipitation and column water vapor on daily and longer time scales (e.g Sherwood, 1999; Raymond, 2000; Bretherton et al., 2004). The intrusion of dry air into the mid troposphere is also observed to halt self organisation over west Pacific ocean (e.g Numaguti et al., 1995; Redelsperger et al., 2002).

Various RCE simulations using CRMs have been conducted to investigate the impact of water vapor on the organisation of convection. For example, RCE simulations using a 2D CRM were conducted by Held et al. (1993) finding the moisture field to be key for the localization of convection. This result is consistent with Tompkins (2001a), who used a three dimensional CRM to

show the critical role of free-tropospheric humidity field for the organisation of convection. In sensitivity tests, a moisture perturbation was applied (removing 60% of the moisture) above 900 and 700 hPa levels respectively. Convection was immediately extinguished by the low level perturbation (900 hPa), while the latter case continued to simulate convection but with reduced mass fluxes. As a result of this, Tompkins argued that lower tropospheric humidity is most critical in controlling moist convection.

Tompkins (2001c) conducted additional experiments to show the importance of moisture in a domain with an imposed SST gradient. It was found that the convection initialized over warm SST and suppressed over cooler SST as expected. The air above the cooler SST dries as a result of the subsidence that balances the remote convection. In idealized experiment the location of the hot and cold spots was interchanged. However, convection failed to initialize instantly over the new warmest SST due to overlying dry air, inherited from the earlier subsidence over cold SST. The moistening process propagates with an advection time scale and thus it required several days to create a conducive environment for convection to recommence. This experiment highlighted the importance of water vapor feedback for the organisation of convection.

Further experiments by Grabowski and Moncrieff (2004) imposed a Newtonian relaxation of the moisture profile back to the domain mean value in order to remove large-scale moisture gradients. Essentially, the relaxation hugely increases the mixing of water vapour between the moisture and dry domains, which is usually a relatively slow process relative to the time scales that create anomalies (Pierrehumbert, 1995; Zhang et al., 2003). Grabowski and Moncrieff (2004) showed that reducing the ability of convection to set up large scale gradients of moisture destroyed the strong organisation of convection that was apparent in the control integration. While more recent work has acknowledged the role that water vapor may play, it has tended to have been downplayed in importance relative to radiative feedbacks (e.g Wing and Emanuel, 2014).

1.5.2 Cold pools

The drag of falling precipitation and negative buoyancy resulting from precipitation evaporation and mixing forms downdrafts which inject cold and dry

air from the mid troposphere into the boundary layer (Zipser, 1977) (figure 1.1). Cold pools can play a dynamical role in triggering new convection, as well as a more recently suggested thermodynamical role. Dynamical lifting of the boundary layer air by the spreading cold pool can lead to the convective inhibition energy (CIN) being overcome leading to new convective cells, and which can be especially pronounced when they interact with environmental wind shear leading often to the formation of squall lines (e.g Simpson, 1980; Thorpe et al., 1982; Rotunno et al., 1988). This documented role of cold pools in higher shear environments in the triggering of convection and the formation of organized squall lines has been widely studies (Rotunno et al., 1988; Moncrieff and Liu, 1999; Boing et al., 2012; Khairoutdinov and Randall, 2006).

There has also been a thermodynamical role of cold pool suggested. Evaporation of rainfall has the role of moistening and cooling the sub-cloud layer before the onset of the cold pool is observed (Betts, 1984). The spreading cold pool advected this moist but negatively buoyant band out at the cold pool edges. The higher water vapour value at the gust front and drier air at the center of the cold pools was observed by Addis et al. (1984). Due to entrainment from the area above the boundary layer and gust-enhanced surface fluxes (Redelsperger et al., 2000) the central regions of the cold pools recover in temperature quickly while moisture perturbation is enhanced (Tompkins, 2001b). Tompkins (2001b) demonstrated the importance of cold pools in low wind shear situations in high resolution CRM experiments (over a water surface). It was showed that new deep convective cells emerge due to high equivalent potential temperature air at the boundary of the spreading cold pools. Enhanced sensible heat fluxes reduce convective inhibition (CIN) as the cold pool spreads while latent heat fluxes increase the moist static energy (h) and associated convection available potential energy (CAPE) further, facilitating the formation of deep convection at the mature cold pool boundary. This makes the thermodynamic behavior of cold pools to be a key mechanism that organize tropical deep convection in low shear conditions (Tompkins, 2001b). Tompkins (2001b) acknowledged that both dynamics and thermodynamics can contemporaneously play a role in triggering, as in the case where two cold pools collide. Jeevanjee and Romps (2015) recently studies these relative roles in more detail and concluded that the dynamical effect of cold pool collision could be important.

Over a land surface, one reason for not observing deep convection during maximum solar heating (noon) is associated with cold pools (although water vapour is also important as outlined below). For instance, Lima and Wilson (2008) observed that shallow convection produces small cold pools during early afternoon and these cold pools eventually merge with others to form larger cold pools with near-circular gust fronts. The time scale of the cold pool formation and merger played a role in the triggering delay. This phenomena was observed during the Tropical Rainfall Measuring Mission-Large-Scale Biosphere-Atmosphere (TRMM-LBA) project that was conducted to identify storm triggering mechanisms using a combination of ground-based radar and geostationary satellite observations. The impact of cold pools on the diurnal cycle of convection over land is parameterized by a single column model of Rio et al. (2009). They found enhanced convection maintains active convective precipitation until early evening.

It is also observed over land surfaces that cold pools are important in transforming shallow to deep convection. (Grabowski et al., 2006; Khairoutdinov and Randall, 2006; Boing et al., 2012) demonstrated the critical role of cold pools for the development of deep convection, by suppressing the formation of cold pools in large eddy simulation (LES) and CRM experiments. Without cold pools convection remained shallow even in the presence of high CAPE values and almost zero CIN values due to the lack of momentum input to overcome frictional drag and mixing effects. This suggests the importance of precipitation and cold pools for the formation of deep convection.

The effect of cold pools over the the tropical western Pacific ocean was observed by Chuda et al. (2008) using ship measurements. The effect of cold pools on the variability of sensible and latent heat fluxes of the ocean was shown. Parameterizations of surface fluxes that take into consideration the effect of cold pools on enhancing the surface latent and sensible heat fluxes through wind gustiness were introduced for coarse-scale model in which convection is also parameterized (Redelsperger et al., 2000; Zeng et al., 2002). They presented the gustiness of the wind as functions of precipitation or updraft and downdraft mass fluxes generated by deep convective cells.

In addition to the significant thermodynamic and/or dynamic role of cold pools for the triggering of deep convection, cold pools are also observed to facilitate stronger and more organized convection when many cold pools are

interacting. Boing et al. (2012) use Lagrangian parcel analysis to highlight the important role of convective organisation within sub-cloud layer for the development of deep convection. The relative contributions of isolated and interacting cold pools in triggering deep convection is quantified by Feng et al. (2015). They describe the result obtained from their high-resolution regional model simulation as "intersecting cold pools last more than twice as long, are twice as large, 41% more intense (measured with buoyancy), and 62% deeper than isolated cold pools. Consequently, intersecting cold pools trigger 73% more convection than do isolated ones." They attribute this behavior to the closeness of clouds formed by intersecting cold pools moistens the local environment and reduces entrainment drying, increasing the probability that the clouds further develop into deep convection. Jeevanjee and Romps (2013) also quantified the thermodynamic versus dynamic role of cold pools, and the thermodynamic role of cold pools suggested by Tompkins (2001b) was confirmed, while the dynamic influence of cold pool collision has also emphasized.

1.5.3 Radiation

In addition to the interaction of water vapor and cold pools with convection, the role of radiation is also important for the organisation of convection. Gray and Jacobson Jr (1977) hypothesized a role for cloud-radiation feedbacks for driving the observed diurnal cycle of convection over oceans. Using observations, the interaction of cloud and radiation was diagnosed to increase convergence in cloudy areas over the pacific (Bergman and Hendon, 2000). A number of studies had shown the importance of cloud-radiation interaction to drive dynamical circulation in global general circulation model (GCMs) such as the seminal studies of Slingo and Slingo (1988) and Slingo and Slingo (1991).

One of the first studies to identify the critical role of radiation for formation of self organisation of convection in CRM studies of RCE was by Tompkins and Craig (1998a). They showed (in figure 1.3 c) the disappearance of the organized structure of convection within a few days of simulation when radiative heating rate is horizontally uniform but separate experiments were not performed to discern whether the effect was driven by cloud anvil radiative effects or the response to the large scale variability in the water vapor field, nor whether the longwave or shortwave feedback dominated. This inhomogeneous radiative

heating rates were assumed to increase convergence into cloudy region.

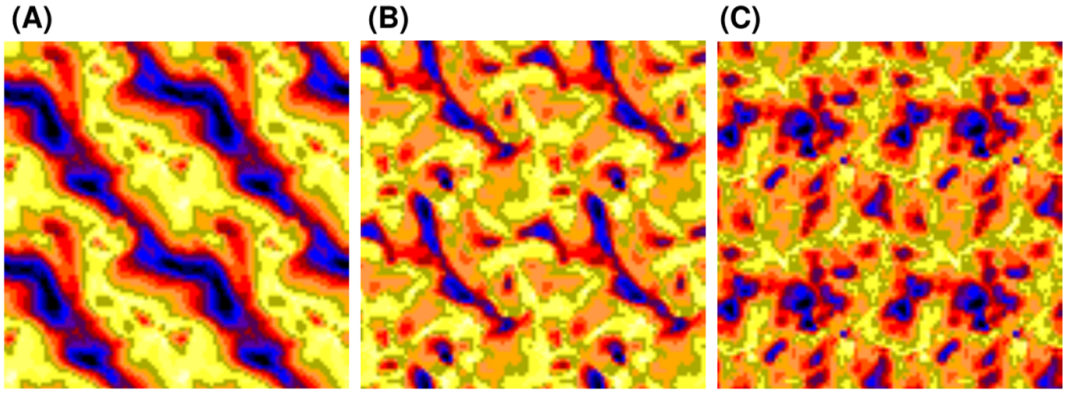

Figure 1.3: Water vapor mixing ratio at the lowest model level in long term CRM simulations of RCE by Tompkins and Craig (1998a). The domain is repeated twice in each direction to emphasize any organisation present. a) radiation and wind surface flux (control experiment) b) after 4 days of simulation from the control experiment with interactive radiation and wind insensitive surface fluxes c) after 4 days of simulation from the control experiment with non-interactive radiation and wind sensitive surface fluxes. From Tompkins and Craig (1998a).

The differential horizontal radiative heating between cloudy and clear regions was found to be important in localizing convection in later studies. Stephens et al. (2008) found that the presence of high anvil cloud resulting from convection introduces gradients of radiative heating which determine the location of organized convection structure. This result is consistent with Bretherton et al. (2005), who highlighted the initialization of self-organisation to be a result of reduction of radiative cooling of air columns in the moistest region due to the presence of extensive anvil cirrus. In contrast, the driest columns are characterized by extensive radiative cooling (Bretherton et al., 2005) shown in three dimensional CRM integrations. The enhanced cooling serves as a positive feedback for self-aggregation since the subsidence that compensate the cooling will facilitate the transport of moist static energy from dry to moist columns. The upgradient transport of moist static energy preferentially removes energy from the driest columns, was also shown by Muller and Held (2012); Wing and Emanuel (2014) to be a positive feedback for the self-organisation of convection.

Muller and Held (2012) noticed different critical mechanisms operating during the initial and matured state of self-aggregation. These are, longwave

cooling from low clouds and clear sky longwave cooling in dry regions are the responsible mechanisms for initializing and maintaining of the self-organisation process respectively. In contrast, interactive shortwave radiation extracts energy from the high energy columns (moist regions) through the action cloud anvils and it provides a negative feedback to self organisation process (Muller and Held, 2012).

Similarly Wing and Emanuel (2014) recently argued that the mechanisms required to initialize self-organisation might be different from those required to maintain it. For instance, contrasts in longwave cooling rates between moist and dry regions is initially a positive feedback for organisation. They associate this effect with the reduction of water vapor in the upper troposphere which is opposed by anomalous longwave cooling in the lower troposphere. However, as the self-organisation process intensifies, the lower troposphere also becomes drier, which in turn reduces low level longwave emissivity. As a result less radiative cooling occurs in the dry region. Hence, in their simulations they showed a change from positive to negative feedback of longwave radiation during the evolution of the self-organisation process. In contrast, shortwave radiation was a positive feedback throughout the evolution of self aggregation. This is due to the increasing absorption of shortwave radiation with the increasing total column water vapor. The longwave positive feedback appears once again in the moistest region during the matured stage of self-organisation process. This is due to the reduction of longwave cooling by longwave opacity and low temperature of high clouds.

Emanuel et al. (2014) have further recently argued that the longwave feedback between dry and moist regions operates when lower tropospheric humidity is so large that the opacity approaches unity. It is argued that convection thus organizes over warmer oceans when SST exceeds a critical threshold of around 300-305 K. This raises the intriguing prospect that convection organisation acts as a strong negative feedback on surface temperatures since mean humidity is lower in all organized state. Indeed Mauritsen and Stevens (2015) argue that such an iris effect (Lindzen et al., 2001) could greatly reduce the climate sensitivity of global models. However opposing this Muller and Bony (2015) show other processes such as cold pools still initiate organisation at cooler temperatures.

1.5.4 Surface fluxes

Convective activity increases boundary layer winds and depresses temperature and humidity through the generation of cold pools which enhances surface energy fluxes. The local enhancement of moist static energy by elevated fluxes could lead to convective organisation. Removing this interaction shown (figure 1.3 b) to destroy the organisation structure in three dimensional CRM of Tompkins and Craig (1998a). This implies that surface flux feedback could also play a role in addition to radiation, water vapor and cold pools feedbacks for the self-organisation process.

In the three dimensional CRM of Bretherton et al. (2005), it was demonstrated that surface fluxes play a role in exporting high energy air from dry to moist columns. This effect is due to convective gustiness which is shown to be a positive feedback on self aggregation during the first 20 days of their simulations. Later on, the air-sea humidity difference is intensified in the dry regions and as a result these regions are subject to enhanced surface fluxes. The surface flux feedback for organisation is thus negative as the dry perturbation amplifies.

In the recent work of Wing and Emanuel (2014), the surface feedback was partitioned into the variation in surface wind speed (gustiness) and the thermodynamic disequilibrium between the ocean and the overlying atmosphere. They found the gustiness in moist regions to enhance surface fluxes there, considered as a positive feedback for self-aggregation process (Tompkins and Craig, 1998a). This feedback is related to the WISHE mechanism for cyclone intensification suggested by Neelin et al. (1987); Emanuel (1987). This feedback is specially dominant in the early stage of the simulation of Wing and Emanuel (2014), the result was also supported by Bretherton et al. (2005). In contrast, the feedback from air-sea enthalpy disequilibrium is found to have negative feedback throughout the simulation but this effect becomes dominant during the later stage of the self organisation process, as shown by Wing and Emanuel (2014).

1.5.5 Summary of the feedbacks

Previous studies have investigated various mechanisms such as water vapor, cold pools, radiation and surface fluxes for the self-organisation using CRMs.

Processes	References
Water vapor	Held et al. (1993), Tompkins (2001a)
Cold pools	Tompkins (2001b),Feng et al. (2015),Muller and Bony (2015) Jeevanjee and Romps (2013), (Muller and Held, 2012)
Gustiness	Neelin et al. (1987), Emanuel (1987), Bretherton et al. (2005), Wing and Emanuel (2014)
Radiation	Tompkins and Craig (1998a)
Low clouds (longwave)	Muller and Held (2012)
High clouds (longwave)	Bretherton et al. (2005), Wing and Emanuel (2014), Stephens et al. (2008)
Water vapor (longwave)	Muller and Held (2012), Emanuel et al. (2014)
Water vapor (shortwave)	Wing and Emanuel (2014)
Surface flux	Tompkins and Craig (1998a)

Table 1.1: Summary of positive feedbacks for the organisation of convection

The feedbacks of these mechanisms are summarized in table 1.1 and the following points highlight some of the key characteristics of the feedbacks observed in previous studies:

- Convective local moistening and the associated subsidence drying creates vapor gradients, while moist air supports deep convection: a positive feedback for self-organisation.
- CRM experiments are found to produce this bimodal vapour behavior (moist-convective and dry-subsidence) if they produce self-aggregated states.
- The effect of variations in humidity (moist and dry regions) are highly modulated by feedbacks of radiation, surface fluxes and cold pools.

1.6 CRM as a tool to investigate organisation

The majority of the studies into spontaneous organisation of convection used cloud resolving models with horizontal resolutions of the order of 1 to 4 km. While much has been learned from these tools, there are some caveats to both

the modelling framework and the idealized experimental framework that must be considered, and which will form the crux of this thesis work.

Considering the resolution employed, these models can be regarded at best as convective permitting, rather than convective resolving, and Bryan et al. (2003) argued strongly that an order of magnitude higher resolution on the order of 100 m was desirably for most modelling applications. One issue is that the grid spacing is too coarse to explicitly represent sub-plume turbulence and entrainment processes. Such mixing is thus almost entirely represented by the sub-grid scale turbulence parameterizations that are employed in such models. The RCE states in these CRMs simulation are likely to be sensitive to the model configuration as a result, in particular, the sub-grid mixing scheme employed. These are often simple in nature, employed first order Smagorinski or 1.5 order TKE closures, although Krüger (1988) employed a third order closure scheme on the basis of the argument that sub grid processes were important to model accurately. Romps (2010) did compare entrainment rates with 100 m and 1 km horizontal resolutions and found them to be surprisingly similar. This issue will be addressed in chapter 4 of the thesis, where the sensitivity of self-organisation process is discussed using various sub-grid turbulent mixing options.

The idealized experimental frameworks represent another concern. The domains used may not always be adequate to represent the scale of the organisation. This was certainly the case in the earlier RCE work, both in 2D and 3D, where convection collapsed to a single cluster (Held et al., 1993; Tompkins and Craig, 1998a). Tompkins and Craig (1998a) used a smaller domain size (100x100 km) that didn't artificially restrict subsidence, but the convective band oriented itself on the diagonal to ensure the maximum inter-cluster spaces; a obvious marker than the domain size was insufficient.

Dimensionality of the CRMs are also important issue during the set up the simulations Tompkins (2000*b*). Tompkins demonstrated the effect of the dimensionality by comparing 2D and 3D CRMs having the same number of grids and zero mean wind. The 2D simulation indicated to develop unrealistic large wind shears which suggested the need to use three dimensional model to sufficiently represent cloud scale motions and their associated transport of water vapor.

In recent studies due to the advancement of computational resources and

the need to study a wide range of scales in organisation, larger domains of several hundred km have been used (e.g Bretherton et al., 2005; Muller and Held, 2012; Wing and Emanuel, 2014), but convection is still often restricted to a single location or band. During the investigation of self-organisation process, variation in the choice of domain size and horizontal resolution is found to affect the organisation (Muller and Held, 2012). The main cause for the sensitivity of self-organisation to these model configuration is the sensitivity of the distribution of low clouds to the domain size and horizontal resolution (Muller and Held, 2012). In contrast, Jeevanjee and Romps (2013) associate the sensitivity of CRM to the domain size with the effect of cold pools. Wing and Timothy (2015) outlines an exciting recent simulation which has the capacity to represent several bands.

Finally, the simulation boundary conditions are often also highly idealized. Low mean wind conditions, where domain mean winds are often close to (or even relaxed to) zero, exacerbate the impact of cold pool gustiness on flux enhancement. In the presence of a mean wind, cold pool wind perturbation both reduce and enhance fluxes, which may reduce their overall impact on organisation. Likewise, replacing a fixed lower boundary temperature with an reactive SST may also enhance or reduce organisation. Bretherton et al. (2005) briefly report the result of using a slab ocean of 2 metre depth which considerably slowed the formation of organisation due to the short-wave radiative feedback.

1.7 Objective of the thesis

The main objective of this thesis is to gain a better insight into the mechanisms that control the self-organisation process of convection in convection permitting simulations of radiative-convective equilibrium. Towards this goal, various controlled experiments are conducted using a three dimensional cloud resolution model, to address the following questions:

- Using a fixed-SST, convection permitting CRM experiment, can we reproduce the results of previous research regarding the spontaneous organisation and its key drivers?
- How does the basic experimental framework such domain size and imposed wind affect the organisation?

- How does the updraught entrainment process and its representation in the subgrid parameterization affect the equilibrium state?
- How does the boundary conditions such as employing an interactive SST affect the self-aggregation state?

Chapter 2 will outline the model used in the work, and its setup for the experiments. A new diagnostic index for the degree of organisation is introduced, which is used to quantify the level of organisation at each stage of the self-aggregation process. The control experiments and all the sensitivity tests have used it to understand the impact of the physical mechanisms. In chapter 3, a control experiment with a fixed SST is conducted to investigate the evolution of the self-aggregation process. The dominant mechanisms at different stage of the organisation process is analyzed using frozen moist static energy budget. In chapter 4, the sensitivity of the model to sub-grid mixing and numerical filters are discussed in detail, while chapter 5 discusses the role of interactive SST in the self-organisation process. Additional sensitivity experiments are conducted to investigate the role of imposed winds. Chapter 6 concludes the work and makes further recommendations.

Chapter 2

Model description, general model setup and diagnostics for organisation

This chapter provides an overview of the model including information concerning the governing equations and some of its key parametrizations. Details are also given of the basic model setup such as domain size, horizontal and vertical resolutions. The chapter also describes the radiation, surface flux and microphysical schemes used in the model. Furthermore, it provides a brief description of a new statistical diagnostic metric that will be used to quantify the characteristics of convection's spatial distribution and degree of clustering.

2.1 Model Description

2.1.1 Governing equations

The Weather Research Forecast (WRF) version 3.5.1 is used as a cloud resolving model (CRM). It is non-hydrostatic and uses a flux form of Euler equations. These equations are formulated based on a terrain following mass vertical coordinate (Laprise, 1992) as defined in equation 2.1

$$\eta = (p_h - p_{ht})/\mu \tag{2.1}$$

where $\mu = (p_{hs} - p_{ht})$. The pressure variables p_h, p_{hs} and p_{ht} are the hydrostatic, surface and top pressure, respectively.

The values of η varies from 1 at the surface to 0 at the upper boundary of the model, μ represents the mass per unit area within the column in the

model domain that is used to define the appropriate flux form of the variables as shown in equation 2.2

$$U = \mu u, V = \mu v, W = \mu V, \Theta = \mu \theta, \tag{2.2}$$

where U is the flux form of velocity in east-west direction, V is the flux form of velocity in south-north direction, W is the flux form of velocity in vertical direction, Θ is the flux form of potential temperature.

Using the variables defined in 2.2, it is possible to write the flux form of Euler equations as shown below; further detail of these equations can be obtained from Skamarock et al. (2008).

$$\frac{\partial U}{\partial t} + (\bigtriangledown.\mathbf{V}u) - \frac{\partial (p\phi_\eta)}{\partial x} + \frac{\partial (p\phi_x)}{\partial \eta} = F_U, \tag{2.3}$$

$$\frac{\partial V}{\partial t} + (\bigtriangledown.\mathbf{V}v) - \frac{\partial (p\phi_\eta)}{\partial y} + \frac{\partial (p\phi_x)}{\partial \eta} = F_V, \tag{2.4}$$

$$\frac{\partial W}{\partial t} + (\bigtriangledown.\mathbf{V}w) - g(\frac{\partial p}{\partial \eta} - \mu) = F_W, \tag{2.5}$$

$$\frac{\partial \Theta}{\partial t} + (\bigtriangledown.\mathbf{V}\theta) = F_\Theta, \tag{2.6}$$

$$\frac{\partial \mu}{\partial t} + (\bigtriangledown.\mathbf{V}) = 0 \tag{2.7}$$

where F_U, F_V , F_W, and F_Θ represent forcing terms arising from model physics, turbulent mixing, spherical projections, and the earth's rotation, $\mathbf{V} = \mu\mathbf{v} = (U, V, W)$ are the flux form of horizontal and vertical velocities, g is gravitational acceleration, p is pressure and $\phi = gz$ is a geopotential term.

2.1.2 Miscellaneous technical details

The model uses Arakawa type C grid staggering where the horizontal velocities are normal to the respective faces of the grid cell while the mass, thermodynamic and scalar variables are located in the center of the cell. The model implements a time-splitting integration scheme where slow or low-frequency modes are integrated using a third-order Runge-Kutta (RK3) time integration scheme, while the high-frequency acoustic modes are integrated over smaller time steps to maintain numerical stability (Klemp and Skamarock, 2007). The

time step is limited by the advective Courant number and the choice of advection schemes (Skamarock et al., 2008).

The WRF model has both even and odd order advection schemes. The even-order advection operators are spatially centered and thus contain no implicit diffusion outside of the diffusion inherent in the RK3 time integration, while the odd-order schemes are upwind-biased and the spatial discretization is inherently diffusive (Skamarock et al., 2008). Thus, the odd-ordered flux divergence schemes are equivalent to the next higher ordered (even) flux-divergence scheme, with the addition of a dissipation term of the highest even order with a coefficient proportional to the Courant number as the formulation (detailed in Skamarock et al., 2008). The 5^{th} order advection scheme is used for both momentum and scalar horizontal fields in the setup used in this thesis.

Traditional Rayleigh damping is used in the model for absorbing vertically-propagating gravity waves. This is important to prevent unphysical wave reflection off the domain upper boundary from contaminating the solutions (Skamarock et al., 2008). The damping coefficient is inverse of the time scale (0.03) and damping is applied in the top 5 km of the model.

2.1.3 Turbulence parametrizations

Eddy diffusivity coefficients are used to parametrize the sub-grid atmospheric mixing caused by the macroscopic eddy diffusion process for models with horizontal grid spacing that is not able to resolve boundary layer turbulent eddies. The main assumption is the turbulent flux of an adiabatically conserved quantity "a" is related to its gradient as shown in equation 2.8.

$$\overline{w'a'} = -k_a \frac{d\overline{a}}{dz} \tag{2.8}$$

where $\overline{a}$ is turbulent ensemble horizontal mean of advected item, $\overline{w'a'}$ is the vertical flux and k_a is the eddy coefficient. There are a number of options in WRF to calculate k_a so that its CRM and global model versions include the effect of sub-grid eddy mixing. The sensitivity of the CRM to the choice of sub-grid eddy mixing options will be discussed in chapter 4.

a) Smagorinsky scheme

One widely used method to calculate the eddy diffusion coefficient is the first order closure (Smagorinsky scheme) which specifies k_a in the form of vertical shear and static stability. WRF provides two and three dimensional versions of this scheme, where the former one only considers horizontal mixing and needs to employ an additional planetary boundary layer (PBL) scheme to represent the vertical mixing. As a result the 2D Smagorinsky only uses the horizontal deformation to obtain k_h (horizontal eddy diffusion coefficient):

$$k_h = C_s^2 l^2 [0.25(D_{11} - D_{22})^2 + \overline{D_{12}^2}^{xy}]^{\frac{1}{2}} \tag{2.9}$$

where C_s is a constant with typical value of 0.25, $l = (\Delta x \Delta y)^{\frac{1}{2}}$ is a mixing length scale, D represents the deformation and for scalar mixing the k_h has to be divided by the Prandtl number ($\frac{1}{3}$).

The 3D Smagorinsky scheme, which can be used without a PBL scheme, calculates both the horizontal and vertical mixing as shown in equation 2.10:

$$k_{h,v} = C_s^2 l_{h,v}^2 max[0, (D^2 - P_r^{-1} N^2)^{\frac{1}{2}}] \tag{2.10}$$

where $D^2 = \frac{1}{2}[D_{11}^2 + D_{22}^2 + D_{33}^2] + (\overline{D_{12}}^{xy})^2 + (\overline{D_{13}}^{x\eta})^2 + (\overline{D_{23}}^{y\eta})^2$, $l_h = h_v = (\Delta x \Delta y \Delta z)^{\frac{1}{3}}$, N = Brunt - Vaisala frequency and scalar values obtained by dividing $k_{h,v}$ by the Prandtl number.

b) TKE scheme

A Turbulence Kinetic Energy (TKE) or 1.5 order closure scheme is also available in the WRF model, in which k_a is obtained from prognostic TKE equation and length scale as shown in equation 2.11. Like the 3D Smagorinsky scheme it can be used without the PBL scheme, since the TKE closure method can handle both horizontal and vertical sub-grid mixing, also in the boundary layer. The formulation for the eddy coefficient is:

$$\begin{aligned} k_{h,v} &= c_k e^{\frac{1}{2}} l_{h,v} \\ \Delta s &= (\Delta x \Delta y \Delta z)^{\frac{1}{3}} \\ l_s &= 0.76 e \frac{1}{2} (\frac{g}{\theta} \frac{\partial \theta}{\partial z})^{-\frac{1}{2}} \end{aligned} \tag{2.11}$$

where c_k is a constant with a default value of 0.15, $e = \frac{1}{2}(u'^2 + v'^2 + w'^2)$, l_h and h_v are horizontal and vertical length scales, respectively. Δs is length

scale for neutral and unstable cases ($l = \Delta s = l_h = h_v$). l_s is the length scale for stable situations, in this case the length scale is $l = min(\Delta s, l_s)$.

The sub-grid mixing coefficients k_h and k_v calculated by the above schemes are represented in the model by xkmh and xkmv for the horizontal and vertical mixing terms, respectively.

2.1.4 Planetary boundary layer (PBL) schemes

The WRF model can use PBL schemes such as the Medium Range Forecast Model (MRF) or Yonsei University (YSU) scheme to represent vertical mixing. The PBL schemes determine the flux profiles within the well-mixed boundary layer and thus provide atmospheric tendencies of temperature, moisture (including clouds), and horizontal momentum in the entire atmospheric column (Skamarock et al., 2008). In the experiments where a PBL is employed, we employ the Yonsei University (YSU) PBL scheme (Hong et al., 2006). The momentum diffusivity coefficient provided by this scheme is shown below (equation 2.12):

$$K_m = k w_s z (1 - \frac{z}{z_{pbl}})^2 \tag{2.12}$$

where k is Von Karman constant, w_s is mixed layer velocity scale (2.13), z is the height from the surface and z_{pbl} is the height of the PBL.

$$w_s = (u_*^3 + \phi_m k w_b^3 \frac{z}{z_{pbl}})^{\frac{1}{3}} \tag{2.13}$$

u_*^3 is the surface frictional velocity, ϕ_m is the wind profile function evaluated at the top of the surface layer, w_b convective velocity scale given the surface buoyancy flux ($\frac{g}{T_o}\overline{w'\theta'_o}$) and the ratio of the surface layer height to the PBL height.

The counter gradient term for potential temperature (θ) and momentum is also included in the PBL scheme. Water substances including water vapor are not affected by this counter gradient mixing term. Hence, the only variables that contribute for nonlocal term due to the counter gradient mixing are potential temperature and horizontal velocity, in the prognostic diffusion equation 2.14.

$$\gamma_c = b \frac{\overline{w'c'}}{w_{so} z_{pbl}} \tag{2.14}$$

where γ_c is a counter gradient term for θ and momentum (these two terms are represented by c) and w_{so} is the mixed-layer velocity scale at the level of $0.5z_{pbl}$.

Turbulence diffusion equations for the prognostic variables (horizontal velocity) (u,v), potential temperature (θ) and water variables (q water vapor , q_i ice, q_c cloud droplets) can be expressed as follows:

$$\frac{\partial C}{\partial t} = \frac{\partial}{\partial z}[K_c(\frac{\partial C}{\partial z} - \gamma_c) - (\overline{w'C'})_{z_{pbl}}(\frac{z}{z_{pbl}})^3] \tag{2.15}$$

where C is the general term for prognostic variables, K_c is the eddy diffusivity coefficient (based on the prognostic variable), γ_c is the correction to the local gradient, $-\overline{w'C'}_{z_{pbl}}(\frac{z}{z_{pbl}})^3$ is the flux at the inversion layer, includes an asymptotic entrainment flux term at this layer.

The YSU PBL scheme has counter gradient terms to represent fluxes due to non local transport and it also includes an explicit treatment of the entrainment layer at the PBL top (equation 2.15). This method was successfully implemented in WRF model and found to produce a realistic PBL structure (Hong et al., 2006). Note that when any of the PBL schemes are activated in WRF, the explicit diffusion calculated by the turbulence schemes will not be used and is replaced by the dedicated PBL scheme. Thus, despite their name, if switched on, the planetary boundary layer (PBL) schemes are responsible for vertical sub-grid-scale fluxes due to eddy transports in the whole atmospheric column, not just the boundary layer. If two closure schemes such as 3D Smagorinsky and TKE are both using the same PBL then the difference between the two cases is only due to the horizontal sub-grid mixing throughout the domain.

2.1.5 Surface layer schemes

The surface layer scheme is responsible for calculating friction velocities and exchange coefficients in the model. For land surfaces these are an input to calculate surface heat and moisture fluxes while these values are directly obtained within the surface layer over water surfaces.

Monin-Obukhov similarity theory uses stability functions from Paulson (1970), Dyer and Hicks (1970) and Webb (1970) to compute surface exchange coefficients for heat, moisture, and momentum, as shown in equation 2.16 and

2.17.

$$\phi_M(\frac{z}{L}) = \frac{kz}{u_*}\frac{\partial u}{\partial z} \tag{2.16}$$

$$\phi_H(\frac{z}{L}) = \frac{kz}{\theta_{v*}}\frac{\partial \theta_v}{\partial z} \tag{2.17}$$

where z is the vertical space coordinate, L is Monin-Obukhov length scale, k is the Von Karman constant, u_* is the friction velocity, θ_{v*} a scaling temperature, θ_v potential temperature and ϕ_M and ϕ_H are momentum and turbulent heat flux similarity functions, respectively.

The similarity functions are defined based on the local bulk Richardson number (R_{bulk}) for stable conditions. According to Zhang and Anthes (1982), if R_{bulk} is greater than 0.2, stable (night time) conditions are assumed and no turbulence exists, with the stability function set to zero. If the R_{bulk} is between 0.2 and zero, then the surface layer assumes a state of mechanical turbulence with a stability function given by equation 2.18. When R_{bulk} is less than or equal to 0 and $|\frac{z_h}{L}|$ less than or equal to 1.5 (z_h is the height of mixed layer), it is called forced convection occurs. The layer is unstable and it's stability function is given by equation 2.19.

$$\begin{aligned} \frac{z_a}{L} &= \frac{R_{bulk}}{1 - 5R_{bulk}} ln\frac{z_a}{z_o} \\ \phi_M = \phi_H &= -5\frac{z_a}{L} \end{aligned} \tag{2.18}$$

$$\begin{aligned} \frac{z_a}{L} &= Ri(z_1) \\ \phi_M = \phi_H &= 0 \end{aligned} \tag{2.19}$$

where z_a , z_1 the vertical coordinate value inside and above the surface layer respectively , Ri is Richardson number, z_o vertical coordinate at the ground.

In contrast, under conditions of free convection, the exchange of heat, moisture and momentum occurs through mixing between convective elements originating at the surface and environmental air in the PBL. This condition is considered when the R_{bulk} value is less than 0 and $|\frac{z_h}{L}|$ greater than 1.5, it as often happens usually during the day when there is a strong solar heating.

2.1.6 Microphysics schemes

For the CRM configuration, Purdue Lin microphysics scheme that includes six classes of hydrometers (water vapor, cloud water, rain, cloud ice, snow

and graupel) is included. The terminal velocity of cloud water and cloud ice particles are considered to be negligible when compared to the other hydrometeors (Lin et al., 1983). The microphysical processes used by this scheme is summarized in figure 2.1 using the Lin et al. (1983) description.

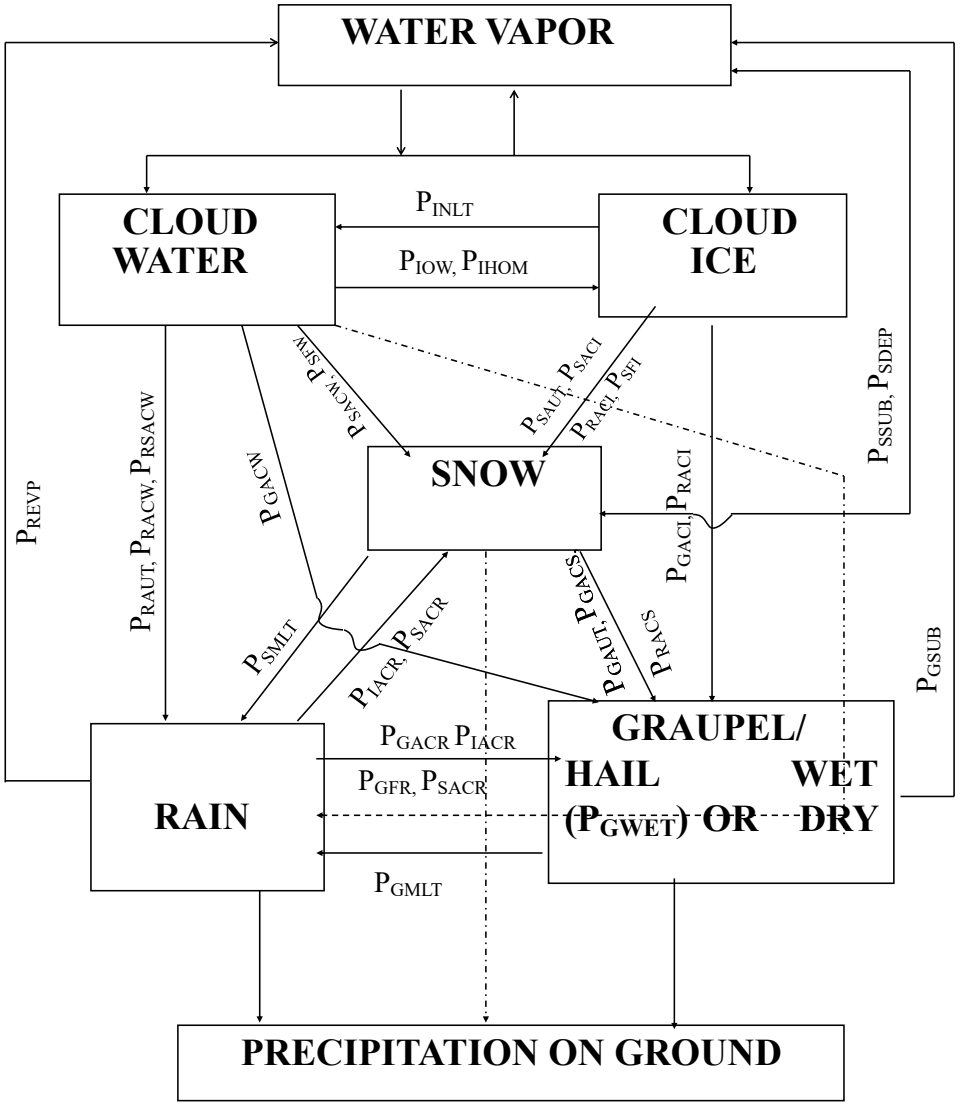

Figure 2.1: Microphysics processes simulated in the CRM adopted from Lin et al. (1983).

Description of figure 2.1

- P_{IMLT} - Melting of cloud ice to form cloud water, T $\geq$ To.
- P_{IDW} - Depositional growth of cloud ice at expense of cloud water.
- P_{IHOM} - Homogeneous freezing of cloud water to form cloud ice.

- P_{IACR} - Accretion of rain by cloud ice; produces snow or graupel depending on the amount of rain.
- P_{RACI} - Accretion of cloud ice by rain; produces snow or graupel depending on the amount of rain.
- P_{ROUT} - Autoconversion of cloud water to form rain.
- P_{RACW} - Accretion of cloud water by brain.
- P_{REVP} - Evaporation of rain.
- P_{RACS} - Accretion of snow by rain; produces graupel if rain or snow exceeds threshold and T $\leq$ To.
- P_{SACW} - Accretion of cloud water by snow; produces snow if T $<$ To or rain if T $\geq$ To. Also enhances snow melting for T $\geq$ To.
- P_{SACR} - Accretion of rain by snow. For T $<$ To, produces graupel if rain or snow exceeds threshold; if not, produces snow. For T $\geq$ To, the accretion water enhances snow melting.
- P_{SACI} - Accretion of cloud ice by snow.
- P_{SAUT} - Autoconversion (aggregation) of cloud ice to form snow.
- P_{SFW} - Bergeron process (deposition and riming) - transfer of cloud water to form snow.
- P_{SFI} - Transfer rate of cloud ice to snow through growth of Bergeron process embryos.
- P_{SDEP} - Depositional growth of snow.
- P_{SSUB} - Sublimation of snow.
- P_{SMLT} - Melting of snow to form rain, T $\geq$ To.
- P_{GAUT} - Autoconversion (aggregation) of snow to form graupel.
- P_{GFR} - Probablistic freezing of rain to form graupel.
- P_{GACW} - Accretion of cloud water by graupel.
- P_{GACI} - Accretion of cloud ice by graupel.
- P_{GACR} - Accretion of rain by graupel
- P_{GACS} - Accretion of snow by graupel.
- P_{GSUB} - Sublimation of graupel.

- P_{GMLT} - Melting of graupel to form rain, T $\geq$ To. (In this regime, P_{GACW} is assumed to be shed as rain.)
- P_{GWET} - Wet growth of graupel; may involve P_{GACS} and P_{GACI} and must include P_{GACW} or P_{GACR}, or both. The amount of P_{GACW} which is not able to freeze is shed to rain.

The parametrization of production terms are mainly taken from Lin et al. (1983) and Rutledge et al. (1984). The prognostic equations of water variables given in equations 2.20 to 2.23 based on Lin et al. (1983):

$$\frac{\partial q_c}{\partial t} = -V. \bigtriangledown q_c + \bigtriangledown . K_h \bigtriangledown q_c - P_R - P_S - P_G, \tag{2.20}$$

$$\frac{\partial q_R}{\partial t} = -V. \bigtriangledown q_R + \bigtriangledown . K_m \bigtriangledown q_R + P_R + \frac{1}{\rho}\frac{\partial}{\partial z}(U_R q_R \rho), \tag{2.21}$$

$$\frac{\partial q_S}{\partial t} = -V. \bigtriangledown q_S + \bigtriangledown . K_m \bigtriangledown q_S + P_S + \frac{1}{\rho}\frac{\partial}{\partial z}(U_S q_S \rho), \tag{2.22}$$

$$\frac{\partial q_G}{\partial t} = -V. \bigtriangledown q_G + \bigtriangledown . K_m \bigtriangledown q_G + P_G + \frac{1}{\rho}\frac{\partial}{\partial z}(U_G q_G \rho) \tag{2.23}$$

where q_c is sum of q_{cw}, q_{ci}, q_r representing cloud water, cloud ice and water vapor mixing ratio, respectively. The prognostic equation for the mixing ratio of rain q_R, snow q_S and graupel q_G is given in equation 2.21, 2.22 and 2.23, respectively. P_R, P_S and P_G are the production terms for rain, snow and hail. The first terms on the right hand side in all the above equations are advection terms and the second terms are diffusion terms. The last terms on the right of equations 2.21, 2.22 and 2.23 are the fallout terms. Some modifications such as saturation adjustment and ice sedimentation over the micro-physics parametrization were introduced by Tao et al. (1989).

2.1.7 Radiation schemes

The radiative transfer scheme RRTMG is used in configuration of the CRM. It serves to calculate shortwave ($RRTMG\_SW$) (Mlawer and Clough, 1997) and longwave ($RRTMG\_LW$) (Mlawer et al., 1997; Mlawer and Clough, 1997) fluxes and heating/cooling rates efficiently and accurately using the correlated K approach. Sixteen contiguous bands are used to calculate cooling rate for longwave fluxes while fourteen contiguous bands are implemented to calculate shortwave fluxes and heating rates. The k-distribution data for both shortwave

and longwave flux absorption coefficients are obtained directly from the line-by-line radiative transfer model (LBLRTM) (Mlawer et al., 1997; Mlawer and Clough, 1997), which has been extensively validated against observations as detailed in Clough and Iacono (1995).

2.2 General model setup

The lateral boundary conditions are periodic and the initial SST is constant with a value of 301.5 K for the control run. The initial horizontal homogeneous environment is specified based on Jordan mean hurricane sounding for the West Indies area Jordan (1958)

The domain size (500 km by 500 km) of the control run is similar to Bretherton et al. (2005). It is based on the suggestion of Muller and Held (2012) who found self-aggregation on domain size larger than 200 km. A long channel geometry (Tompkins, 2001a; Stephens et al., 2008; Wing and Timothy, 2015) is also used to study the sensitivity of the self-organisation to a domain geometry.

All CRM simulations in this thesis use a 2 km horizontal spacing similar to Tompkins and Craig (1998a); Bretherton et al. (2005); Muller and Held (2012). This is also consistent to the recommendation of Muller and Held (2012), who found self-organisation with resolutions coarser than 2 km. Since this grid spacing can only resolve deep convective cores marginally, a number of sensitivity tests to mixing scheme will be conducted to identify how the sub-grid mixing affect the self-organisation.

In the vertical, the model elongates to its top value of around 25 km having 62 levels of stretched grid points for all experiments. The lowest model level is at 39 m with grid spacing of only 50 m to the second level, then the spacing extends to 100 m, 200 m, 500 m and 1 km for the first 1 km, 1 km to 5 km, 5 km to 15 km and 15 km to 25 km respectively. This approach allows more levels to be placed in and near the boundary layer (e.g Tompkins and Craig, 1998a; Bretherton et al., 2005; Muller and Held, 2012).

2.2.1 Relaxation of horizontal wind

A Newtonian relaxation towards specified fixed values of wind speed (0 for the control experiment) both in west-east and south-north direction on velocity

tendency terms are applied as shown in equation 2.24:

$$\frac{\partial U}{\partial x} = \frac{U_{target} - \overline{U}}{\tau}$$
$$\frac{\partial V}{\partial y} = \frac{V_{target} - \overline{V}}{\tau} \tag{2.24}$$

where U_{target} and V_{target} are imposed wind in west-east and south-north direction respectively, $\overline{U}$ and $\overline{V}$ are domain average wind values, τ is the velocity relaxation time scale.

In order to determine the appropriate values of τ, additional experiments are conducted for the duration of five days. These experiments use different relaxation time scale of 10, 3600, 21600 and 86400 s, respectively while the other model settings are identical to the control run. The five day domain average horizontal velocities of U and V are constrained to imposed wind of 0 m s^{-1} as shown in figure 2.2. The restriction of the horizontal velocities are stronger for shorter relaxation time scale as clearly indicated in the experiment with τ value of 10 s. On the other hand, the deviation from imposed wind can extend to the values of 0.01 m s^{-1} and 0.014 m s^{-1} in west-east and south-north direction, respectively as observed in the experiment with τ value of 24 hours but is nevertheless small. This indicates that the choice of τ is not important if the values is less than 1 day.

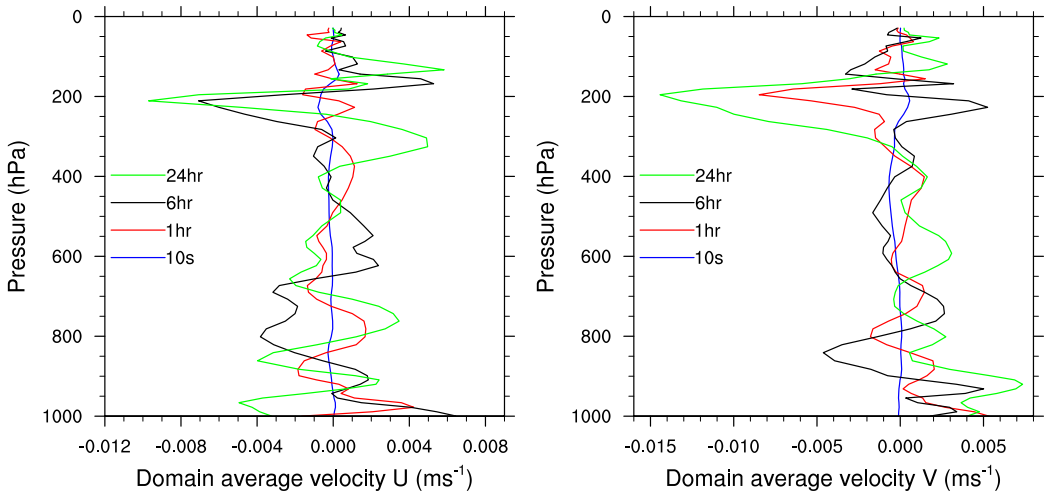

(a) (b)

Figure 2.2: Five days domain average of horizontal velocities a) U b) V for relaxation time scale of 10 s, 3600 s (1 hour), 21600 s (6 hours) and 86400 s (24 hours).

It should be emphasized that the imposed wind is not limiting the local flow

since it is applied to the mean state of the horizontal velocities. Figure 2.3, is a column average of five days horizontal wind in west-east direction, demonstrates the presence of local variability of the flow in all relaxation time scales. Hence, the Newtonian relaxation towards an imposed wind with smaller values of τ essentially keeps the mean wind (not local) exactly at the target value. This relaxation prevents the build up of wind-shear during the experiment, which has been observed in a variety of models (Held et al., 1993; Tompkins and Craig, 1998a; Tompkins, 2000*b*). As a result all the simulations in this thesis use 10 s as a relaxation time scale to prevent large scale drift without affecting the local flow.

2.2.2 Slab Ocean model

While some of the experiments use a fixed imposed lower SST, in chapter 5, experiments are also conducted using two different slab ocean models. The first slab model imposes a fixed mixed layer depth z_{mo}. The local temperature SST is affected by the latent and sensible heat fluxes, in addition to the radiative fluxes. An additional relaxation term with time scale (τ_{sst}) of 1 hour is applied to ensure that the domain mean SST remains close to a target value (SST_0) and effectively extracts heat at each time step that in reality is heat either mixed to the deeper ocean and/or advected out of the domain.

$$\frac{dSST}{dt} = \frac{-LH - HFX + GLW + SW - \varepsilon\sigma SST^4}{\rho C_{pl} z_{mo}} + \frac{SST_0 - \overline{SST}}{\tau_{SST}}, \quad (2.25)$$

where the negative/positive sign indicates the outgoing/incoming flux at the surface, LH is latent heat, HFX is sensible heat flux, GLW is longwave radiation arriving at the surface, SW is net shortwave radiation arriving at the surface, ε is the emissivity of the atmosphere, σ is Stefan-Boltzmann constant, SST is ocean mixed layer temperature, ρ is density of water and C_{pl} is specific heat capacity of water.

Further experiments are also conducted with the standard mixed layer ocean scheme available in WRF which is based on Pollard et al. (1973). This scheme incorporates a wind driven prognostic model for the local mixed layer depth and also represents the mixing of heat between the shallow mixed layer and the upper 200 m of the ocean. Further details of this model are given in Pollard et al. (1973).

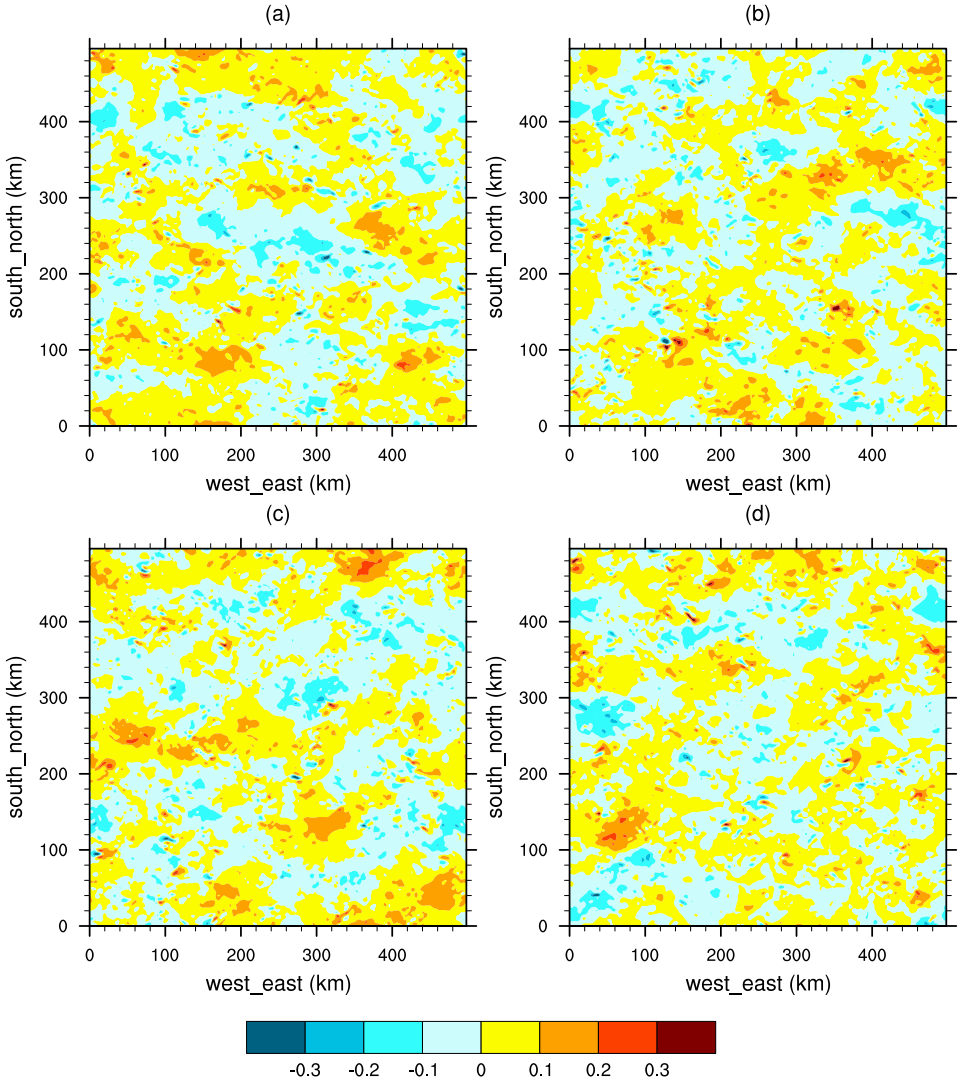

Figure 2.3: Column average of five days horizontal wind in west-east direction U (m s^{-1}) with τ values of a) 10 s b) 3600 s (1 hour) c) 21600 s (6 hours) and d) 86400 s (24 hours).

2.2.3 Model configuration

In the process of model configuration a number of experiments are conducted to obtain an appropriate CRM setup that can explain the self-organisation process. Table 2.1 summarizes four experiments that vary the shape of the domain and initial conditions. The first experiment (config1) uses a square domain (500x500 km) using an initial condition of higher moisture and temperature values at the center of the domain. The initial conditions adopt the thermodynamic anomalies that are used in an idealized tropical cyclone (TC) initialization technique that uses analytic axisymmetric vortex at the center

Name	Initial condition	Domain shape
config1	TC	square(500x500 km)
config2	TC	rectangle(1024x256 km)
config3	Random	square(512x512 km)
config4	Random	rectangle(1024x256 km)

Table 2.1: Lists the number of simulations conducted with varies values of domain size and initial condition.

of the domain to initialize convection (Rotunno and Emanuel, 1987). Note that this initialization technique thus enforces some measure of organisation on the initial state, as opposed to using randomly distributed perturbations as is more commonly the case. Thus if convective reverts in some experimentation formats to a random distribution, this will be due to negative spatial feedbacks.

In the second experiment (config2) is the same as config1 but with rectangular shape (1024x256 km), using the same TC initialization. This channel-like configuration was originally introduced by Tompkins (2001a) to study the effect of convective ensemble in a large enough 3D domain and recently this approach was adopted by Stephens et al. (2008); Wing and Timothy (2015). The third experiment (config3) is a square domain (512x512 km, very similar to config1) using instead random perturbations to initialize the simulation in order to examine the impact of the form of the initial anomalies. The last experiment (config4) is the same as the third experiment using a rectangular shape of 1024x256 km.

Figure 2.4 presents the TCWV during day 70 of all the experiments, and it demonstrates a well developed organisation structure in all the experiments. However, the shape of the organized structure is affected by the choice of domain shape and initial conditions. In the narrower channel domains with a cross domain distance of 256 km, the convection organises into a strong band-like structure, which does not occur using the square domain format. Although the form and location of the convection evolves throughout the simulation, examination of similar snapshots at all other days (not shown) shows that this distinction is robust, that is, the narrow domains always show a much stronger linear organisation. This is consistent with Muller and Held (2012), who note

a strong variation in organisation structure as a function of the domain set up. Experiments config2 and config4 have a band like structure stretched in south-north direction, while this structure is not apparent in config3, and is also less defined in config1 (Fig. 2.4); both of the latter experiments employing the square domain. It is noted that the scale of the moist region in config1 and config3 exceeds the width of the narrow channel domain indicating the possible reason for the disposition of these domains to form linear organisation.

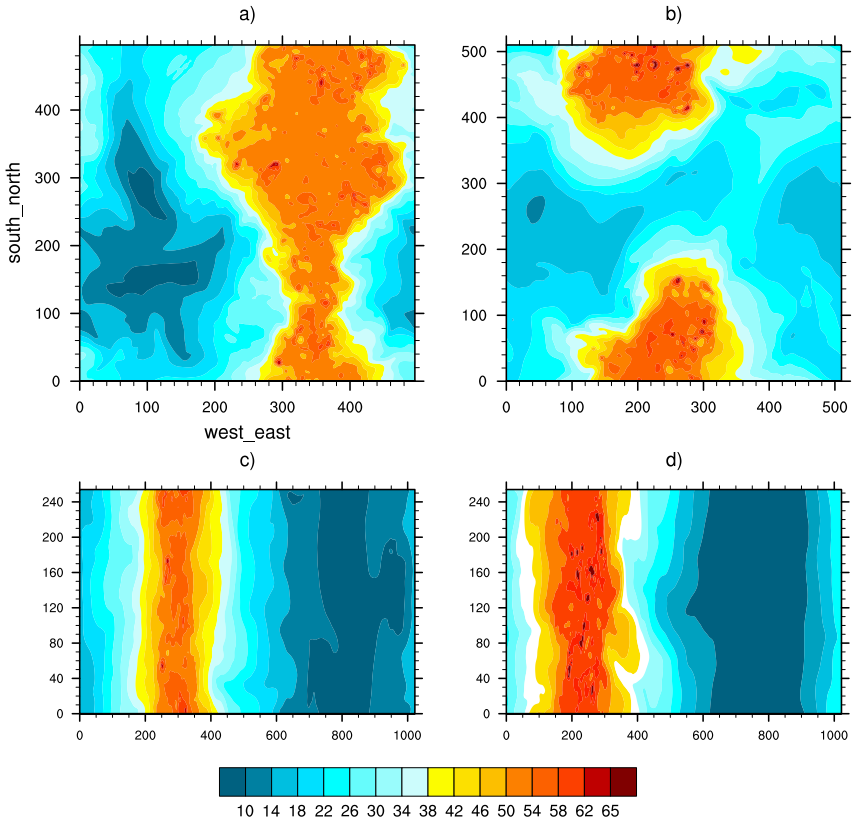

Figure 2.4: Column integrated water vapor(kg m^{-2}) on day 70 of experiments a) config1 b) config3 c) config2 and d) config4.

In addition to the difference in the shape of the cluster structure, config2 and config4 display lower TCWV values (less than 10 kg m^{-2}) in the subsidence region of the domain. These lower relative humidities are the result of the increased organisation scale using the channel-like configuration; the distance from the convective regions is increased and the horizontal advective source of humidity is reduced. This indicates that while these configurations are adequately large to represent organisation they are constraining the scale of the organisation, also evidenced by the formation of a single moist regions

in all experiments. It is noted that Wing and Timothy (2015) uses a channel of several thousand kilometres in order to achieve several distinct moist areas of convection, although the cross-domain width was considerably smaller in those experiments. Comparing the pairs of experiments using different initial conditions (config1 with config3 and config2 with config4), no strong dependence on the initial perturbations is seen.

All the experiments can be a good candidate to investigate the self organisation process, and the main experiments in the paper are conducted with the 500 by 500 km domain size as it allowed the 3D organisation to establish. This domain choice was made with the appreciation of the caveat that the domain appears to be inadequate to represent several moist convective 'centers' contemporaneously, but is computationally economic enough to allow a wide range of sensitivity experiments to be conducted.

Further sets of sensitivity tests were conducted concerning the set-up, concerning the choices of the radiation scheme and subgrid-scale diffusion. While the radiation scheme did not impact the organisational scale strongly, and is not reported here, the choice of sub-grid mixing schemes resulted in a significant difference in terms of level of organisation. These experiments are the topic of chapter 4 where an explanation will be presented to explain the underlying mechanism for this sensitivity.

2.2.4 Summary of default configuration

For purpose of investigating the physical mechanisms that affect the self organisation process, a cloud resolving model (CRM) is configured with a domain size of 500 by 500 km with a horizontal grid length of 2 km. The top vertical value of the setup is 25 km with 62 levels of stretched grid points. The lowest model level is at 39 m with grid spacing of only 50 m to the second level, then the spacing extends to 100 m, 200 m, 500 m and 1 km for the first 1 km, 1 km to 5 km, 5 km to 15 km and 15 km to 25 km respectively.

The control experiment uses 3D Smagorinsky scheme with YSU PBL for the horizontal and vertical sub-grid eddy mixing, respectively. An imposed horizontal wind of 0 m s^{-1} with relaxation time scale of 10 s is applied to prevent the build up of wind-shear.

The lateral boundary conditions are periodic and the initial environmental

Domain size	500 x 500 x 25 km^{-3}
Horizontal grid length	2km
Number of vertical levels	62 with stretched grid
Time step	12 s
Sea surface temperature	301.5 K
Imposed wind	zero
Coriolis parameter	zero
Boundary conditions	periodic lateral boundary
Initial/Environmental Profile	Mean sounding from the west indies Jordan (1958)

Table 2.2: Summary of the setup of the control simulations

condition is specified based on Jordan mean hurricane sounding for the West Indies area (Jordan, 1958). To initialize convection an analytic axisymmetric vortex specified by Rotunno and Emanuel (1987) is placed at the center of the domain and the simulation is run for duration of 70 days. This experiment excludes the Coriolis effect and all large scale mass and moisture forcing. The absence of moisture convergence is observed to be consistent with zero monthly mean values for specific times during the year in certain mid-Pacific regions (Dodd and James, 1996). Table 2.2 presents the summary of the model setup.

2.3 Diagnostics for organisation

In the introduction chapter it is shown that suppressing surface flux or radiation feedback had an impact on the level of convective organisation as shown in figure 1.3. However, when comparing the two experiments in panal B and C it is not obvious in which experiment clustering is greater. It is therefore necessary to determine a set of appropriate metrics to show the level of clustering in simulations. Using such metrics the strength of mechanisms that are responsible for the organisation/disorganisation of the system can be quantified.

2.3.1 OLR

In the case of self-aggregated system, the convective region with higher values of humidity and cloudiness are limited into a small proportion of the domain. Whereas, the dominant convection-free environment is characterized by a large increase in outgoing longwave radiation (OLR). As a result the increase in domain average OLR value can be used as indicator of self-aggregation (Wing and Emanuel, 2014). This is demonstrated in figure 2.5 a, where the experiments with higher domain average OLR value indicate higher level of organisation. Further discussion about the mechanisms that affect the level of organisation will be presented in section 5.1 that discusses the impact of horizontal imposed wind.

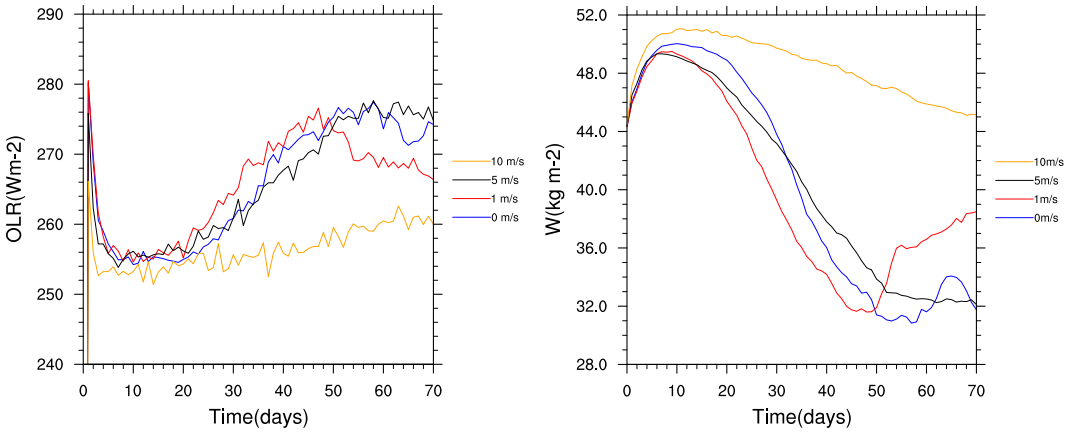

(a) (b)

Figure 2.5: Time series of domain average a) OLR b) TCWV value for experiments with horizontal imposed wind value of 0 ms^{-1}, 1 ms^{-1}, 5 ms^{-1} and 10 ms^{-1}.

2.3.2 TCWV

During the self-organisation process, a small dry patch at the beginning of the process expands as the organisation process matures and covers the majority of the domain. This can be an indicator of self-aggregation (Bretherton et al., 2005; Wing and Emanuel, 2014). Figure 2.5 b shows a comparison among domain average total column water vapor (TCWV) of the same experiments used for OLR. In this case also it is apparent to identify the experiments with higher/lower level of organisation. The system with higher level of organisation

gets drier while the experiment with low level of organisation doesn't show significant difference in TCWV during the evolution of the organisation (figure 2.5 b).

2.3.3 Organization index

The organisation index (I_{org}) method is based on a statistics of the nearest neighbor cumulative distribution function (NNCDF). If convection were randomly organized, and thus can be considered as a Poisson point process. The distribution function is given by Weibull distribution (Stoyan et al., 1987) as shown in equation 2.26. In this case, a stationary Poisson point process is considered as a possible model for cloud nearest neighbor distributions in a bounded region (Weger et al., 1992).

$$NNCDF_{ran} = 1 - exp(-\lambda\pi r^2). \tag{2.26}$$

Here λ is the number of points per unit area (a normalizing factor) and r is the nearest neighbor distance.

To apply the NNCDF distribution method to the model output, one should first identify the convective cores. We focus on the updraught cores since these cover a small fraction of the domain (Craig, 1996) and thus the contamination of the statistics by edge effects and merging are minimized (Weger et al., 1992). Convective columns are identified based on the vertical velocity at the level of 730 hPa (2680 m). If the vertical velocity at the given height is greater or equal to the threshold velocity of 1 m s^{-1} then it is considered as a convective core according to a widely used definition of convection updraft (e.g LeMone and Zipser, 1980; Robe and Emanuel, 1996).

Once the convective cores are identified then it is important to recursively trace each updraft element to find the centroid of each updraught. In other words, all adjacent updraught cells combined together to be considered as a single core (figure 2.6). This is important since it excludes a possible interactions among these convective cores. For each centroid, the nearest neighbor distance (NND) to the closest convective cores is then calculated, taking care to account for the periodic boundary conditions (figure 2.6)

After obtaining the PDF of NND, the cumulative density function is calculated as a function of NND and it is referred here as the simulated NNCDF

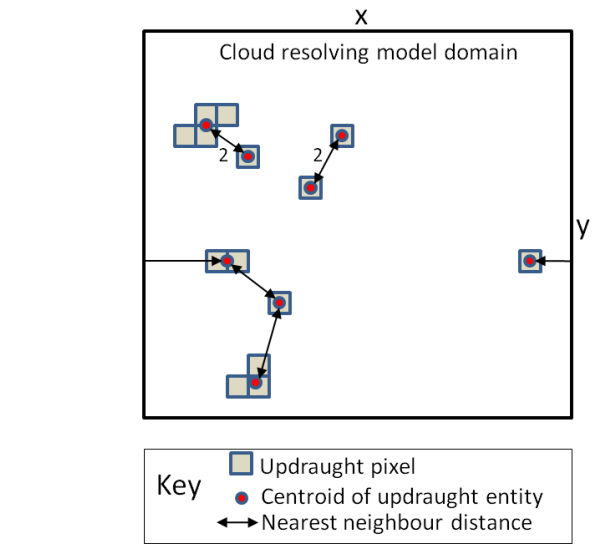

Figure 2.6: Centroid of each updraught, updraught pixel and nearest neighbor distance between two convective cores.

($NNCDF_{sim}$). The graph of simulated versus Poisson NNCDF can provide important information about the characteristics of the distribution (figure 2.7). The simulated NNCDF will increase faster for organized states since a system with clustered distribution will have more NN pairs for a given NND than expected for the Poisson distribution. As a result the $NNCDF_{sim}$ value is larger than the corresponding Poisson NNCDF. Thus the curve will be above the diagonal as shown in figure 2.7. On the other hand, a system with a regular distribution will have fewer NN pairs separated by a given distance than it would be expected by the Poisson NNCDF as a result the NNCDF curve lies below the diagonal. The $NNCDF_{sim}$ have the same value as Poisson NNCDF for the case of random distribution and the curve will lie on the diagonal.

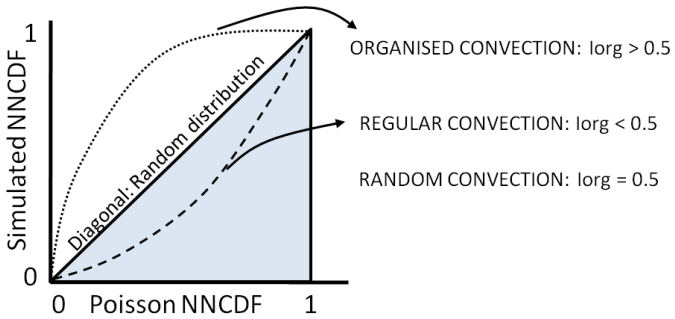

Figure 2.7: NNCDF curve for regular, random and clustered distributions.

In order to document the degree of clustering accurately, the area under

the graph of the $NNCDF_{sim}$ versus Poisson NNCDF is integrated. In this thesis, this integrated value is perceived as index of organization (I_{org}). The trapezoidal rule is used to approximately calculate the I_{org} value of the simulation. The NNCDF comparison for the possible distribution of updrafts is given in 2.7, which results in representation of regular, random and clustered hypothetical situations. The I_{org} value is calculated for each day of the simulation (control run), using velocity snapshots from each experiments, to observe the evolution of self-organisation during the simulation, as shown in figure 2.8.

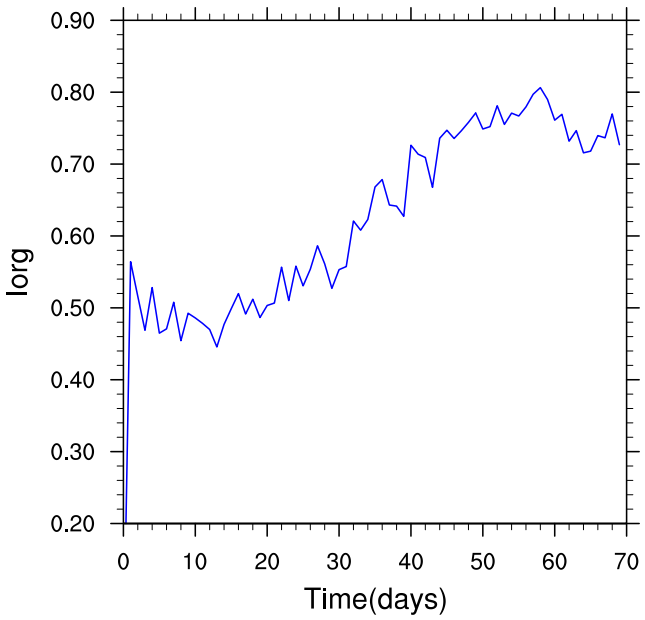

Figure 2.8: Time series of daily I_{org} values for the control experiment (detail discussion will be given in chapter 3).

In general, the method is applied to the whole simulation domain and thus measures the overall level of organisation as λ is calculated for the domain mean. It is also possible to calculate I_{org} for subregions of the domain which would allow one to document the degree of spatial organisation as a function of spatial scale. This would be an interesting additional step since the mutual inclusivity of certain processes may lead to convection being organized over mesoscale while the action of cold pools or shortwave feedback might generate regularity over smaller spatial scales.

2.3.4 Summary of diagnostics for organisation

All the diagnostics introduced in this section properly differentiate whether a given experiment has higher or lower level of organisation. However, the organisation metrics that use OLR and TCWV don't have a precise value for the extent of organisation. This value can be easily obtained from I_{org} to analyze the the level of clustering, randomness and regularity in convective field at equilibrium.

Chapter 3

Convective Organization

The main objective of this chapter is to investigate whether convective organisation occurs in the control experiment, where the summery of its model setup is given in table 2.2. This CRM is also used to identify the role of various physical mechanisms which are responsible for the self-organisation of convection.

3.1 Equilibrium state

Figure 3.1 presents the instantaneous snapshot of clouds, which is identified using the values of the mixing ratio of all liquid and ice phase precipitating and non-precipitating condensates. The isosurface values of these hydrometers greater than 0.15 g kg^{-1} is used to visualize the horizontal and vertical distribution of clouds in the simulation.

During day 10 the hydrometers are distributed all over the domain with cores of varying height (shallow and deep convection) (Fig. 3.1 a). This highlights the random distribution of convection during the initial stage of the simulation. Later on (day 70), the distribution of the condensates are restricted to a specific location of the domain and this marks the presence of a strong organisation (Fig. 3.1 b).

Significant variations in the distribution of hydrometeors, radiation and surface fluxes are observed inside the domain of self-organized systems (e.g Bretherton et al., 2005). These variations depend on the evolution time scale of self-organisation process. Fig. 3.2 shows the distribution of total column water vapor (TCWV) at different stages of the simulation. During the initial

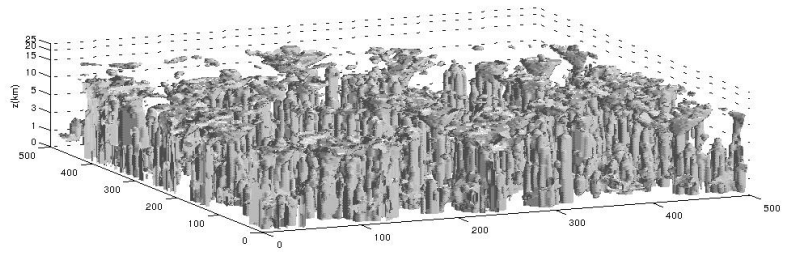

(a)

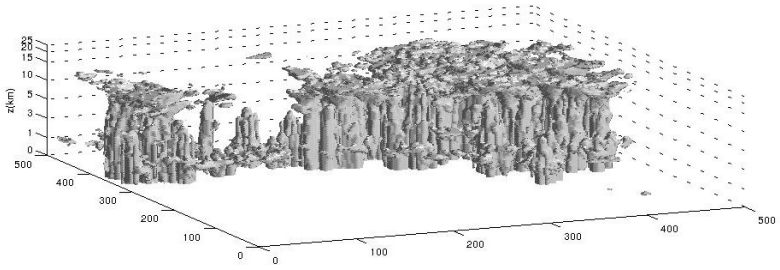

(b)

Figure 3.1: Isosurface values of hydrometers greater than 0.15 g kg^{-1} on a) day 10 and b) day 70 of the simulation.

period there is a small dry patch around 110 km and 40 km in the west-east and south-north directions respectively. This dry patch expands as the self-organisation process evolves in time and eventually confine the moist region into a band like structure. The expansion of the dry patch with the convection eventually restricted to a small region of the domain is also observed in a number of previous CRM simulations such as Held et al. (1993); Sui et al. (1994); Tompkins and Craig (1998a); Bretherton et al. (2005); Muller and Held (2012) and Wing and Emanuel (2014). However, the shape of the moist convective region can vary based on the choice of model and different model settings, as pointed out by Muller and Held (2012).

The domain is partitioned based on the TCWV values of the domain into four quartile regions (moistest, moist, dry and driest) which should reveal large differences in energy budget components because of the large differences within the domain of self-organized systems. For the discussion of the equilibrium state, the time series of TCWV and temperature field is used as shown in figure 3.3. The domain average TCWV value initially increase from 44 to 49 kg m^{-2} during the first 10 days then it slowly declines to 32 kg m^{-2} by day 50. It remains close to this value until the end of the simulation. However,

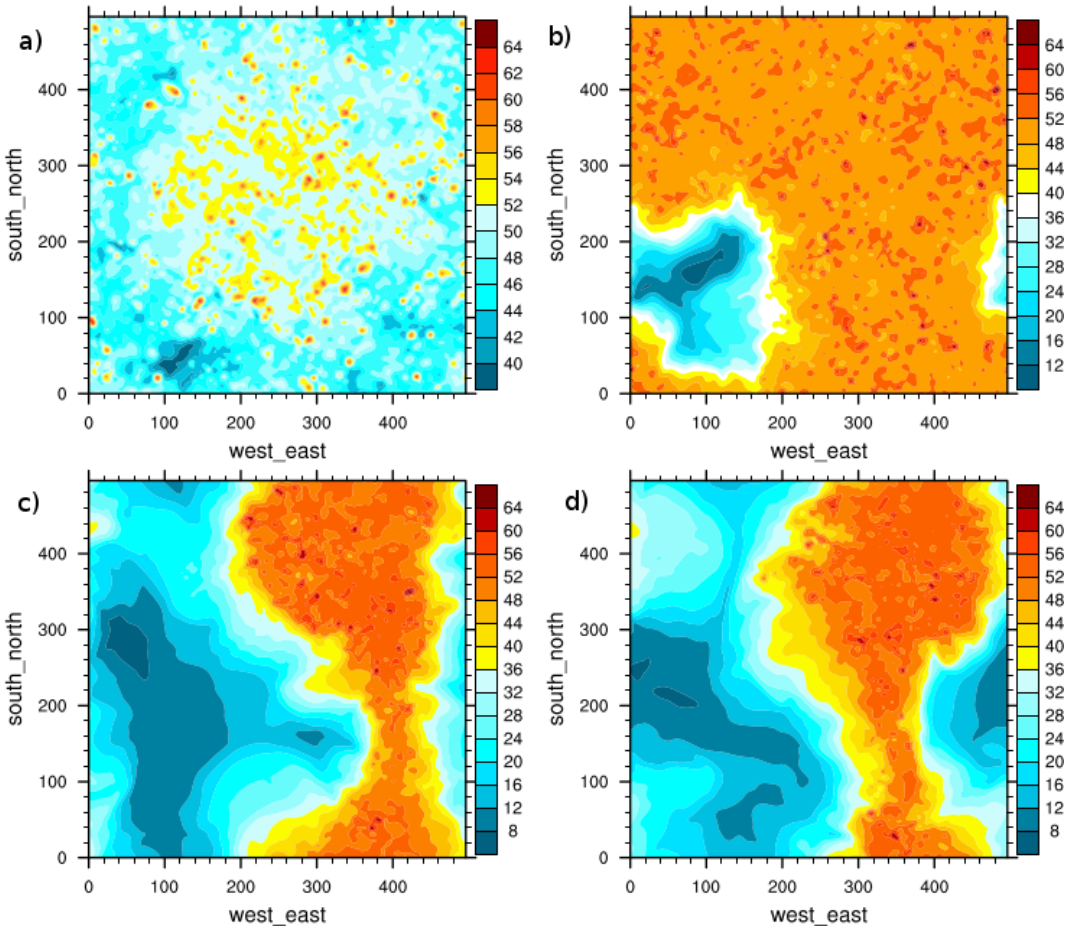

Figure 3.2: Column integrated water vapor values on day a) 5 b) 25 c) 50 and d) 70.

there is a large variation between the quartiles in terms of the adjustment to the respective equilibrium values. The moistest quartile reaches 52 kg m^{-2} during the first 4 days and then remains close to this value for the rest of the simulation of the control run, while the second moistest quartile takes more than 50 days to reach equilibrium (Fig. 3.3), since these regions are the last to be impacted by the growth of the dry patch. Similar observations that highlight the varying time scale between the quartiles are reported by Bretherton et al. (2005), in which they have used a square domain of 576 by 576 km and run their simulation for the duration of 100 days.

The main reason for the variation in adjustment time scale of TCWV is related to the organisation process. During the first 10 days the difference among the quartiles is small since the dry patch grows in a top-down manner, with the upper troposphere drying first (see also Tompkins and Craig, 1998b; Emanuel et al., 2014). The upper tropospheric dry anomalies have a limited

impact on convection through entrainment processes as humidity is limited there. After day 10, the driest part dramatically declines due to the impact of the initiation of the self-organisation process. At this point the dry anomaly has started to reach the lower troposphere and have an significant influence on suppressing convection (this entrainment mechanism will be investigated in further detail in chapter 4). This is also clearly visible in the domain average TCWV values (Fig. 3.3).

The variation in domain average temperature value is limited to less than 0.7 K which shows that the initial state is close to the model equilibrium value. The differences between quartiles are small since the horizontal atmospheric virtual temperature gradient is removed by gravity wave propagation over relatively fast time scales, leading to a weak horizontal temperature gradient (e.g Bretherton and Smolarkiewicz, 1989; Sobel et al., 2001). The dry bulb temperature variations between the quartiles (Fig. 3.3) at around 0.7 K is due to the moisture gradients. Thus the moistest regions are cooler to offset the virtual temperature effect of the humidity (Fig. 3.3).

3.2 Vertical profile of the equilibrium state

3.2.1 Skew-T

To examine the vertical profile, a skew-T diagram of a five day domain average thermodynamic variables of the moist and dry regions is considered. All the variables are sorted by the TCWV value and the first and last 25% (quartiles) of these values are binned together and taken as driest and moistest part of the domain respectively.

The skew-T plot of the driest quartile for average values of days 5 to 9 is shown in figure 3.4 a. The lifting condensation level (LCL) temperature and pressure are 21 C and 934 hPa respectively, but these values change to 14 C and 858 hPa on the last period of the simulation. The showalter index is an index used to assess 850 hPa parcel instability/stability, and indicates the driest quartile in the early stage to be marginally instable while stable conditions are observed in the later stages of the simulation.

Convective available potential energy (CAPE) is a measure of the energy

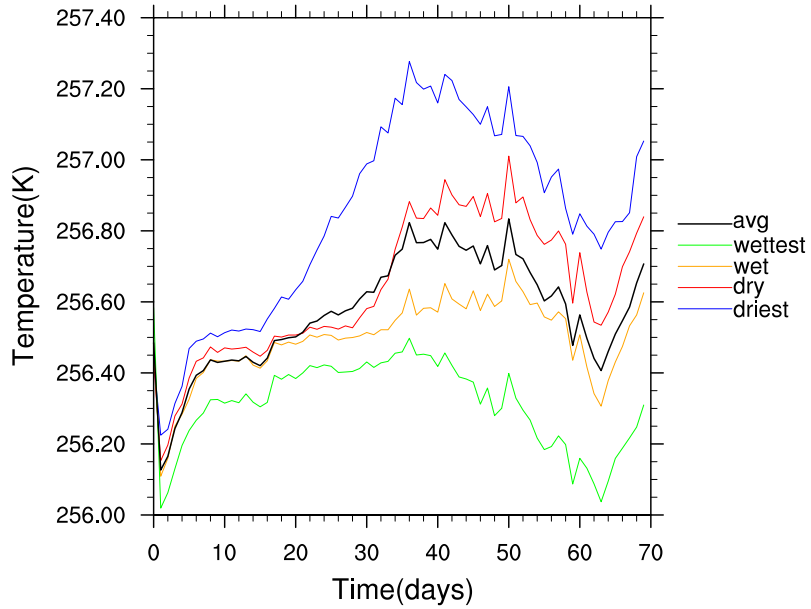

(a)

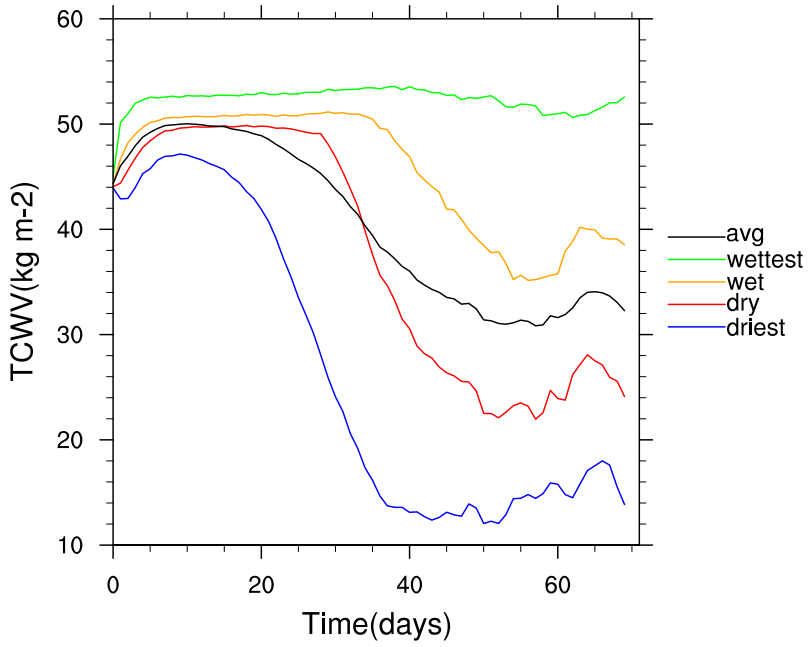

(b)

Figure 3.3: Time series of domain average a) Temperature and b) TCWV for the entire integration. The black lines are domain means and the other curves are means of sub domain region sorted into four quartiles on the basis of their daily mean of column integrated water vapor content.

available to an ascending parcel:

$$CAPE_p = g \int_i^{LNB} (\frac{T_u - T_{env}}{T_{env}}) dz, \tag{3.1}$$

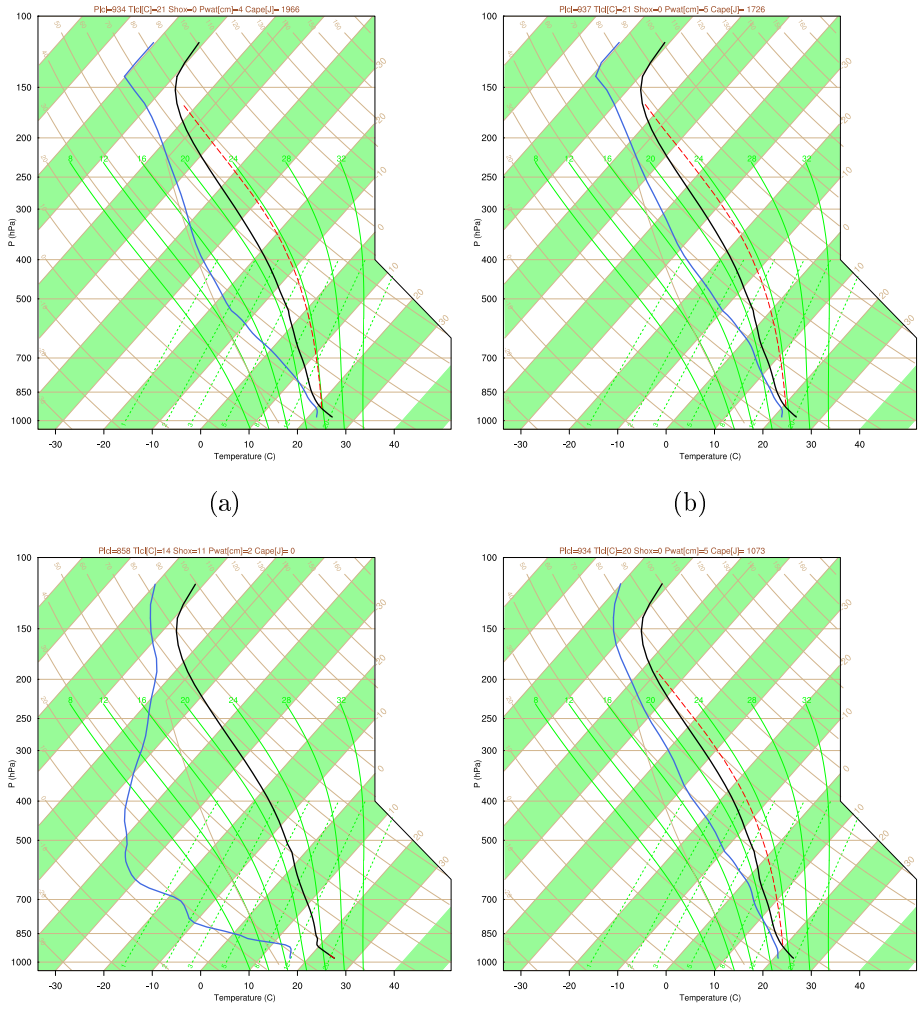

Figure 3.4: Skew-T diagram of a five day domain average of a) 25% of driest part(days 5-9) b) 25% of wettest part(days 5-9) c) 25% of driest part(days 65-69) b) 25% of wettest part(days 65-69).

where $CAPE_p$ is convective available potential energy at pressure level p, T_u is updraft parcel temperature, T_{env} environmental temperature, integrated from certain level (i) up to level of neutral buoyancy (LNB). CAPE is zero by the end of the simulation (day 65 to 69) in the driest region. The contrast between the initial and final stage of thermodynamic values in the driest region is significant, marking the intensification of the dry region due to self-aggregation processes.

There is a minor difference in the moistest region between the initial and final stage of the simulation as shown in figure 3.4 b and d. This is consistent

to the wettest total column water vapor value (figure 3.3 b), which indicates a small variation throughout the simulation. The skew-T plots underscore the remarkable effect of organisation of convection on the vertical distribution of moisture and temperature.

3.2.2 Moisture, vertical motion and cloud profiles

The effect of self-organisation is also found to modulate the vertical structure of relative humidity, vertical motion, mixing ratio of rain and cloud water. These values are binned into four quartiles based on TCWV values on day 5 and 70 that represent the initial and final stage of the simulation respectively.

The moistest quartile on day 5 has a higher relative humidity (RH) than the domain average above the boundary layer (Fig. 3.5). The interplay of cumulus clouds with environmental humidity can be the cause for this variation in vertical structure (Bretherton et al., 2005). This difference is quite extreme by day 70, as the two driest quartiles have less than 20% RH throughout much of the free troposphere while the moistest quartile has more than 80% in the mid-troposphere as shown in figure 3.6. Examples of such extremely dry atmospheric columns were also observed over the Pacific Ocean during the Tropical Ocean Global Atmosphere Coupled Ocean-Atmosphere Response Experiment (TOGA COARE) by Mapes and Zuidema (1996), and are thus not necessary unrealistic in terms of the dry anomaly magnitude. The domain average RH decreases as the organisation progresses.

A similar behaviour is observed for the mass weighted vertical velocity where the top heavy vertical structure of moistest quartile is obvious by day 70 relative to day 5. In both periods the domain average value is zero by construction due to the periodic boundary conditions. The vertical structure of mixing ratio of rain and cloud disappear in the dry quartiles during the last period of the simulation. This is also an impact of self-organisation that intensifies/suppresses precipitation and deep clouds in the moistest/driest quartile due to a vigorous/weak convective activity in the corresponding moist quartiles (Fig. 3.6). The observed strong relation of deep convection (cloud) and humidity is the main characteristic of tropical regions where convective activity is the main source of moisture in the free troposphere (Grabowski and Moncrieff, 2004), and dry tropospheres may suppress convective activity (Maloney and

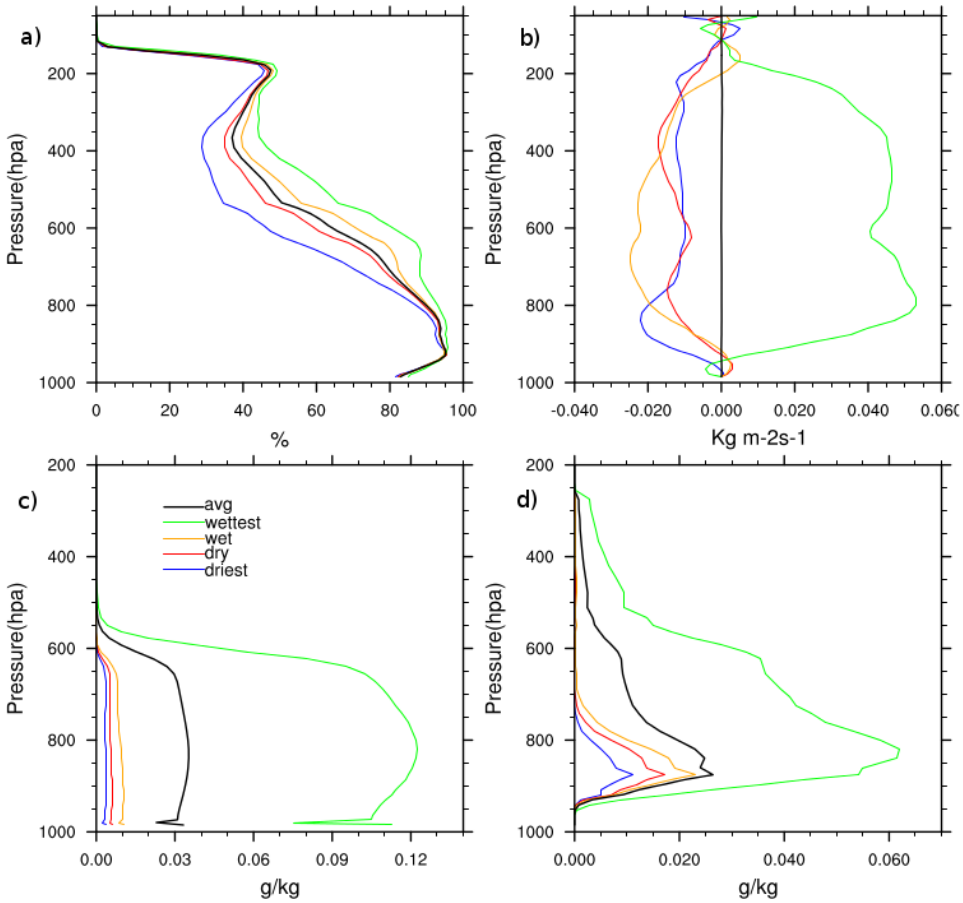

Figure 3.5: Vertical profile of 5 day (65-69) average value of a) Relative humidity b) Mass weighted vertical velocity c) Rain water mixing ratio d) Cloud water mixing ratio.

Hartmann, 1998; Derbyshire et al., 2004).

3.3 Organization process in equilibrium state

In this section the evolution of self organisation is analyzed using the frozen moist static energy (h_f) budget as used by Bretherton et al. (2005) and Muller and Held (2012). It is a useful thermodynamic variable which is conserved during phase change and is thus not affected by convection processes. Hence, h_f is conserved during moist adiabatic process including the freezing and melting of precipitation as shown in equation 3.2. Moreover, the correlations terms of feedbacks due to diabatic processes as in Wing and Emanuel (2014) is used to identify the mechanisms that are responsible for positive/negative feedbacks

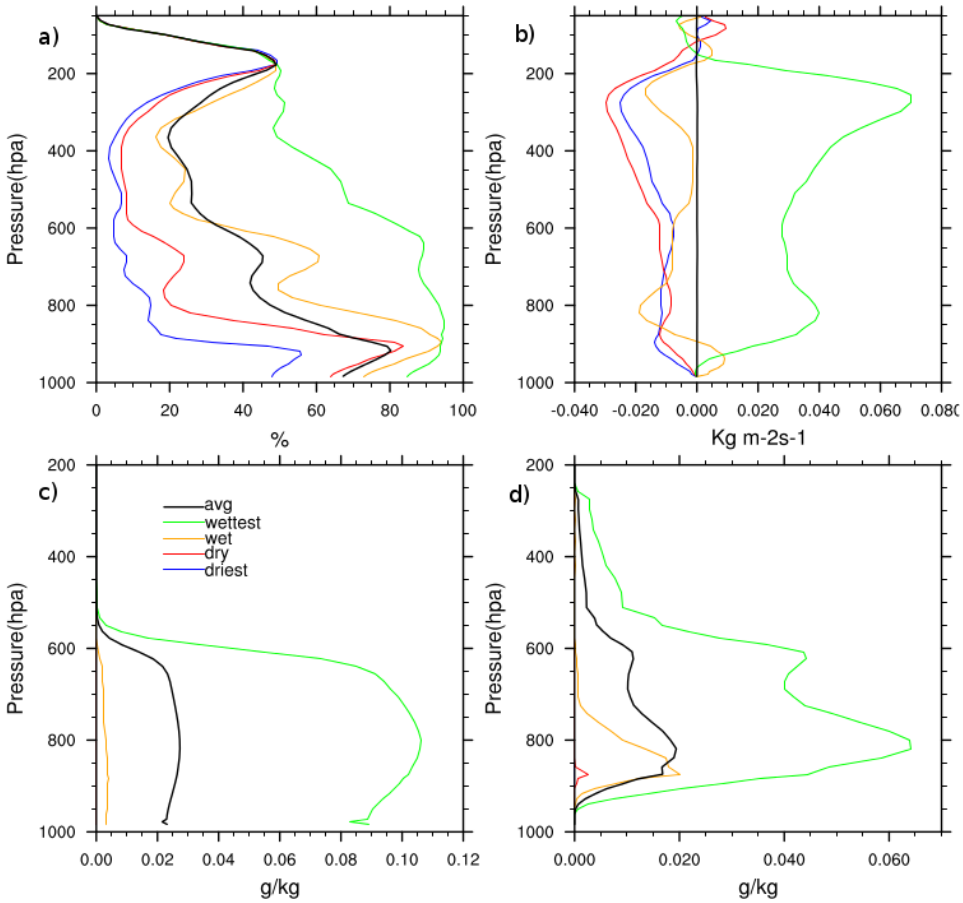

Figure 3.6: Vertical profile of 5 day (65-69) average value of a) Relative humidity b) Mass weighted vertical velocity c) Rain water mixing ratio d) Cloud water mixing ratio.

to the organisation process.

$$h_f = c_p T + gz + L_v q_v - L_f q_i \tag{3.2}$$

where h_f is the frozen moist static energy, c_p is isobaric specific heat of dry air, T is temperature, g is gravitational acceleration, L_v is latent heat of vaporization, q_v is water vapor mixing ratio, L_f is latent heat of fusion and q_i is ice phase condensate.

3.3.1 Evolution to self organisation state

Although this control experiment is initialized by introducing a significant positive perturbation of moisture and temperature at the domain center, an evenly distributed temperature and moisture field with convective grid points distributed throughout the domain are observed by day 5. Self-organisation is

not apparent in the field of vertical velocity, outgoing longwave radiation(OLR) and total heat fluxes during the initial period (Fig. 3.7). However, the vertical velocity at the level of 730 hPa, which serves as a proxy for locating deep convective towers, reveals a small fraction of the domain is free from convection centered at x = 150 km and y = 60 km. This same location exhibits enhanced top of atmosphere (TOA) OLR values and depressed water vapor values. This indicates the location of the small dry patch in the early stage of the self-organisation process. The values of latent and sensible heat fluxes are found to be small and distributed non-uniformly as shown in figure 3.8 a and b, with enhanced values near convection due to the action of cold pools (raise air-sea differences and enhanced gustiness).

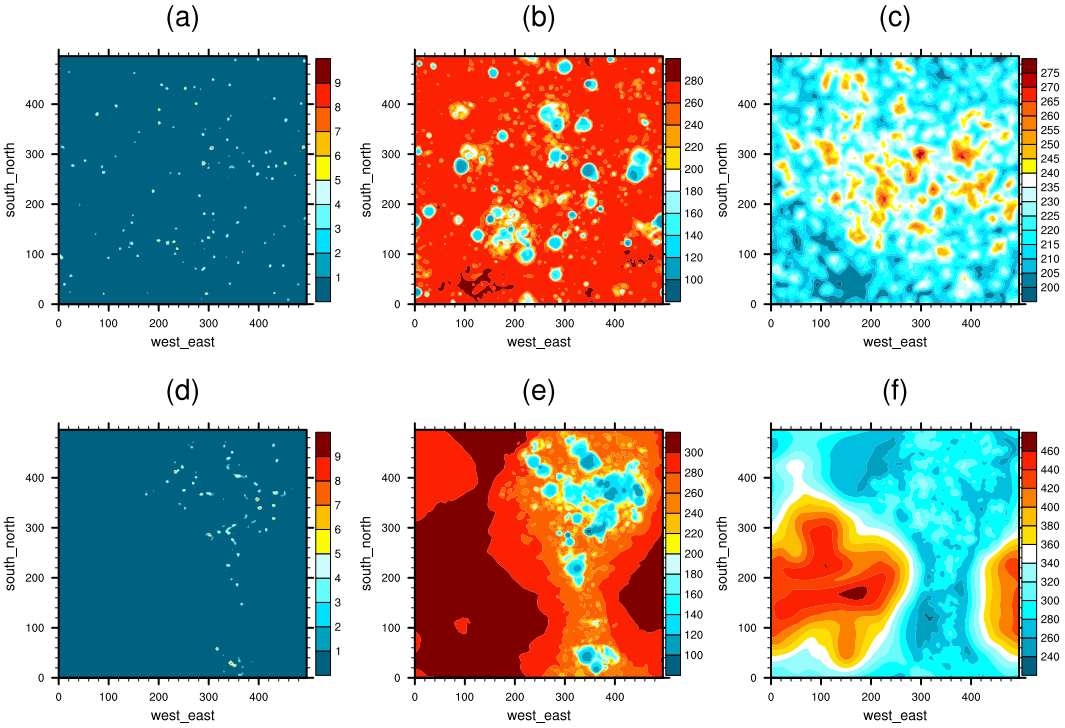

Figure 3.7: a) Vertical velocity at the level of 730 hPa (day 5) b) outgoing long wave radiation (day 5) c) total surface heat flux (day 5) d) Vertical velocity at the level of 730 hPa (day 70) e) outgoing long wave radiation (day 70) f) total surface heat flux (day 70) in the control run.

Eventually, these fluxes become well structured as self-organisation matures and this is clearly visible in figure 3.7 f. During this period, there is a higher moisture gradient between the surface and the atmosphere in the dry zone. This enhances the latent heat fluxes in this region as shown in figure 3.8 d.

The opposite is true for sensible heat fluxes as shown in 3.8 c. These fluxes are enhanced in the convective regions due to the cold pools that increases the temperature gradient. They are depressed in dry region as a result of strong subsidence warming.

The small dry patch continues to expand and confine the moist region into a small band as the self-organisation process evolves. By day 70 the driest region is so dry that all convection is suppressed in figure 3.7 d and e. On the contrary, the moist part gets progressively moister and an enhancement of convection is observed during the last period of the simulation (day 70). An Enhancement of OLR values on the dry and cloud free region is clearly visible while a decrease in convective region is indicated due to deep cumulus anvil cloud that can limit outgoing infrared radiation.

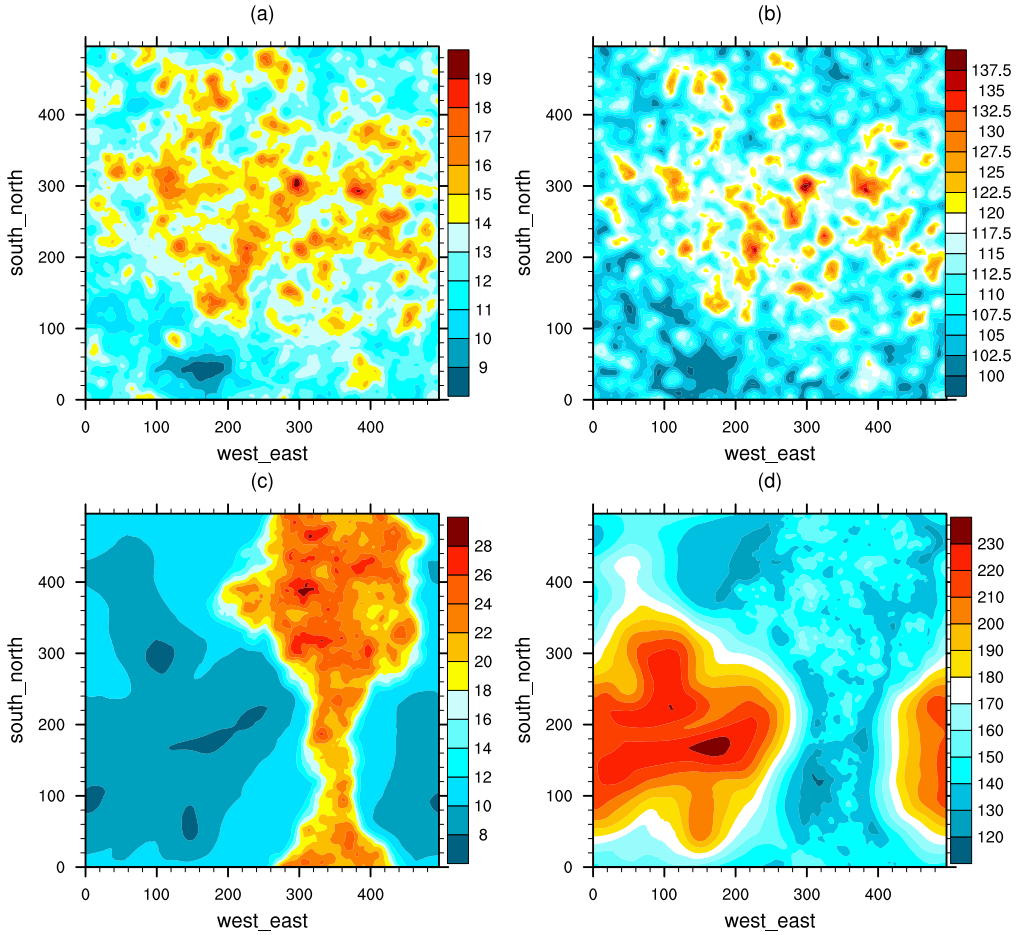

Figure 3.8: a) Sensible heat flux (day 5) b) latent heat flux (day 5) c) Sensible heat flux (day 70) d) latent heat flux (day 70) in the control run.

Model variables such as OLR, TCWV and others can be useful in iden-

tifying the location and organisation of convection. The organisation index method introduced earlier provides further information about the model's evolution towards an organized state. For the first 3 weeks of the simulation the I_{org} is not significantly different from 0.5 (2-tail student T-test) indicating randomly organised convection. Around day 20, the index starts to increase, indicating the onset of organisation. Thus the diagnostic indicates the control experiment starts to transform from random to a clustered spatial distribution of convection around day 20 of the simulation (Fig. 3.9). The organisation index increases approximately linearly over a period off 20 days to reach a new equilibrium around day 40-45, with a value of 0.8 indicating strongly organized convection. Temporal random fluctuations are also apparent as expected due to sampling and the stochastic nature of convection (Plant and Craig, 2008). The S-shaped adjustment curve of I_{org} is partly an artifact of the method being used in a domain with doubly periodic boundary conditions. These enforce a maximum separation between the convective towers to be $\frac{D}{\sqrt{2}}$, where D is the size of the square domain. Thus even though figure 3.7 and 3.8 show dry patch formation and growth starting from the beginning of the integration, it is not detectable by I_{org} until dry patch grows sufficiently to start to cluster convection at the scale below $\frac{D}{\sqrt{2}}$. Once organisation is established it appears robust since the existence of past clouds affects the location and mesoscale spatial arrangement of future clouds, as it is observed by Houze et al. (1981) for the case of cloud distribution in the inter-tropical convergence zone. Similarly the organisation index diagnostic shows the pattern of the initial, intermediate and matured states of cloud distribution for the control experiment.

3.3.2 Time series of diabatic forces

The time series of the atmospheric diabatic flux convergence are shown in figure 3.10 and 3.11 to examine their evolution during the organisational onset. The net shortwave and longwave radiation is obtained by taking the difference between the top of atmosphere (TOA) and surface radiative fluxes. All fluxes are partitioned into four quartiles based on TCWV values. The fluxes confirm the pattern observed with the organisation index in that the quartiles have similar values for the first 15 to 20 days. After the first ten days of simulation the infrared values of the driest quartile start to increase and are doubled by

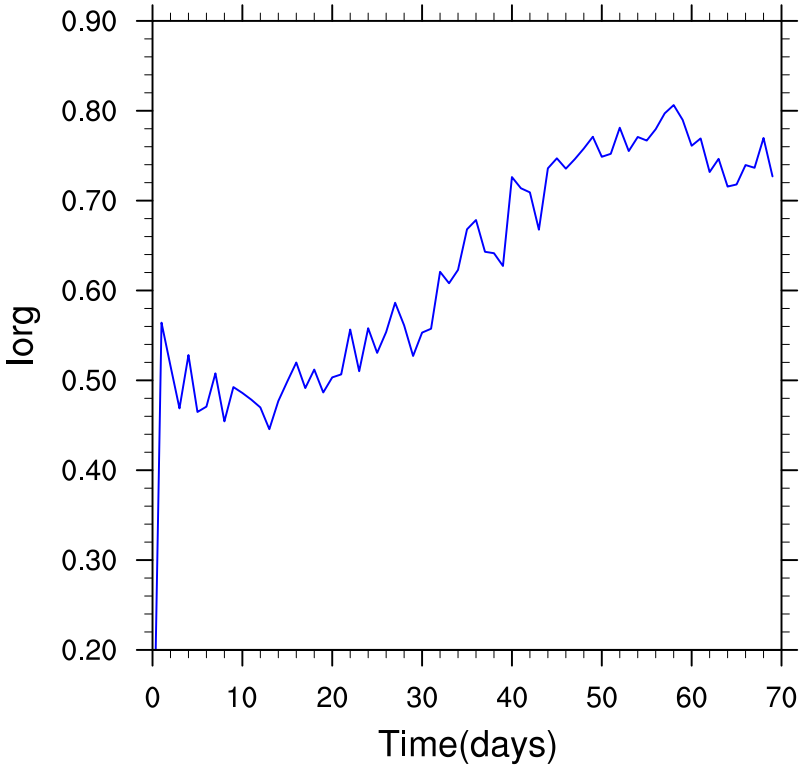

Figure 3.9: Time series of daily I_{org} value in the control run.

day 36 as organisation establishes (Fig. 3.10 a). After this period the driest quartile remains close to the values of 120 W m^{-2} at the surface until the end of the simulation. However, there are limited fluctuations (2 W m^{-2}) of surface longwave radiation value in the wettest quartile throughout the simulation period (Fig. 3.10). The observed adjustment time scale for the driest and wettest quartiles are directly related to corresponding TCWV quartiles as shown in figure 3.3 b.

To describe the relationship between the emitted longwave radiation from the surface and the amount of TCWV in different parts of the quartiles, a simple one layer representation of infrared radiation flux is considered in which the surface emits as a black body over which a given atmosphere lies:

$$LW_s = \sigma T_s^4 - \varepsilon \sigma T_a^4, \tag{3.3}$$

where LW_s longwave radiation at the surface, σ Stefan-Boltzmann constant, T_s is surface temperature, ε the emissivity of the atmosphere and T_a is atmosphere temperature.

The control experiment has fixed SST and assume a weak horizontal temperature gradient, thus the surface temperature doesn't contribute to the varia-

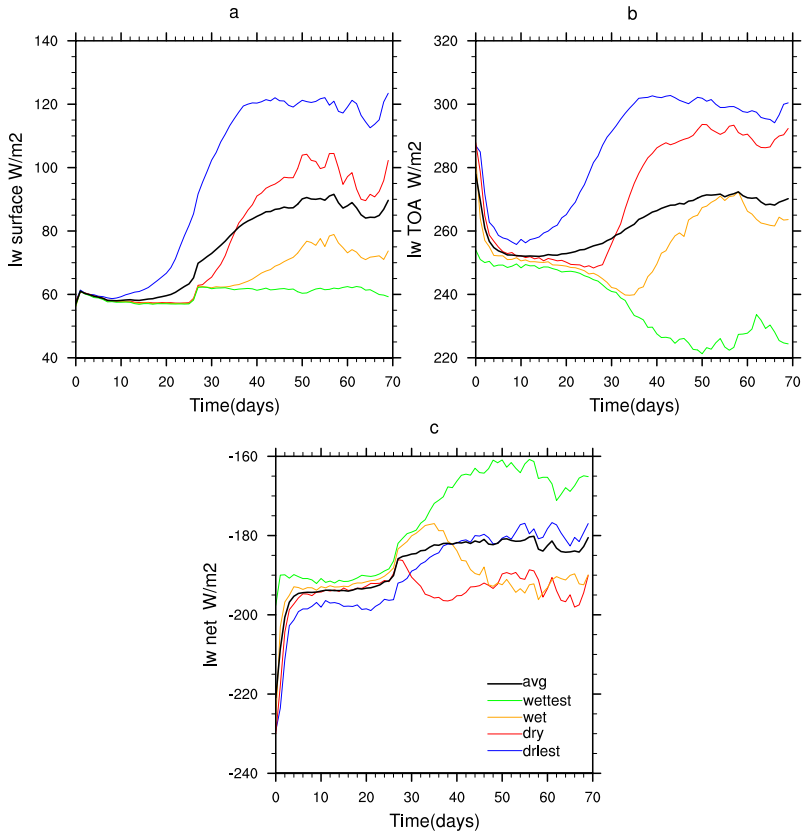

Figure 3.10: Time series of a) longwave radiation at the surface b) longwave radiation at TOA c) net longwave (surface minus TOA) radiation in the atmospheric column for domain average and 4 quartiles.

tion in the longwave radiation budget. Hence the values of longwave emissivity, that in turn depends on the moisture content of the atmosphere, is mainly responsible for the variation in surface longwave energy budget in dry and moist regions. This implies that in this control experiment the longwave emissivity in the dry region is reduced relative to the moist part of the domain. This can also explain why the intermediate dry and wet quartiles also follow their corresponding TCWV value for the relative increase in the amount of the longwave radiation at surface as the self-organisation matures.

The outgoing longwave radiation at TOA partitioned into quartiles based on TCWV is presented in figure 3.10 b. The amount of longwave radiation released at TOA from the moistest quartile is much smaller (by about 75 W m^{-2}) than the driest quartile after the self-organisation matures. As a result, the moistest quartile is characterized by higher value of net longwave radiation in the column (Fig. 3.10 c). This effect can be related to the absorption of

infrared radiation by the green house gases (e.g Weaver et al., 1994; Bony et al., 1997).

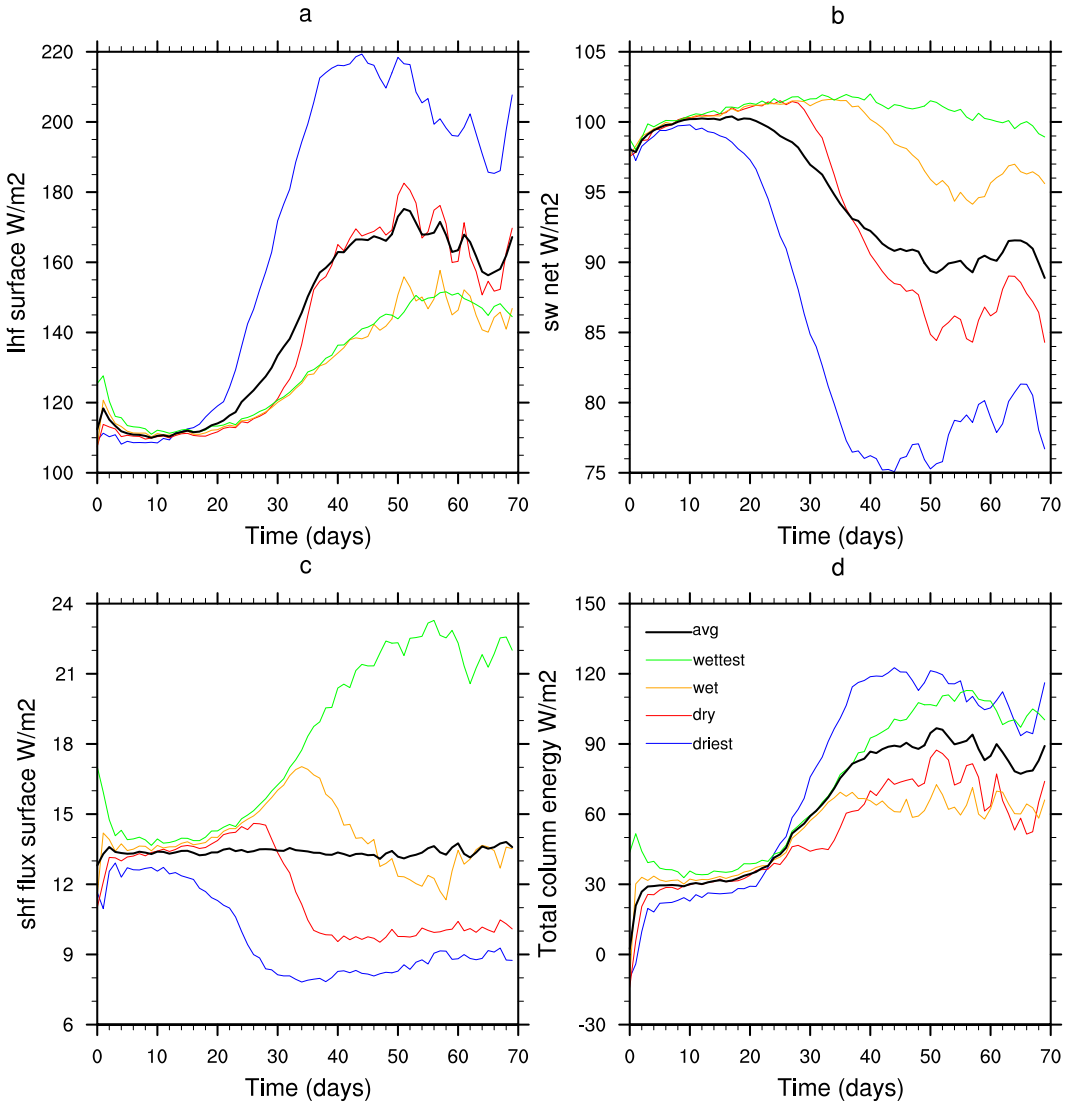

Figure 3.11: Time series of a) latent heat flux at the surface b) net shortwave (TOA minus surface) radiation in the atmospheric column c) sensible heat flux at surface and d) net total energy in the atmospheric column for domain average and 4 quartiles

.

Similarly, shortwave radiation flux in the atmospheric column is considered in figure 3.11b for the domain partitioned into the four quartiles. The moistest quartile of the shortwave radiation has a small variation (around 3 W m^{-2}) throughout the simulation similar to the evolution of the corresponding quartile's TCWV values (Fig. 3.3 b). However, a slight decreasing trend in the shortwave radiation is observed as the organisation intensifies due to the

radiative effects associated with clouds; anvil cirrus clouds in particular. The absorbed shortwave radiation of the driest quartile instead declines sharply in the same way as the corresponding TCWV trends. Similarly, the intermediate quartiles show a decreasing trend in the column shortwave radiation, in association with the decreasing column moisture. This highlights the critical role of water vapor in dictating the amount of absorbed radiation (shortwave and longwave) in the atmosphere (e.g Wing and Emanuel, 2014).

Figure 3.11a presents the daily quartile average value of latent heat heat flux from the surface. As already pointed out, the sensible surface heat flux is dominated by latent heat flux over the ocean surfaces. It is shown that the latent heat flux increases dramatically as the atmosphere gets drier (Fig. 3.11 a). This is the reason for not observing a significant difference between the quartiles until the organisation process intensifies. For instance, the latent heat of the driest quartile increases substantially after day 16 due to an increasing difference between the saturated surface and the humidity of the boundary layer air.

The sensible heat flux from the surface is found to decrease in the driest zone due to the influence of subsidence after the onset of self-aggregation (Fig. 3.11 c). In contrast, there is enhancement of the sensible heat flux in the moistest quartile. This is caused by the effect of cold pools and convective gustiness, which are a key positive mechanisms for self-organisation processes (e.g Tompkins, 2001b; Bretherton et al., 2005). The sensible heat flux is smaller by an order of magnitude when it compares to latent heat flux. As a result the effect of sensible heat flux is barely discernible when one considers the contribution of total heat flux from the surface.

Figure 3.11d shows the total amount of absorbed energy in the atmospheric column. The driest and moistest quartiles have reached to similar value (around 110 W m^{-2}) as the organisation process matures. The reason for higher values in the driest quartile is because of large contribution of latent heat flux from the surface, while in the moistest quartile there is increasing absorption of the radiations as the organisation process intensifies. All the calculations of net energy in the atmospheric column highlight how the incoming and outgoing energy from the surface and the sun can be modulated by the organisation process, in the meantime these diabatic processes have significant positive or negative feedback to the self-aggregation process.

3.3.3 Frozen moist static energy budget

The mass weighted vertically integrated h_f is identified as an important diagnostic to study the roles of varies mechanisms in the self organisation of convection (Bretherton et al., 2005; Muller and Held, 2012; Wing and Emanuel, 2014). The temporal rate of change of this value depends only on advection and diabatic heating processes of surface fluxes and radiation as shown in equation 3.4, while convection does not affect its mass weighted vertical integral:

$$\frac{d}{dt}\int h_f = THF + NetSW + NetLW + C_{hf} \tag{3.4}$$

where the $\int h_f$ is mass weighted integral of equation 3.4, THF is sum of latent heat flux and sensible heat flux, $NetSW$ is column shortwave radiative flux convergence, $NetLW$ is column longwave radiative flux convergence and C_{hf} is vertically integrated horizontal convergence of h_f.

The adiabatic term C_{hf} is calculated as a residual term by taking the difference between $\frac{d}{dt}\int h_f$ and diabatic terms of equation 3.4 (Bretherton et al., 2005; Muller and Held, 2012; Wing and Emanuel, 2014). The h_f budget is used to identify the dominant mechanisms in the evolution of the system to self organisation. It has already been shown how diabatic and adiabatic processes set up the large scale gradient in total column water vapor during the evolution to the organized state. To quantify their respective role on different stage of the evolution, a comparison of the various terms of h_f budget of equation 3.4 as a function of h_f tendency term is shown in figure 3.12.

Figure 3.12 shows various terms of moist static budget in different stages of the simulation. This includes the total diabatic term (the sum of surface and radiation fluxes), the advective term (C_{hf}) and the storage term ($\frac{d}{dt}\int h_f$). The y-axis indicates the variation from the domain average of these terms and they are sorted based on the system's TCWV values (x-axis).

During the early period of the simulation (Days 5-9, figure 3.12a), the advective term shows a downgradient horizontal transport of h_f from high energy columns to low energy columns as observed by Muller and Held (2012) for the case of unorganized convection. It indicates the advective term is not contributing positively for the self-aggregation process at this period. On the other hand, the total diabatic term is a positive feedback in most of the columns. This shows more cooling from dry regions and warming in moist

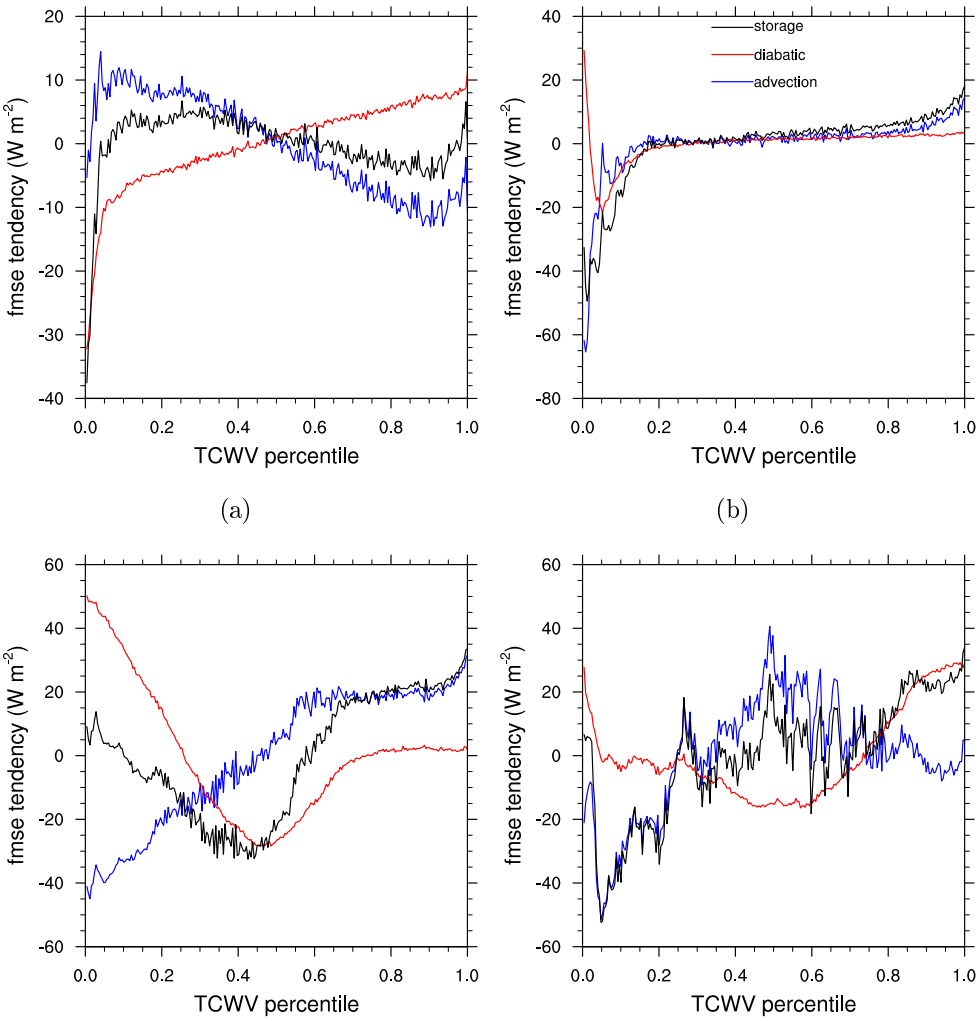

Figure 3.12: Five day mean values of h_f tendency terms of both adiabatic(advection) and diabatic processes (total heat flux, net column convergence of longwave and shortwave flux) plotted as departure from domain averages a) average h_f budget of day 5-9 b) average h_f budget of day 15-19 c) average h_f budget of day 35-39 d) average h_f budget of day 65-69 . All these values are binned together and sorted based on column integrated water vapor content.

regions. A detail discussion of diabatic feedback will be presented in the next section.

During day 15 to 19 (3.12 b), a small portion of the domain (8% of the driest region) horizontally transports h_f from low energy to high energy columns which results a decrease in moist static energy in the dry region. This upgradient transport of energy represents a positive feedback that will lead to self-

organisation. The contribution of the advective term to the self-organisation process intensifies during day 35 to 39 (3.12c). This is consistent with Bretherton et al. (2005); Muller and Held (2012), who also found a positive feedback to the self-aggregation process when there is an upgradient horizontal transport of moist static energy. On the other hand, spatial fluctuations in the advection term lead to changes in storage term during the last stage of the simulation (day 65-69). As a result positive and negative feedback to the self-organisation process appears interchangeably throughout the domain.

Note that care has to be taken when interpreting these plots due to the fact that columns are constantly changing their water vapour and thus the TCWV to which they are allocated during the experiment. For example, one might expect to diagnose a balance between the terms during day 65-69 as the experiment has reached quasi-equilibrium by this point. But the imbalance in, for example, the very driest bin implies that the columns in this bin are becoming moister and thus on subsequent time steps are replaced by other columns undergoing a drying tendency. In other words, there is no temporal coherency in the columns contributing the statistics of each bin and no equilibrium can be expected. This is also true for the Hovmuller plots that will be shown in the subsequent section.

3.3.4 Diabatic feedback

A powerful diagnostic method that was first introduced by Wing and Emanuel (2014) is used to quantify the role of diabatic feedback on the self-organisation process. This method calculates the correlation values for each diabatic terms based on their relation with the anomaly of the mass-weighted vertical integral of h_f:

$$\int h_f^{'} \frac{d}{dt} \int h_f^{'} = \int h_f^{'} THF' + \int h_f^{'} NetSW' + \int h_f^{'} NetLW' + \int h_f^{'} C_{hf} \quad (3.5)$$

where $\int h_f^{'}$ is anomaly of the density weighted vertical integral of h_f, $\int h_f^{'} THF'$, $\int h_f^{'} NetSW'$, $\int h_f^{'} NetLW'$ and $\int h_f^{'} C_{hf}$ represent the correlations of total heat flux, column shortwave convergence, infrared convergence and horizontal divergence of the density weighted vertical integral of h_f respectively with the variance of the density weighted vertical integral of h_f.

As self-organisation is associated with an increase in the variance of vertically integrated h_f, all processes that increase the variance favor self-aggregation. These correlation terms are obtained by taking the anomaly from domain average of all the terms in equation 3.4 and multiply them by anomaly of vertically integrated h_f as shown in equation 3.5. If the correlation term in equation 3.5 is positive, there is either an anomalous source of h_f in a region of already high h_f or anomalous sink of h_f in a region of low h_f. Both of these processes are considered to be a positive feedback for self-organisation process (Wing and Emanuel, 2014). Note that the implicit assumption of this analysis is that convection occurs preferentially in areas of high h_f. While this is generally the case, the analysis does not consider how the vertical distribution of the h_f tendencies affect the atmospheric moist static stability. For example, a cold anomaly in the planetary boundary layer will likely have a dramatically different impact on convective activity and the mesoscale circulation than the equivalent (in h_f terms) cold perturbation in the upper troposphere.

The Hovmuller plot of the sum of all diabatic correlation terms is shown in figure 3.13 in moisture-time space. For each day, all the diabatic correlation terms are normalized by domain average of the vertically integrated h_f variance and also the color bar in figure 3.13 and 3.14 is limited to the range of -$5e^{-6}$ day^{-1}and $5e^{-6}$ day^{-1} to make interpretation easier.

Figure 3.13 is partitioned (marked by a solid line) into two by a zero anomaly value of density weighted vertical integral of h_f ($\int h_f^{'} = 0$). There are negative and positive values to the left and right side of this line, respectively. For example, if the anomaly of a certain diabatic term is positive and found on the left side of the figure, it will be considered as negative feedback. Figure 3.13 indicates the correlation terms to be positive during the first 12 days except in small regions close to the zero contour ($\int h_f^{'}$) line. The net effect of the diabatic terms play a significant role for the onset of self-aggregation both in dry and moist regions.

After day 12, the correlation field is classified into four regions. This shows that the diabatic terms are acting as a relative sink (recall that tendency perturbations are examined) of h_f at intermediate ranges of h_f, but as a source for the regions of lowest and highest h_f. Thus the gradients of h_f are reduced by these processes for the driest regions, homogenizing the water vapor, but gradients are enhanced for the moister regions, a positive feedback on convec-

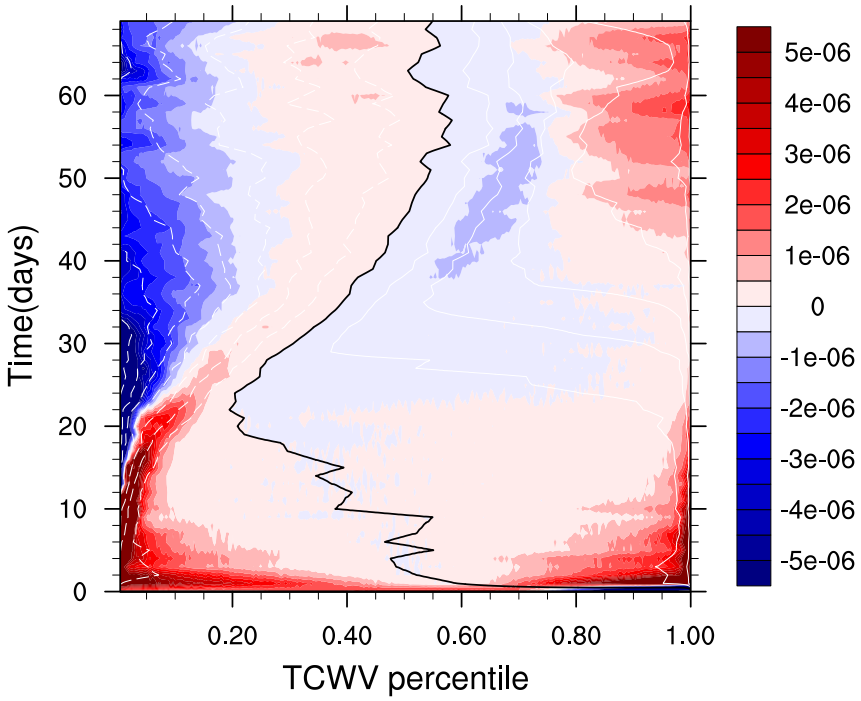

Figure 3.13: The sum of all diabatic correlation values plotted as function of moisture versus time, where the correlation terms are sorted based on the values of total column water vapor. The solid line indicates the zero anomaly value of density weighted vertical integral of h_f ($\int h_f' = 0$), where values on the left and right side of this line have a negative and positive $\int h_f'$ values, respectively.

tive organisation, assuming the convection is occurring in the moistest regions. The figure highlights the existence of competing mechanisms of positive and negative feedbacks during different stages of the organisation process. This behavior is already observed in the analysis of the relative contribution of diabatic and adiabatic terms using h_f budget (shown in figure 3.12). This section takes the discussion further by considering the continuous feedback evolution of diabatic mechanisms and their components as shown in figure 3.13 and 3.14.

Figure 3.14 (a) and (d) show a decomposition of diabatic terms into the radiation and surface flux feedbacks respectively. The radiation feedback has a positive correlation values in almost all part of the domain except some small regions on the left side of the zero contour ($\int h_f'$) for the first 20 days and this shifts to the right side of the zero contour until the end of the simulation. The total surface flux feedback has positive value for almost all part of the domain for the first 10 days. Thereafter, the leftmost and the majority of the right side of the zero contour regions indicate negative correlation values. During

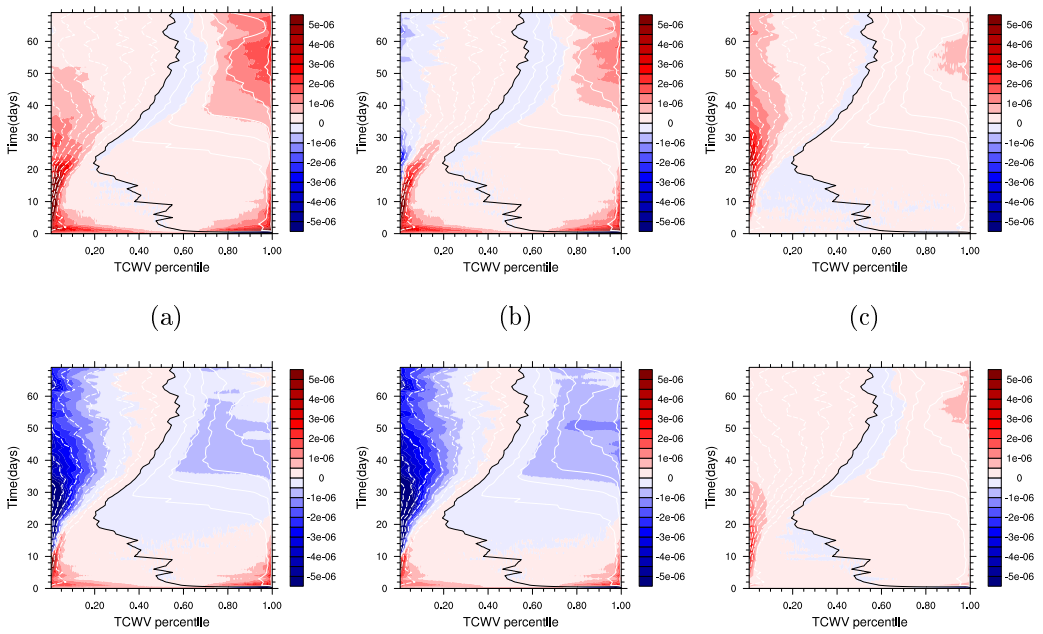

Figure 3.14: Correlation values of a) radiation b) longwave c) shortwave d) surface flux e) latent heat flux and f) sensible heat flux plotted as function of moisture versus time, where the correlation terms are sorted based on the values of total column water vapor. The solid line indicates the zero anomaly value of density weighted vertical integral of h_f ($\int h_f^{'} = 0$), where values on the left and right side of this line have a negative and positive $\int h_f^{'}$ values respective.

the last twelve days of the simulation, positive correlation are found for the surface flux at the right top corner of moisture-time field.

Comparing the radiation and surface flux feedbacks with the total diabatic correlation values provides information on the dominant mechanisms during specific stages of the simulation. For instance, the observed positive correlations for the first 12 days are also reflected in both radiation and surface flux feedbacks. However, the surface flux feedback starts to have negative correlation, and thus opposes organisation, earlier than observed for the total diabatic feedback field. This indicates in the driest part of the domain, the positive feedback of radiation is the dominate mechanism. Thereafter, the surface flux negative feedback started to dominate in the driest, low h_f areas of the domain. While the organisation is controlled by the positive radiation feedbacks. The combined effect of surface and radiation feedback is apparent in figure 3.13, 3.14 (a) and (d) for the intermediate h_f regions as well. It shows

both the surface and radiation flux feedbacks have similar magnitude in terms of $\int h_f^{'}$ budget and they are equally important for self-aggregation processes (Wing and Emanuel, 2014).

Further decomposition of radiation into shortwave and longwave feedbacks highlights the critical role of each of the mechanisms for the self-organisation process in different stages of the simulation. For instance, during the first 18 days the infrared radiation has a positive correlation value for the dry and moist columns. In contrast, shortwave radiation feedback shows a positive feedback in the moistest regions while the left side of the region (from $\int h_f^{'} = 0$ line) is mostly indicates a negative correlation value. During this period, the longwave radiation feedback dominates the total radiation feedbacks.

To further understand the underlying mechanisms of these feedbacks a column longwave and shortwave convergence is considered as shown in figure 3.15. This figure shows the total and clear sky column convergence values of the radiation sorted based on TCWV values. In 3.15 a (on day 10), the driest part (the first 8% of binned columns) is characterized by higher values of longwave radiative cooling. Since the values of TCWV (as shown in figure 3.3 b) are not small enough to reduce the efficiency of longwave radiative cooling during this period (during the first 18 days). However, in the latter stages of the simulation the driest region of longwave radiative feedback start to show negative correlations. This is related to the increasing dryness (as shown in figure 3.3 b) of the non-convective region which makes the longwave radiative cooling less efficient. It is a by-product of the self-organisation process that facilitates the dryness of the dry region. This result is consistent to Wing and Emanuel (2014), who found a shift in longwave radiative feedback from positive to negative as the self-organisation process matures and the dry anomalies in the dry regions reach the lower troposphere.

According to these diagnostics of the diabatic tendencies, the infrared radiation is demonstrated to be the main mechanism for the onset of self-aggregation process in this simulation, as also observed by Bretherton et al. (2005); Muller and Held (2012); Wing and Emanuel (2014). The shortwave radiation appears to have a positive feedback after day 20 in most of the columns. This behavior is related to the total column moisture value of the column, when the TCWV value is higher there there is more absorption of shortwave radiation in the column. This is shown in figure 3.15b and d, which highlight the convergence

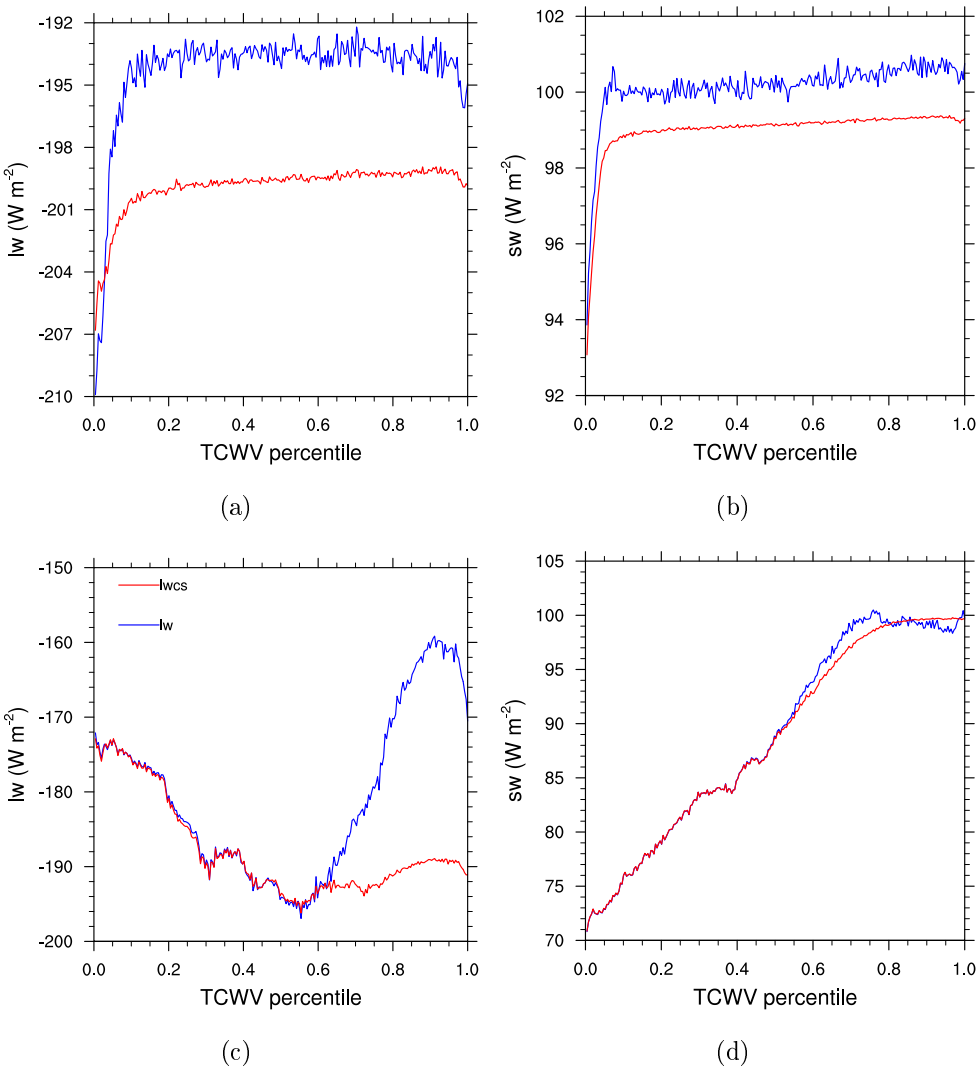

Figure 3.15: (a) and (c) longwave flux convergence on day 10 and 70 respectively, where lwcs is longwave in clear sky and lw is total longwave radiation (b) and (d) shortwave flux convergence on day 10 and 70, respectively, where swcs is shortwave in clear sky and sw is total shortwave radiation All these values are binned together and sorted based on column integrated water vapor content.

of shortwave radiation with an increase of TCWV values. In addition, figure 3.15d shows the clear sky column of shortwave radiation increases with the rate as that of total column shortwave flux convergence increases in almost all the columns. This infer that the positive feedback of shortwave radiation mainly contributed by the clear sky effects rather than clouds radiative feedback, as also stated in Wing and Emanuel (2014).

The effect of clouds is observed (in 3.15 d) to modulate the longwave radia-

tion during the matured state of self organisation in the moistest columns (the last 21% of binned columns). This causes the feedback from infrared radiation to be positive once again. Similar effects are observed by Wing and Emanuel (2014), who suggest the longwave radiation to be an important positive feedback for the maintenance of the organized state in their simulation. It is noted that Wing and Emanuel (2014) uses a different cloud resolving model system (SAM) (Khairoutdinov and Randall, 2003), using different parametrizations, including the microphysics. It is thus encouraging that the radiative contribution to organisation is consistent between these systems.

The aerodynamics bulk formula of latent and sensible heat fluxes depend on the surface wind and thermodynamic imbalance between the surface and the underlying air. The variation in moisture values and surface winds are considered to be the responsible mechanisms for the change in values of latent heat flux. For instance, the latent heat flux of the driest quartile is found to be slightly lower than the wettest quartile during the initial period (the first 14 days) as shown in figure 3.11. In this period, the gustiness of the wind offsets the higher (relatively) air-sea enthalpy disequilibrium value found in the driest quartile. This effect is reflected by having a positive feedback during the first ten days in the moisture-time field of the latent heat flux. The important role of the surface flux feedback for the onset of self-organisation is also observed by Wing and Emanuel (2014).

After day 14, the driest (latent heat flux) quartile (figure 3.11) increases dramatically and causes the air-sea enthalpy disequilibrium to dominate in this region. In addition, the wet quartiles increase at a slower rate than the domain average. As a result, the latent heat flux feedback is shown to have a negative feedback in most of the the region.

According to the aerodynamics bulk formula of sensible heat flux, surface wind and temperature disequilibrium between the surface and underlying air are responsible for the change in values of this flux. According to figure 3.8, higher and lower values of sensible heat flux are observed in convective and dry regions, respectively. The reason for smaller values in dry regions is associated with unsaturated subsidence that warms the air adiabatically in this region, and causes the strong temperature inversions at the boundary layer top in the descending regions of the Walker circulation (not apparent here due to the homogeneous SST applied). On the other hand, higher sensible heat flux is

observed in convective region because of the cold pools and higher values of surface wind due to convectively induced gustiness. Hence, the surface flux is mostly a positive feedback throughout the simulation in most parts of the domain (figure 3.12c).

The dominance of latent heat over sensible heat flux is observed in figure 3.12d, where the pattern of the total surface flux feedback closely follows the feedback behavior of the latent heat flux. However, the signature of the sensible heat flux is also observed at the top right corner of moisture-time field of total surface flux feedback panel (figure 3.12d). The main mechanism for this specific situation is related to cold pools and the gustiness of winds that facilitate the enhancement of sensible heat flux in this location (Tompkins, 2001b).

All the feedback mechanisms in the moisture-time field demonstrate the strong linkages between the organisation processes and the the way the diabatic forces respond. It also indicates that the process that initiates the organisation process might be different from that maintains this process as indicated by Wing and Emanuel (2014).

3.4 Conclusions

A three dimensional CRM with no mean wind and Coriolis force is used to investigate the feedbacks that are responsible for the organisation of convection in RCE above constant SST (301.5 K). This model is integrated for the duration of 70 days and its equilibrium state demonstrates a significant variation in the distribution of hydrometers, radiation and surface fluxes inside the domain. These variations depend on the evolution time scale of the self-organisation process, related to the subsidence time scale for the overturning of the free troposphere (Tompkins and Craig, 1998b). Small variations in temperature are observed due to gravity wave propagation that removes buoyancy gradients and homogenizes the virtual temperature rapidly.

The vertical profiles of RH and hydrometers also highlight the variation between dry and moist regions, where the profiles of the moist quartiles get moister while the dry quartiles get drier as the self-organisation process intensifies. As a result, the domain is divided into moist region where all convection occurs and dry region where all the convection is suppressed, duplicating the results of previous studies (e.g Tompkins and Craig, 1998a; Bretherton et al.,

2005; Stephens et al., 2008; Muller and Held, 2012; Wing and Emanuel, 2014)

The onset of self-aggregation is also reflected on model variables such as TOA OLR and surface latent and sensible heat fluxes. These variables are fairly homogeneous and display small, randomly distributed, perturbations during the initial stages of the simulation, associated with the randomly distributed convective updraught cores. As the organisation process matures, larger variations start to become apparent within the domain, associated with increasing variance of the column integrated moisture content. Dry 'patches' form in the upper troposphere, and then grow in size both horizontally and towards the surface. Higher values of OLR and latent heat flux are observed in the dry region while these values are depressed in moist and convective regions. In contrast, sensible heat fluxes are enhanced in moist regions due to cold pools that increase the temperature gradient while this flux significantly decreases in dry regions due to strong subsidence warming. The self-organisation of convection is also confirmed by higher values of I_{org} starting from day 20 of the simulation.

The time series of the atmospheric diabatic flux convergence is used to examine their evolution during the organisational onset. It is observed that the content of water vapor in the atmospheric column plays a critical role in dictating the amount of absorbed radiation and surface fluxes. This emphasizes how self-organisation through its impact on moisture, modulates the column integrated convergence of the diabatic flux. These diabatic processes can have a significant positive or negative feedback to the self-aggregation process.

The budget of frozen moist static energy and the diabatic correlation terms are used to investigate the mechanisms that are responsible for the organisation of convection. The budget calculation reveals the important role of advective and diabatic terms. The role of these mechanisms is observed to vary during different stages of the organisation process. For example, longwave radiative feedback is positive during the first 20 days of the simulation both in dry and moist regions of the domain but later on the longwave radiative feedback in dry regions changed to a negative feedback. The reason for change of sign in the feedback of longwave radiation is related to the response of longwave cooling to dry perturbation as the perturbation deepens and affects the lower troposphere, as discussed further in Wing and Emanuel (2014) and Emanuel et al. (2014).

In contrast, the shortwave radiation flux is a positive feedback in all stages of the self-organisation process in almost all part of the domain since the amount of shortwave radiation absorbed by atmosphere increases with increasing water vapor content. The small impact of the convective anvils was noted, and it is possible that the strength of the shortwave feedback in sensitive to the microphysical parametrization assumption employed in the model which determine the proportion of the convective updraft's cloud base total water transport which is eventually detrained in the anvil and the horizontal extent of the anvils which is likely to be sensitive to the ice fall speeds.

The surface flux feedback is a positive feedback during the initial stages of the simulation since the gustiness of the wind offsets the air-sea enthalpy disequilibrium value found in the driest regions of the domain. However, in the latter stages of the simulation negative surface flux feedback is indicated due to the dominance of air-sea enthalpy disequilibrium. Furthermore, the upgradient transport of h_f is a positive advection feedback which is observed in the intermediate stages of the simulation. The important role of different mechanisms at different stage of the simulation for the control run is consistent with Wing and Emanuel (2014), who provides evidence for a distinction between the feedbacks that initialize and maintain the self-aggregation of convection.

Chapter 4

Impact of sub-grid mixing on spontaneous organisation of convection

Convective organisation depends on a number of processes, radiation, entrainment and cold pools. In this chapter, several simulations are presented that show organization is dependent on the sub-grid formulation, as the choice of mixing schemes that neglect the horizontal derivative of the vertical velocity fail to produce organized states. This suggests that the entrainment mixing process is a crucial component for organisation, despite recent emphasis on radiative feedbacks as the main driver. This also leads to the slightly concerning conclusion that the occurrence and eventual strength of feedback depends on the sub-grid scale turbulence formulation in models; an aspect of the model setup that receives limited attention. The simulations results are discussed in the context of Emanuel (Emanuel et al., 2014), that while radiation is the driver, we believe the results show entrainment is not simply an amplifier of organization but an intrinsic necessary condition for its occurrence. The results also indicate that simulations with higher horizontal resolution may be required to explicitly represent the entrainment process and observe the organised states with confidence.

4.1 Introduction

As summarized in the introduction to the thesis, a number of feedbacks have been suggested for the spontaneous organisation of convection, involving radi-

ation, water vapour, cloud, and cold pool dynamics. Both the long wave and short wave radiative impact of the heterogeneous water vapour field can drive convergence into moist regions (Wing and Emanuel, 2014; Emanuel et al., 2014). Water vapour not only acts through its influence on the radiative heating; it also has a direct thermodynamical role in regulating convection (Tompkins, 2001a; Grabowski and Moncrieff, 2004). Dry boundary layers will inhibit convection due to the impact on CAPE and CIN, but organisation also operates partly through the entrainment processes whereby dry midtropospheres increase entrainment cooling of updraughts (Derbyshire et al., 2004). Tompkins (2001a) noted a larger impact of perturbations in the 900-700 hPa layer since downdraughts immediately transported the dry anomaly to the boundary layer, effectively killing deep convection, while perturbations above 700 hPa merely reduced the intensity of convection through the entrainment mechanism. Craig and Mack (2013) developed an idealized model of upscale organisation cascade resulting from the water vapour feedback. The maintenance of the dry anomalies is due to low horizontal mixing timescales on the mesoscale (Pierrehumbert and Yang, 1993; Yang and Pierrehumbert, 1994; Zhang, 2005), although it is likely exacerbated in the idealized CRM setup since the periodic boundary conditions imply an absence of eddies and shear near the domain scale, seen in the flattening of the power spectra near the domain scale (Bretherton, 2015). The exact role of water vapour entrainment on organisation is far from clear. Despite Tompkins (2001a) and Grabowski and Moncrieff (2004) arguing for its importance, Emanuel et al. (2014) states that water vapour entrainment feedback can only act to amplify organisation but not play a role in its initialization.

If water vapour entrainment is a factor for either the establishment and/or the amplification of convection organisation, it raises an issue concerning the use of CRMs that is rarely discussed, namely that the organisation strength in these models is likely to be sensitive to the choice of resolution and the model setup in terms of the choice of sub-grid diffusion and mixing. The resolutions employed in such experiments often lie in the 1 to 4 km range, on the same order as the scale of the convective updraughts themselves (e.g Bryan et al., 2003; Khairoutdinov et al., 2009). Simulated convective updraughts consist of one, or at most a handful of model grid points. A consequential alternative nomenclature for these models is therefore 'convection permitting', to emphasize the

fact that the resolutions employed are inadequate to truly resolve the intricacies of the sub-cloud structure, such as evidenced in early aircraft observations (e.g WARNER and Newnham, 1952; Warner, 1955). Somewhat ironically, the representation of convection in these models resembles far more the top-hat, ensemble plumes of mass-flux parametrization schemes Warner (1970); Arakawa and Shubert (1974); Tiedtke (1989) than actual turbulent convection. Lateral entrainment into the updraught cores is driven entirely via the subgrid-scale mixing schemes (and numerical diffusion) and result in uniform entrainment across the core. Comparisons of 100 m and 1 km integrations by Zhang et al. (2015) showed that entrainment rates were similar. While sub-core fluctuations are second-order regarding convection transport Randall (1980), the buoyancy effect of the entrainment has driven efforts such as Raymond and Blyth (1986); Emanuel (1991); Emanuel and Zivkovic-Rothman (1999) to incorporate sub-cloud structure into classical parametrization approaches.

Given these considerations, it is perhaps surprising that the fact that the entrainment relies chiefly on subgrid parameterizations is often overlooked in studies of convective organisation in radiative-convective equilibrium. Experiments are conducted with a single setup, and the choice and impact of the subgrid approach has received limited attention. Pauluis and Garner (2006); Muller and Held (2012) did investigate the sensitivity of organisation to the model resolution employed, with Muller and Held (2012) stating the need to employ resolutions coarser than 2 km for organisation to occur.

The impact of the choice of subgrid mixing parameterization scheme and numerical noise filters has been shown to be important for other simulated situations such as squall lines Takemi and Rotunno (2003); Bryan (2005); Knievel et al. (2007). In idealized simulations of a supercell, Verrelle et al. (2015) showed that increased mixing and entrainment in a 3D subgrid-scale parametrization substantially impacted the cloud microphysics when using a 2 km grid length. Two further recent studies have focused on the subgrid-scale turbulence for simulations of realistic convection (Hanley et al., 2015; Machado and Chaboureau, 2015) and both found that increasing the strength of the subgrid-scale mixing (by increasing the eddy diffusivity parameter or switching from a 1D to 3D scheme that accounts for horizontal shear of the vertical wind speed) increased deep convective entrainment, and lead to fewer more vigorous convective systems, possibly indicating more convective organ-

isation as a result.

The aim of this chapter is to investigate the impact of the subgrid diffusion schemes on the degree of convective organisation in the idealized framework of RCE over homogeneous surface conditions. A commonly used community model is employed that has a wide range of subgrid parametrization approaches available. An ensemble of long term convection permitting simulations are performed, each with a choice of subgrid schemes combinations that are recommended for use by the model designers. It will be demonstrated that the strength of the entrainment into convection is crucial to the formation of an organised state, and the strength of the organisation.

4.2 Effects of subgrid Eddy diffusion schemes

Sensitivity experiments using various options of subgrid Eddy diffusion schemes are used to investigate the impact of the schemes on the degree of convective organisation. Towards this objective, experiments summarized in table 4.1 are conducted, each with a duration of 70 days. All these experiments use the same configuration as the control experiment (c.f. chapter 3) with the exception of the choice of the horizontal and vertical subgrid mixing schemes. The control experiment (bl3ds) is the simulation described in the previous chapter that uses the 3D Smagorinski mixing for horizontal transport, while the YSU PBL scheme handled all vertical transport. The experiment nbl3ds switches off the YSU scheme, and thus the 3D Smagorinksy scheme is responsible for both horizontal and vertical transport. The difference between these two experiments is thus only in the representation of vertical mixing. The bl3ds that uses the YSU PBL scheme has an explicit treatment of the entrainment layer at the PBL top and capability of non local mixture using the counter gradient flux terms (Hong et al., 2006) while this is not explicitly represented in the vertical mixing of 3D Smagorinksy scheme.

A two dimensional Smagorinksy model with YSU PBL scheme is used in the bl2ds experiment. This experiment is used to differentiate the role of horizontal mixing in the 2D and 3D versions of Smagorinksy scheme. It is recalled (chapter 2) that the 2D Smagorinksy scheme only uses the horizontal deformation terms to calculate the horizontal eddy diffusion coefficient (equation 2.9). For the 3D Smagorinksy scheme, the vertical deformation and buoyancy

Name	eddy coefficient option	Boundary layer option
bl3ds	3D Smagorinsky first order closure	YSU scheme
nbl3ds	3D Smagorinsky first order closure	No PBL
bl2ds	2D Smagorinsky first order closure	YSU scheme
bltke	1.5-order TKE prediction	YSU scheme
nbltke	1.5-order TKE prediction	No PBL

Table 4.1: Lists the number of simulations conducted with set of eddy coefficients and boundary layer options.

terms are used in addition to the horizontal deformation terms to calculate the horizontal eddy diffusion coefficient (equation 2.10).

The Turbulence Kinetic Energy (TKE) 1.5 order closure scheme is instead employed for the final two experiments: bltke and nbltke. This scheme uses a prognostic TKE equations and a mixing length scale based on TKE as described in equation 2.11. The TKE scheme can be used without a PBL scheme since it can handle the vertical mixing. Hence, experiment nbltke is used without the YSU PBL scheme while bltke experiment utilize the YSU PBL scheme for the vertical mixing. It should be noted that the 1.5 order TKE closure with and without YSU PBL gave very similar results (not shown) in terms of level of organisation, hence in the following section only bltke experiment is considered for brevity.

Figure 4.1 presents the horizontal slice of the vertical velocity at 730 hPa on day 70. An organised structure of convection is only observed in experiments bl3ds and nbl3ds. These two experiments also characterized by high value of TCWV (moisture) in the convective regions as demonstrated by figure 4.2 a and b. The timeseries of the organisation index confirms the presence of clustering in bl3ds and nbl3ds experiments (figure 4.3). Interestingly, the organisation of convection in the bl2ds and bltke experiments is not random, but is slightly regular, that is to say, convective towers are slight further apart on average than expected from a random distribution. This regularity could be related to the effect of cold pools that trigger new convective updraughts at the gust front when they are mature and almost recovered, when low wind shear conditions persist (Tompkins, 2001b). This regular distribution is observed in figure 4.2 c and d, that display a uniformly distributed TCWV (moisture)

throughout the domain.

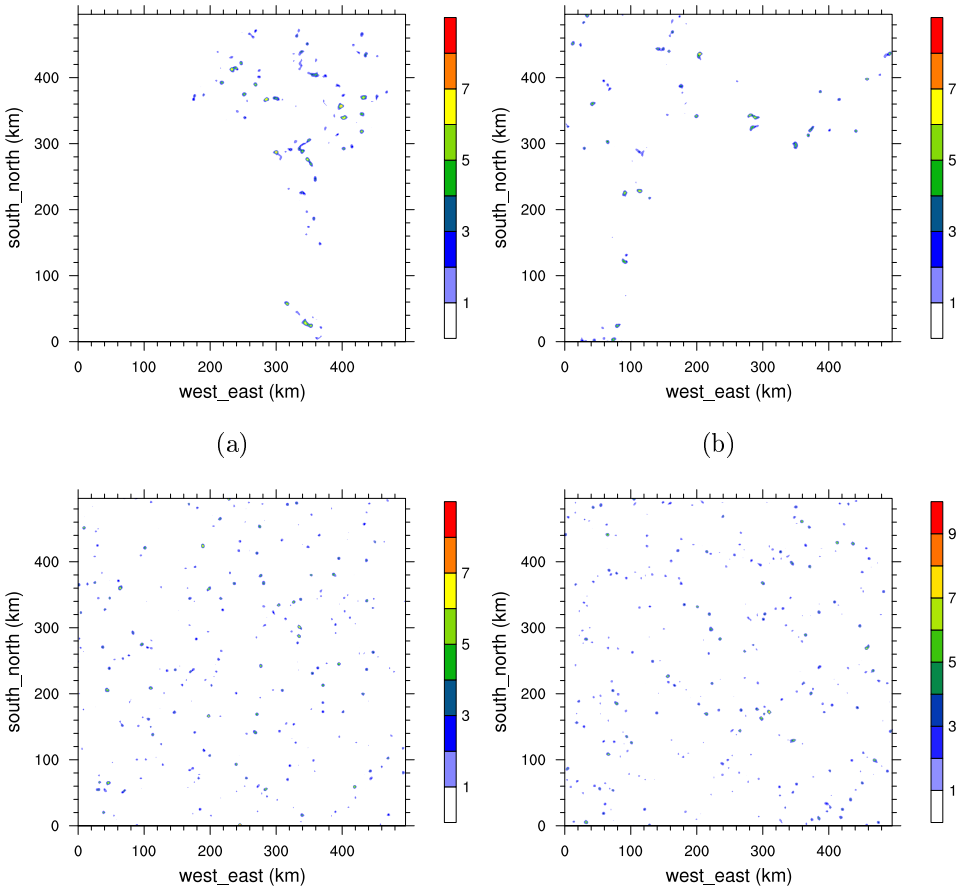

Figure 4.1: Vertical velocity at 730 hPa on day 70 of the simulation for a) 3D Smagornisky with YSU PBL, b) 3D Smagornisky without PBL, c) 2D Smagornisky with YSU PBL and d) TKE closure with YSU PBL.

A difference in rate of adjustment to equilibrium value of domain average TCWV is observed between bl3ds and nbl3ds experiments (Fig. 4.4) which mirrors the I_{org} parameters. In both experiments a decrease in the domain average TCWV is observed as the simulations progress. This is an indication of the onset of self-organisation in the two experiments as already indicated by their I_{org} values. In contrast, the domain average TCWV values of bl2ds and bltke experiments reach the value of 54 kg m^{-2} during the first 5 days and then remain close to this value for the rest of the simulations (Fig. 4.4), highlighting the absence of self-organisation in these experiments.

The I_{org} index in the experiment nbl3ds is higher than bl3ds for the first 40

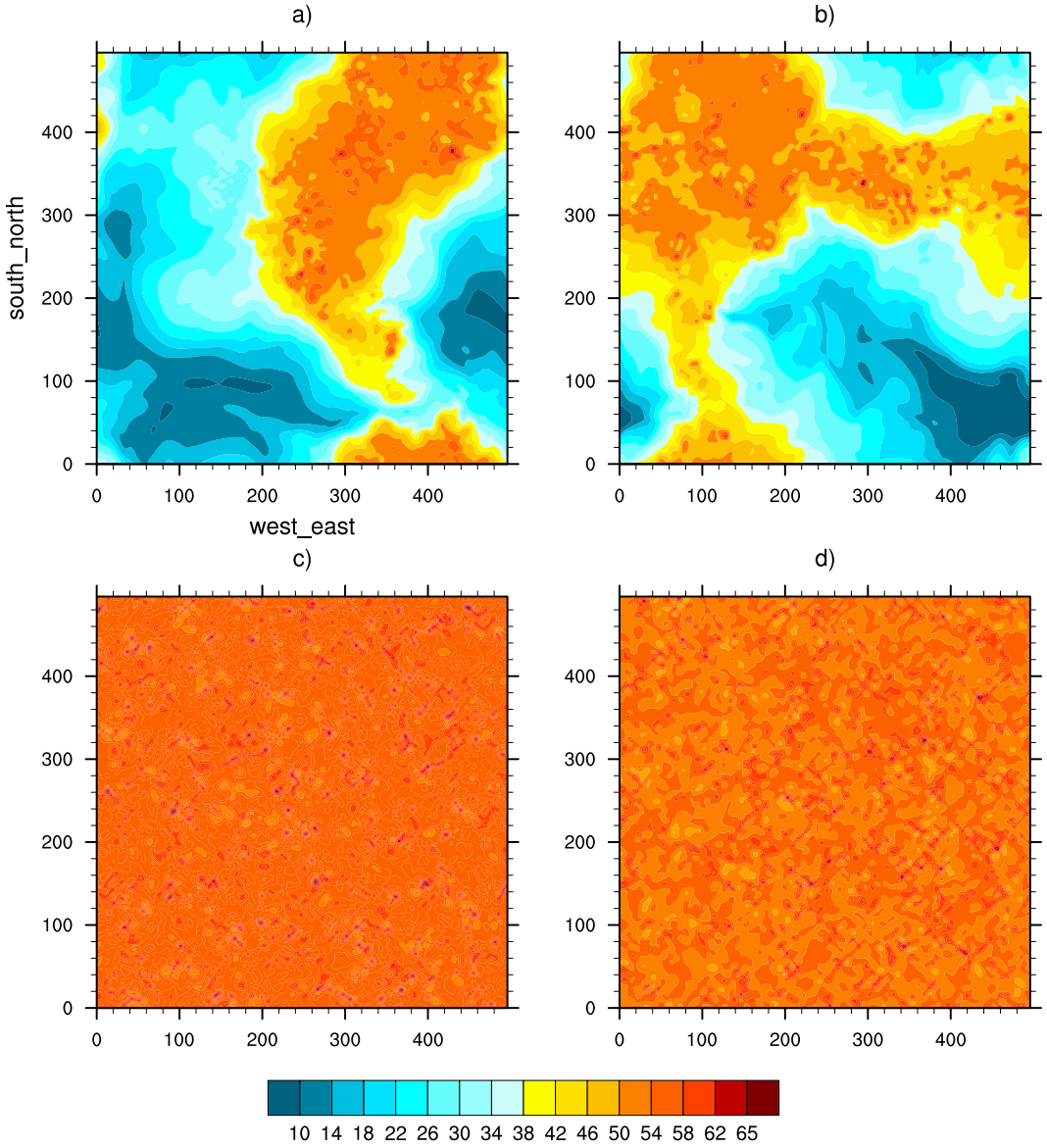

Figure 4.2: Values of TCWV on day 70 of the simulation for a) 3D Smagornisky with YSU PBL, b) 3D Smagornisky without PBL, c) 2D Smagornisky with YSU PBL and d) TKE closure with YSU PBL.

days of the simulation but afterwards is lower than bl3ds experiment. This is due to the variation in vertical mixing in these two experiments, where bl3ds (which uses YSU PBL) has an explicit treatment of the entrainment layer at the PBL top and capability of non local mixture using the counter gradient flux terms (Hong et al., 2006) while this is not explicitly represented in the vertical mixing of 3D Smagorinksy scheme. As a result of these differences in the representation of the vertical entrainment process, the experiments display variation in moisture perturbation. This is clearly observed in figure 4.4 where

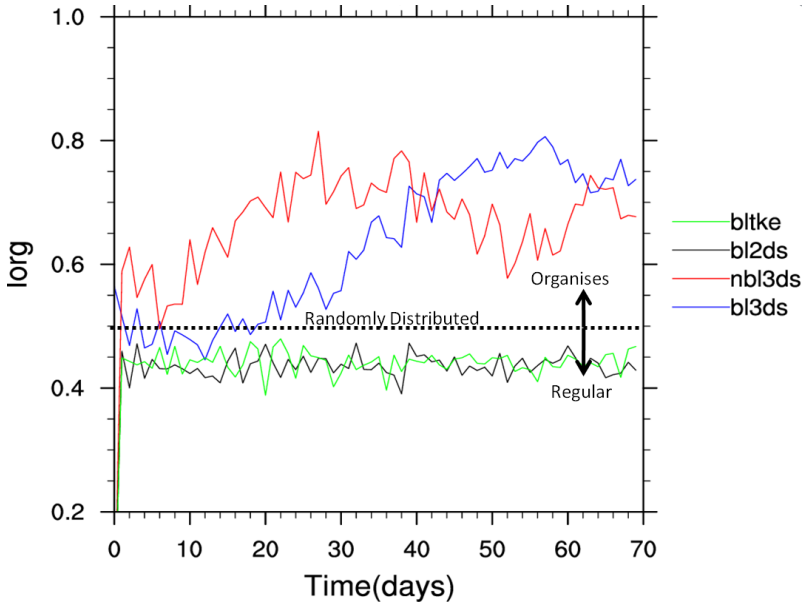

Figure 4.3: Organization index (I_{org}) values of each day of the simulation for the experiments bl3ds, nbl3ds, bl2ds and bltke.

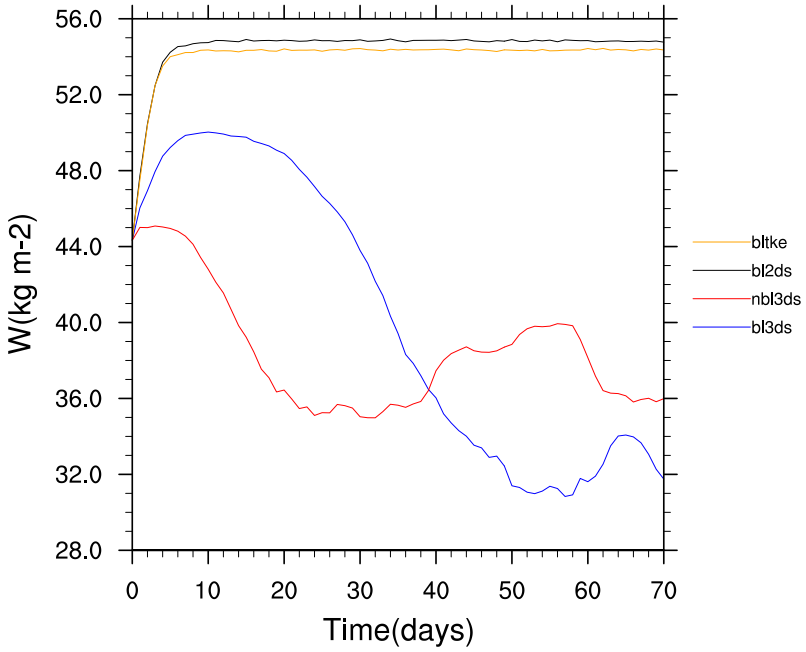

Figure 4.4: Time series of domain average of column integrated water vapor (kg m^{-2}) for experiments bl3ds, nbl3ds, bl2ds and bltke.

the domain average TCWV of nbl3ds experiment decreases faster than bl3ds experiment in the first 40 days of the simulation.

In addition to the analysis based on domain average TCWV, the domain average vertical structure of relative humidity (RH) is also considered. For

each case, the RH domain average value is calculated at the initial (day 10) and final (day 70) stage of the simulation as shown in figure 4.5. The presence of aggregation is indicated in bl3ds and nbl3ds experiments (Fig. 4.5 a and b), since there is variation in the vertical profile of these experiments during the initial and final stage of the simulation. This highlights the expansion of dry region as the self-organisation process intensifies. However, almost identical vertical profile of RH is observed between the two stage of the simulation for the experiment bl2ds and bltke (Fig. 4.5 c and d). This is the consequence of regular distribution of convection in the initial and final stage of the simulation.

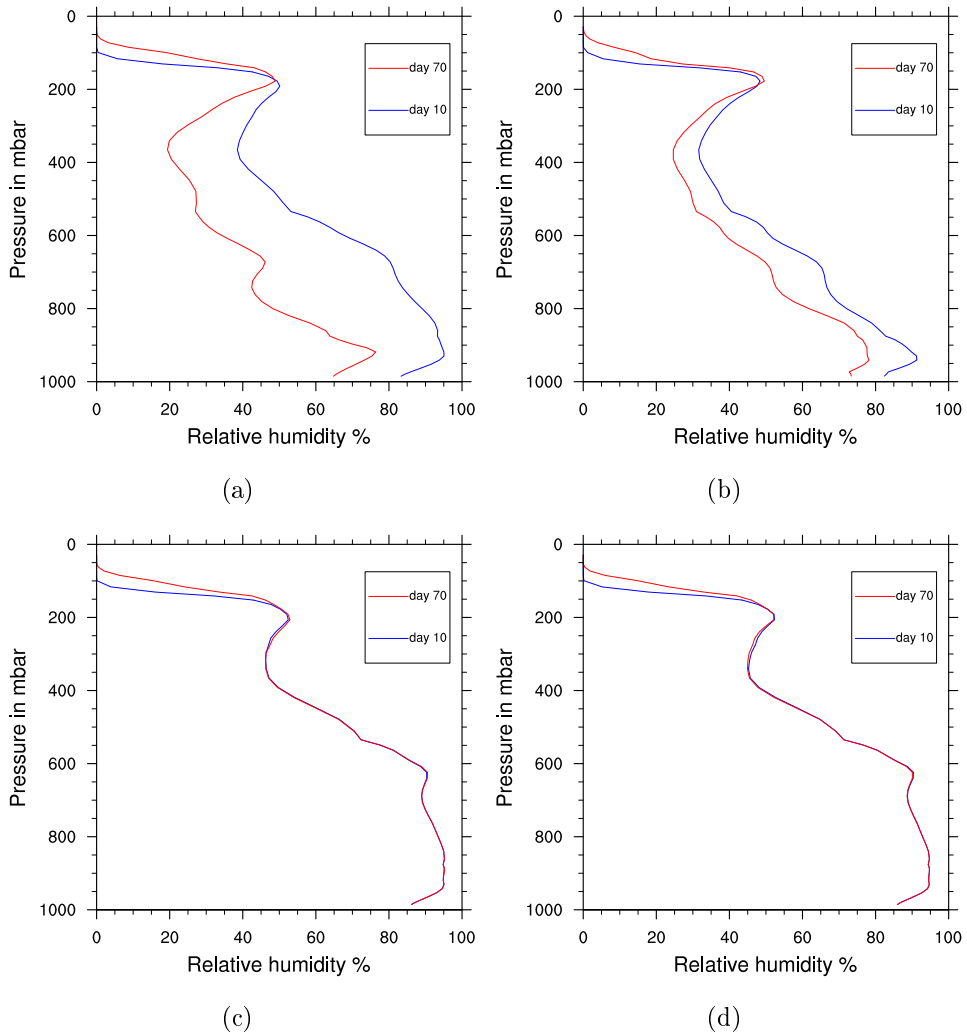

Figure 4.5: Domain average vertical relative humidity of a) 3D Smagornisky with YSU PBL, b) 3D Smagornisky without PBL, c) 2D Smagornisky with YSU PBL and d) TKE closure with YSU PBL.

It should be noted that the only difference between the sensitivity tests of bl3ds, bl2ds and bltke is the representation of horizontal subgrid mixing since these experiments use the same (YSU PBL scheme) vertical mixing. The mixing is quantified by the horizontal eddy viscosity term (xkmh = k_h) as described by equations 2.9, 2.10 and 2.11 for the cases of 2D Smagorinksy, 3D Smagorinksy and TKE closure schemes, respectively.

A comparison of the domain average of xkmh indicates that the experiments bl3ds and nbl3ds have an order of magnitude greater horizontal mixing coefficient than the bl2ds and bltke experiments in the lower troposphere (Fig. 4.6). Boundary layer horizontal mixing is far higher when using the 3D smagorinsky scheme, relative to the TKE and 2D Smagorinski schemes.

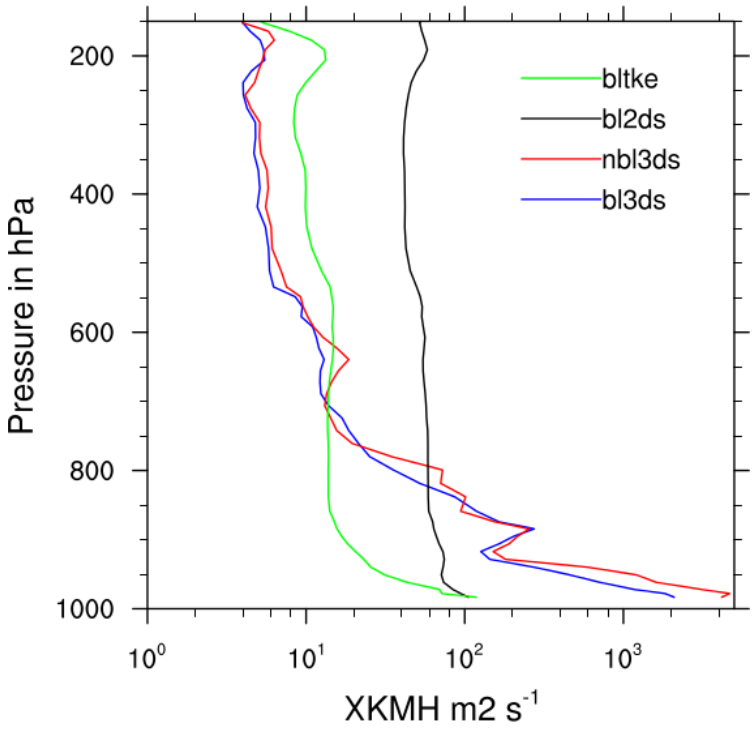

Figure 4.6: Vertical profile of domain average xkmh (horizontal sub-grid mixing coefficient) values of 3D Smagornisky with and without YSU PBL, 2D Smagornisky and TKE closure with YSU PBL.

The domain average xkmh values of bl3ds and nbl3ds experiments are shown to decrease in the upper troposphere as result of self-organisation that makes large proportion of the domain to be dry and stable. This is represented in the model by the square of Brunt - Vaisala frequency (N^2) which will be positive when the atmosphere is stable and will decrease the xkmh as explic-

itly indicated in equation 2.10. This is also revealed in maps showing a slice through the domain at a height of 500 hPa (Fig. 4.7). Thus in most of the domain the mixing coefficient adopt the minimum value of 4 m^2 s^{-1}, with high values only found in the strong shear regions at convective cores.

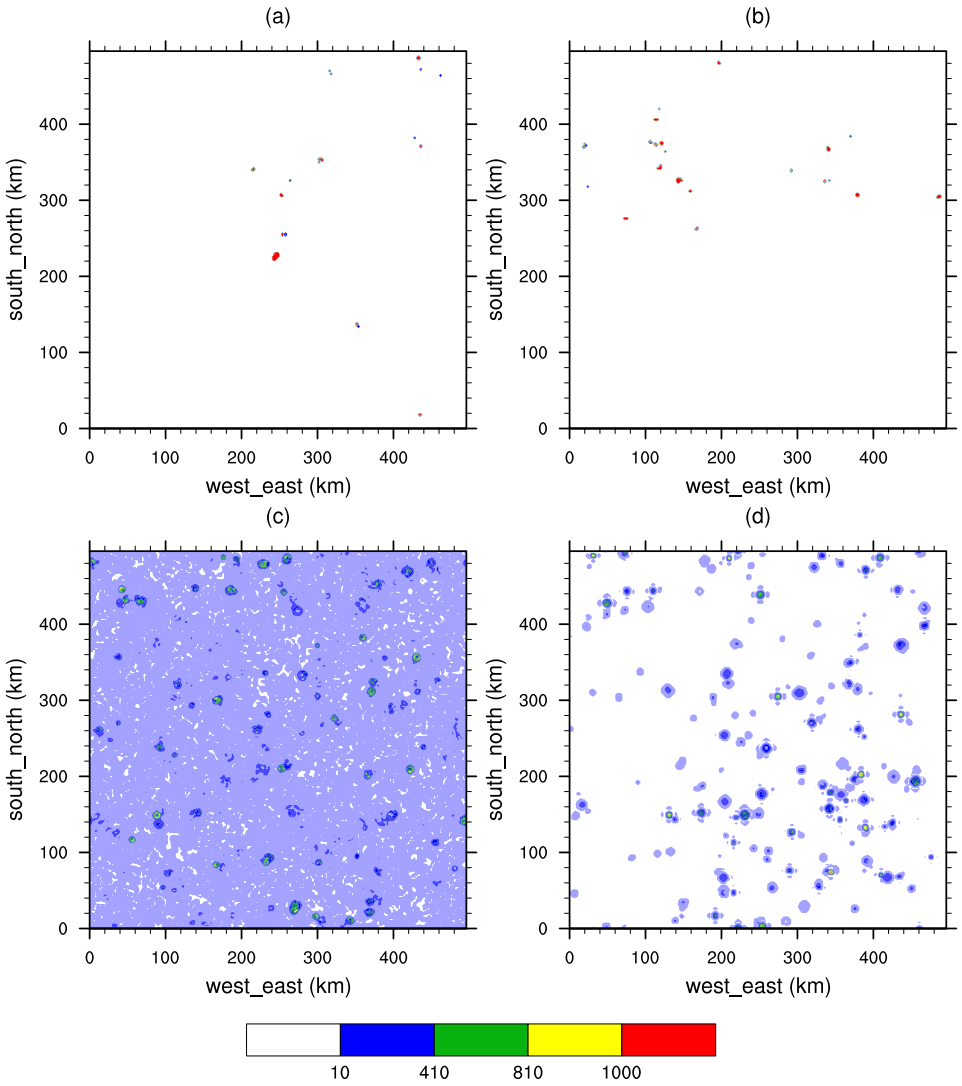

Figure 4.7: xkmh value at 500 hPa for the experiments a) bl3ds, b) nbl3ds, c) bl2ds and d) bltke.

The xkmh slices at the level of 950 hPa (Fig. 4.8 a,b and d) show the the TKE and 3D Smagorinski schemes produce higher mixing near cores and near zero values elsewhere in the domain. The key difference between these schemes is the magnitude of mixing near the cores, with the 3D Smagorinsky scheme produces far higher peak mixing values, on the order of 3 to 10 times higher than the TKE scheme. The TKE domain mean mixing exceeds that of the

3D Smagorinski scheme in the upper troposphere merely because the mixing is spread over more points (Fig. 4.7 d). In contrast to these two schemes, the horizontal shear terms of the the 2D Smagorinski scheme produce lower mixing throughout the domain (Fig. 4.8 c), and is thus generally more diffusive in the subsidence zones, which would act to mixing vapour between the moist and dry regions, while no enhancement of entrainment mixing into the updraughts is noted.

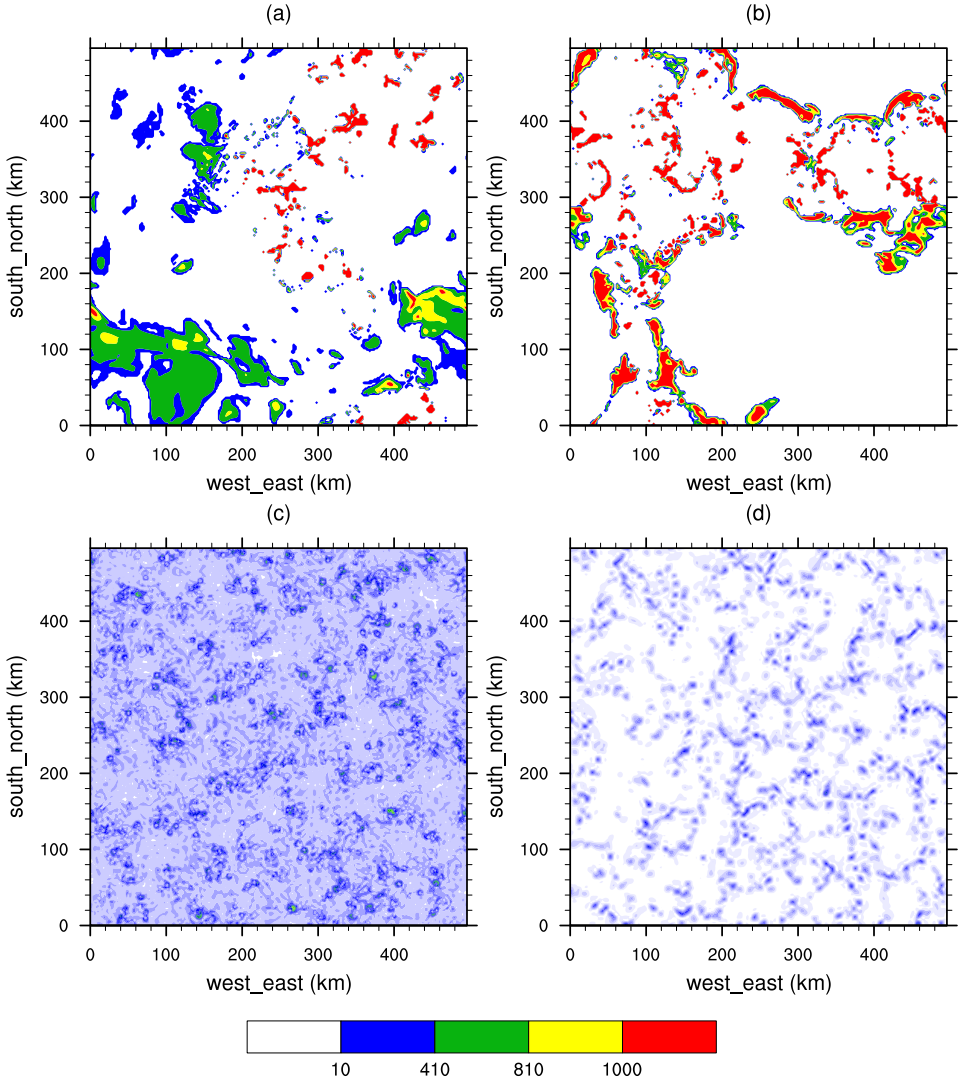

Figure 4.8: xkmh value at 950 hPa for the experiments a) bl3ds, b) nbl3ds, c) bl2ds and d) bltke.

4.3 Effect of sub grid scale constants on TKE experiments

In the earlier experiments, the default TKE did not produce any organisation, despite the fact that the horizontal shear of the vertical velocity $\partial w/\partial x$ features as a source term of TKE. It is assumed that the reason therefore is that the peak mixing values are lower, possibly due to the prognostic rather than diagnostic form of the TKE equation. Additional experiments are conducted which increase the TKE eddy coefficient (c_k in equation 2.11) of 1.5 order TKE closure scheme. The default value is 0.15, and the sensitivity tests increase this systematically to a maximimum of 0.6. The prediction is that higher mixing efficiencies will increase entrainment into convective updraughts and cause deep convection to be more sensitive to the moisture field, encouraging organisation.

Figure 4.9 shows the horizontal cross section of vertical velocity at 730 hPa level and the corresponding time series of the organisation index is provided in figure 4.10. The values of I_{org} indicate an increasing trend as the values of c_k, and thus mixing and entrainment strength, increase. The distribution of vertical velocity at the 730 hPa level shows the presence of convection-free regions starting from the experiment with c_k=0.4 (Fig 4.9 d). Further increasing this value results in more convective-free regions and the system is seen to organize strongly in the early stages of the simulation as shown for c_k = 0.6 in figure (Fig 4.9 f).

A remarkable shift in magnitude and distribution of xkmh values are observed as the magnitude of c_k increases (Fig 4.11). Figure 4.11 a and b present the horizontal slice of xkmh at 950 hPa having c_k values of 0.2 and 0.3 respectively, both of them display almost randomly distributed xkmh throughout the domain. However, the experiment with higher value of c_k started to indicate an elevated values of xkmh. Further increase to the values of c_k (0.4 and 0.5) restrict the distribution of higher values of xkmh to convective regions only (Fig. 4.11 c and d). The magnitude of xkmh near the convective cores of these experiments is in the same order as the 3D Smagorinski scheme.

These results highlight the important role of horizontal mixing. Lower values of c_k result in horizontal subgrid entrainment mixing lower than the threshold that is apparently required to result in the onset of convective or-

ganisation.

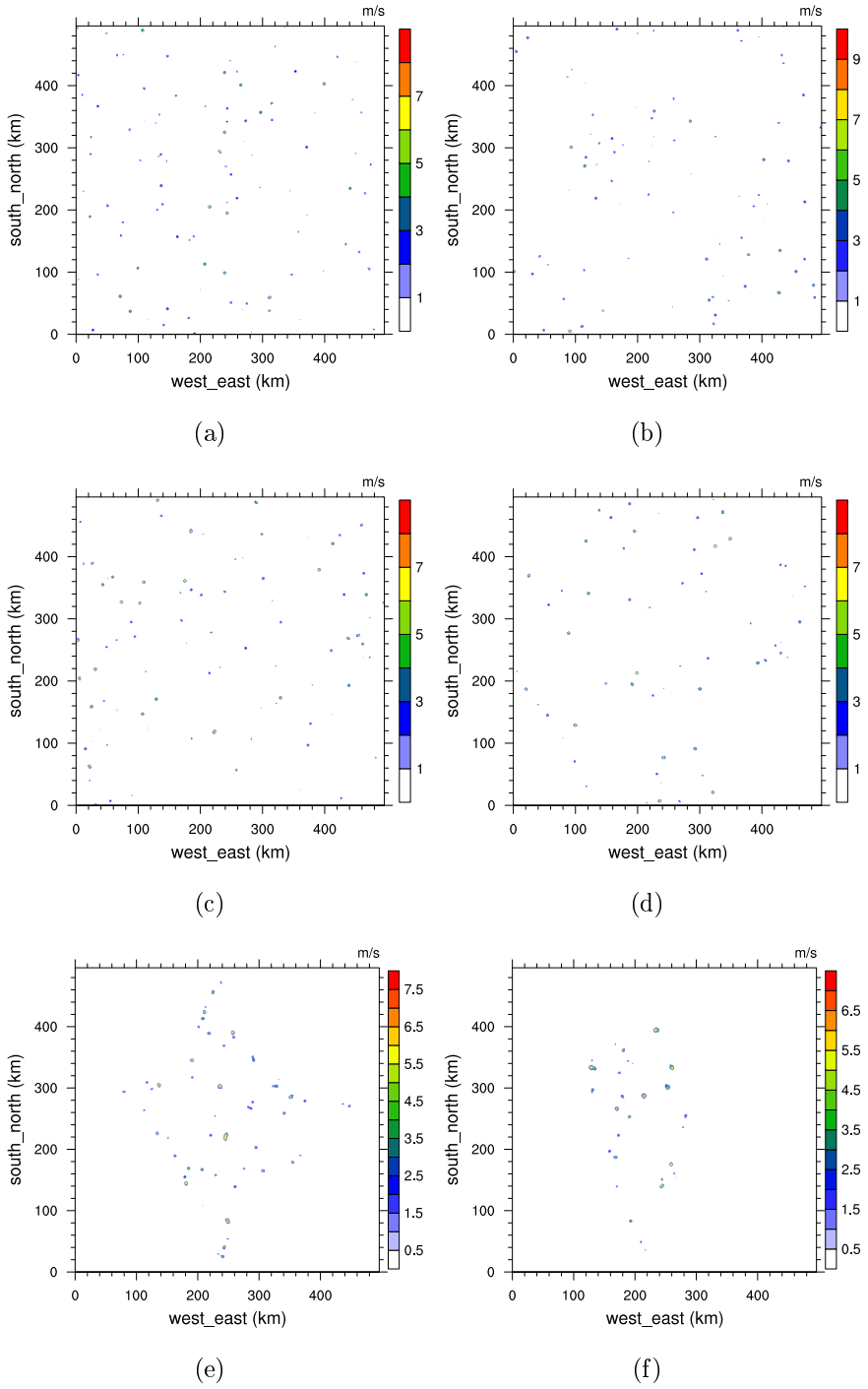

Figure 4.9: Vertical velocity at 730 mb on day 16 for experiments sub grid constants of a) 0.15, b) 0.2, c) 0.3, d) 0.4, e) 0.5 and f) 0.6, respectively.

4.4 Conclusions

The effect of subgrid-scale mixing strength on the organisation of convection is investigated using the WRF model. Experiments employed 3 different subgrid-scale turbulence parametrizations show starkly different behaviour in terms of the convection organisation. Only the experiment employing a 3D Smagorinky closure show aggregation of convection, which is not observed when using the 2D Smagorinksy or TKE schemes.

Two experiments are conducted, bl3ds and nbl3ds, where the difference between them is only representation of subgrid mixing in the vertical direction (xkmv). The physics of the former experiment includes an explicit entrainment term in the turbulence flux equation and capability of non local mixing using the counter gradient flux terms in YSU PBL. This experiment shows slightly stronger organisation, but the differences are small and may not be statistical significant; ensemble integrations rather than single deterministic runs may be required to judge this. Nevertheless, the small differences between these two experiments indicate that it is the horizontal mixing that is key to the onset of organisation. A further pair of experiments that were not reported here, in

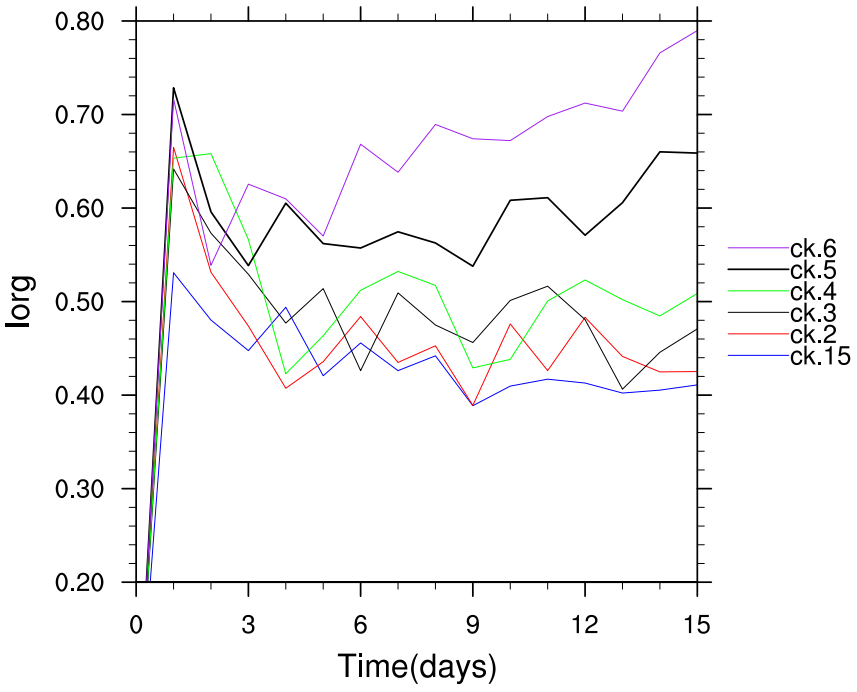

Figure 4.10: Organization index (I_{org}) values of each day of the simulation for the experiments for ck values of 0.15, 0.2, 0.3, 0.4, 0.5 and 0.6.

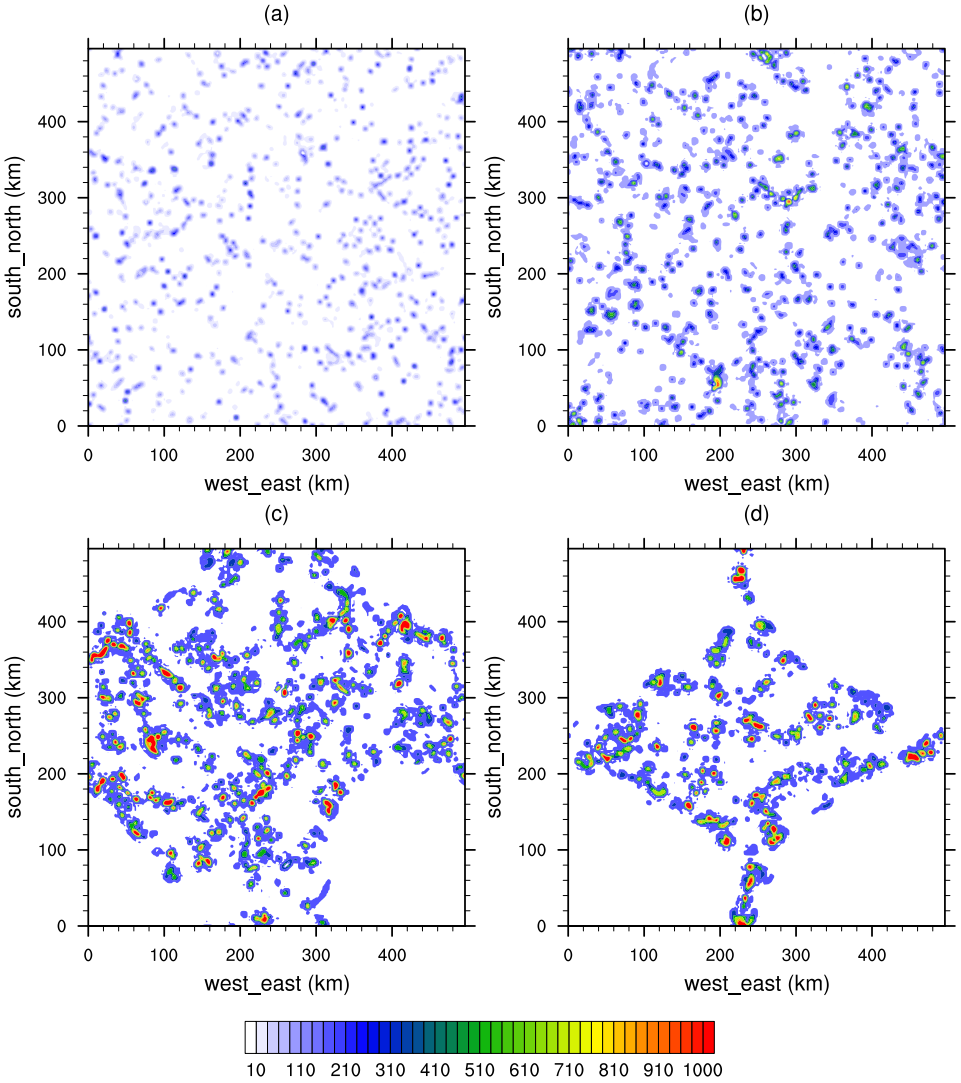

Figure 4.11: Horizontal slice of XKMH at 950 hPa for ck values of a) 0.2, b) 0.3, c) 0.4 and d) 0.5.

which the YSU PBL scheme is added to the TKE scheme confirm the relatively minor impact of vertical mixing on the mean simulated climate.

The variation in the horizontal mixing produced between the three schemes is remarkable. The mixing strength of the 3D Smagorinski scheme is found to be more than an order of magnitude higher than that produced by the TKE or 2D Smagorinski schemes. The higher mixing values are highlighted to play a significant role in the process of organisation of convection by efficiently mixing moisture into the convective updraughts. The importance of vertical wind shear term (and to a lesser extend the stability term) in the representation of subgrid closure schemes is highlighted in the experiment that compares the

difference between 2D and 3D Smagorinksy schemes. The lack of these terms in the 2D scheme reduces entrainment mixing strength greatly and leads to a much lower sensitivity of convection to environmental humidity. Thus, if random variability causes a dry anomaly to form, while the results in chapter 3 indicate that the radiative response is to drive convergence into the moist zone and encourage convective organisation, the results of this chapter indicate that entrainment sensitivity to moisture perturbations is also required to allow organisation to occur. If convective updraughts are not sensitive to moisture, then deep convective may still occur in the locality of the forming dry anomaly, removing it and preventing organisation from progressing. On the other hand, if convection is suppressed in the dry region by entrainment mixing, which reduces the updraught positive buoynancy due to the cooling as cloud droplets evaporate, then this allows the radiative amplication of the moist static energy variance to continue. Thus in contrast to Emanuel et al. (2014), who state that convection-moisture feedback is secondary and does not play a role in the initiation of organisation, even if it might amplify the eventual strength of the organisation, here the results suggest that convective entrainment is a necessary but possibly not sufficient condition for organization to occur.

Chapter 5

Impact of boundary conditions on spontaneous organisation of convection

This chapter investigates the role of boundary conditions on the self-organisation process. Sensitivity tests on an interactive SST lower boundary condition and on the horizontally imposed winds are conducted to discuss their role in respect to the level of organisation. The horizontal wind experiments were observed to affect the organisation structure through their interaction with the gust fronts of cold pools. In the interactive SST experiments, an ocean slab with fixed and varying mixed layer depth is introduced. The effect of interactive SST is found to be related to a reduction of shortwave radiation in the convective regions and enhancement of longwave cooling in a dry regions.

5.1 Sensitivity to horizontal imposed wind

The role of wind sensitive surface flux is one of the critical mechanisms that controls the self-organisation (e.g Emanuel, 1987; Neelin et al., 1987; Tompkins and Craig, 1998a; Bretherton et al., 2005). This is confirmed with the control experiment where the surface flux was seen to have a positive feedback for the onset of the organisation. In the control experiment, a Newtonian relaxation towards zero wind speed in horizontal directions is applied to prevent the build up of wind-shear during the experiment (Held et al., 1993; Tompkins and Craig, 1998a; Tompkins, 2000*b*).

A series of sensitivity tests are conducted using the same Newtonian re-

laxation, but with different target velocities of 1, 5 and 10 m s^{-1}, respectively in the west-east direction, while the imposed wind in south-north direction is zero value for all the experiments. The schematic shown in figure 5.1 demonstrates the interaction of the applied wind to the surface fluxes. When the mean wind speed is very low, that is smaller than the typical velocity associated with downdraft outflow, the gustiness will increase fluxes in all directions, hence the development of parameterizations to represent this effect in the work of Redelsperger et al. (2000). If the mean wind is larger than the gustiness magnitude, then cold pool outflow will enhance fluxes in the downwind direction, while reducing them in the upwind direction. The objective of the sensitivity tests is to understand the impact of this background wind on the self-organisation.

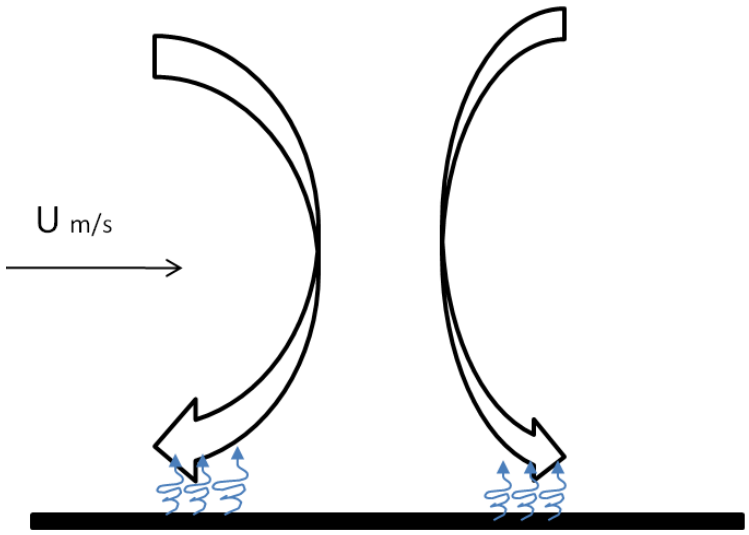

Figure 5.1: A schematic indicating the interaction of downdraughts with imposed wind speed and surface fluxes.

Figure 5.2 shows the time series of TCWV values from the sensitivity experiments and the control run (chapter 3). The TCWV values are partitioned into four quartile regions (moistest, moist, dry and driest) to quantify the spatial variability of the moisture field. The experiments with imposed horizontal wind of 1 m s^{-1} (wind1) and 5 m s^{-1} (wind5) are found to be similar to the control experiment (Fig. 5.2 a, b and c). However, the experiment with applied wind speed of 10 m s^{-1} (wind10) shows a much smaller variation in the TCWV between the quartiles except for the driest quartile, which declines by 20 kg m^{-2} as the end of the simulation approaches. This indicates the presence of

some level of organisation even with the experiment wind10, but establishing on a much slower time scale.

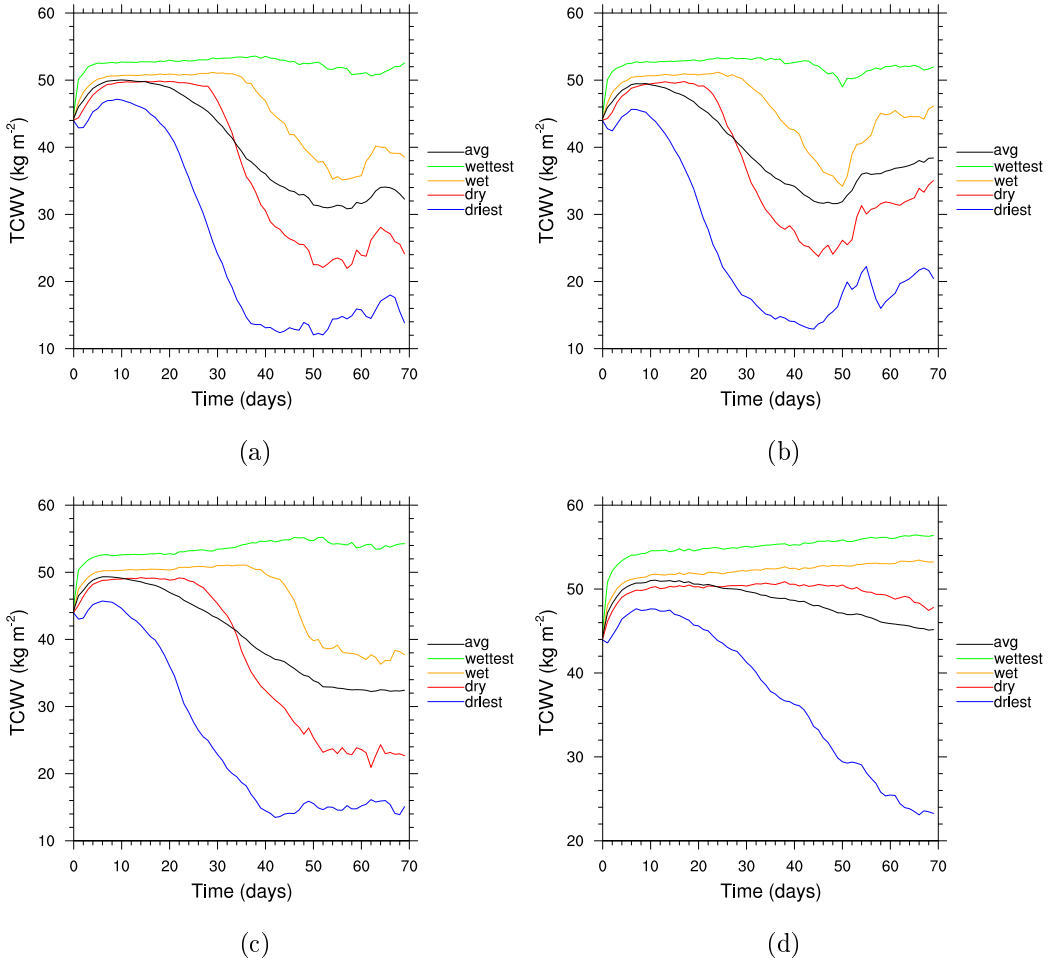

Figure 5.2: Time series of domain average total column water vapor (TCWV) for the entire integration. The black lines are domain means and the other curves are means of sub domain regions partitioned into four quartiles on the basis of their daily mean of column integrated water vapor content a) control experiment 0 m s^{-1} b) 1 m s^{-1} c) 5 m s^{-1} d) 10 m s^{-1} horizontally imposed wind speed.

Figure 5.3 shows the spatial distribution of TCWV on day 70, which also confirms the localization of convection in all the experiments. The level of organisation is quantified by the organisation index as shown in figure 5.4. The experiment wind1 and wind5 reached a self-organized state (I_{org} greater than 0.5) starting from day 20, while in experiment wind10 the system found to be slightly organized for few days during the last stage of the simulation. This indicates applying a constant domain-mean wind (with no vertical shear)

can have a significant effect on the organisation of convection. The following discussion focuses on the contribution of latent and sensible heat fluxes in different parts (dry and moist) of the domain to analyze how the interaction of wind with these fluxes affects the approach to an organized state.

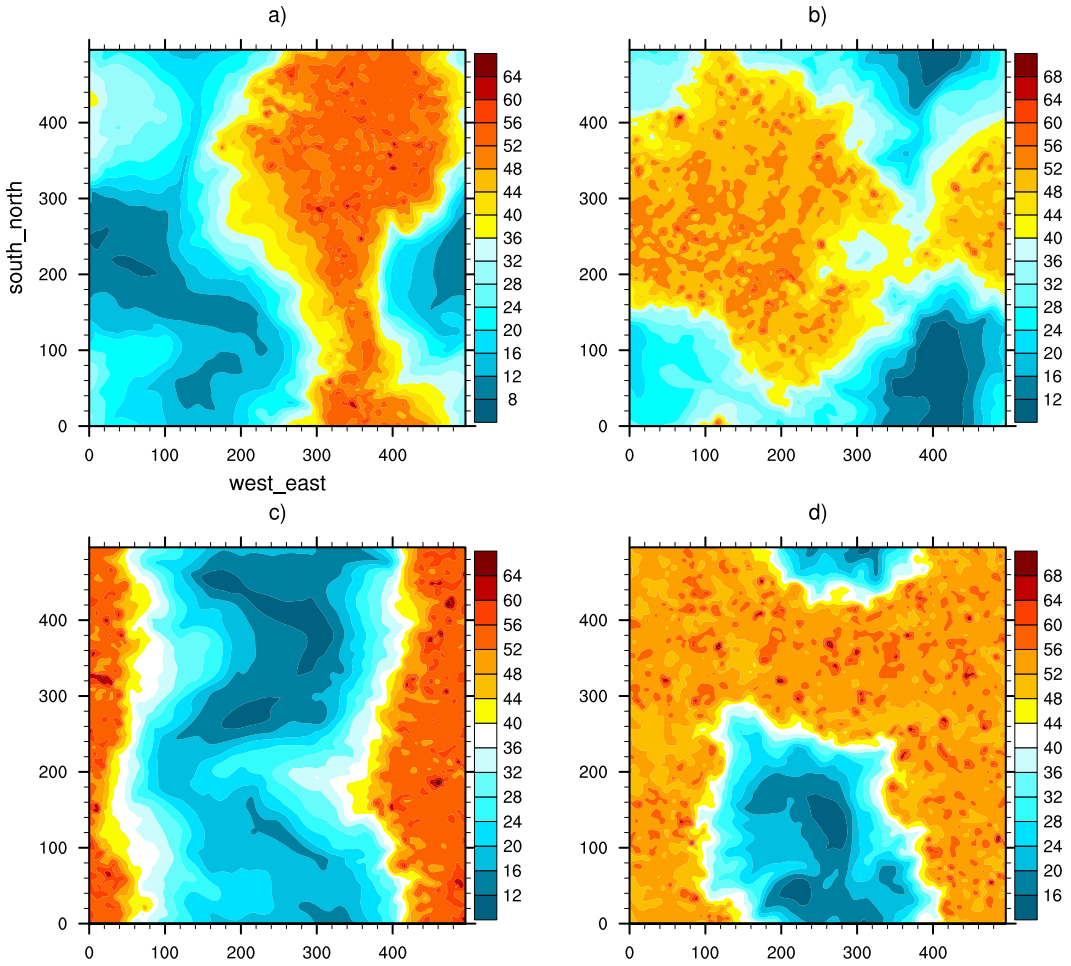

Figure 5.3: Column integrated water vapor (kg m s^{-1}) on day 70 for experiments with horizontal wind speed of a) 0 m s^{-1} b) 1 m s^{-1} c) 5 m s^{-1} d) 10 m s^{-1}.

From the aerodynamic bulk formula it is known that latent and sensible heat fluxes depend on the surface wind and thermodynamic imbalance between the surface and the underlying air. The latent heat flux is driven by surface wind and moisture imbalance between the surface and the underlying air. In the control experiment, it was observed that when the variation in the latent heat flux between the moist and dry regions is small, the gustiness of the wind offsets the higher air-sea enthalpy disequilibrium value found in the driest quartile. The gustiness therefore causes the surface fluxes to be a positive feedback during the onset of the self-organisation, despite the increasing

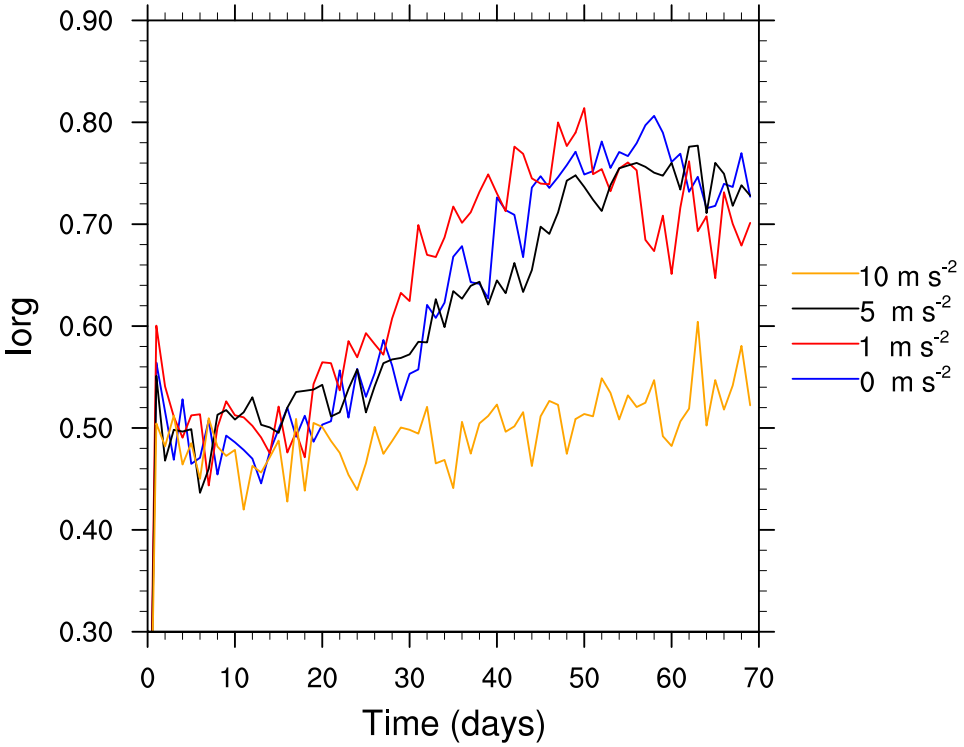

Figure 5.4: Time series of organisation index (I_{org}) for experiments with horizontal wind speed of 0 m s^{-1}, 1 m s^{-1}, 5 m s^{-1} and 10 m s^{-1}.

disequilibrium. This result is consistent with Wing and Emanuel (2014), who reported a net positive feedback of surface flux during the initial period of their simulation.

In order to emphasize on the distribution of the fluxes in dry (leftmost) and moist (rightmost) regions, the deviation from the domain average value of the surface fluxes are arranged based on their TCWV values are shown in figure 5.5 and 5.6. The plots show the initial (day 10) and the last stage (day 70) of the simulation. The deviation from the domain average value of latent heat flux on the initial stage is found to increase in the moistest region for experiment wind1 and wind5, similar to the control experiment. This enhancement of the flux is a result of gustiness observed in convectively active region. This effect is a positive feedback for the onset of self-organisation as indicated in the control run. In contrary, experiment wind10 did not show an increase of latent heat flux in the moistest region. This is due to the fact that the imposed mean wind exceeds the typical wind gust magnitude. Thus the downdraft winds offset the imposed wind in one direction, and increase them in the other. As these effects cancel each other, the wind gustiness does not act as a positive

feedback to organisation in the early stages of this experiment, as it does in the lower wind speed experiments. As a result, the onset of self-organisation is significantly delayed as indicated by organisation index (Fig. 5.4).

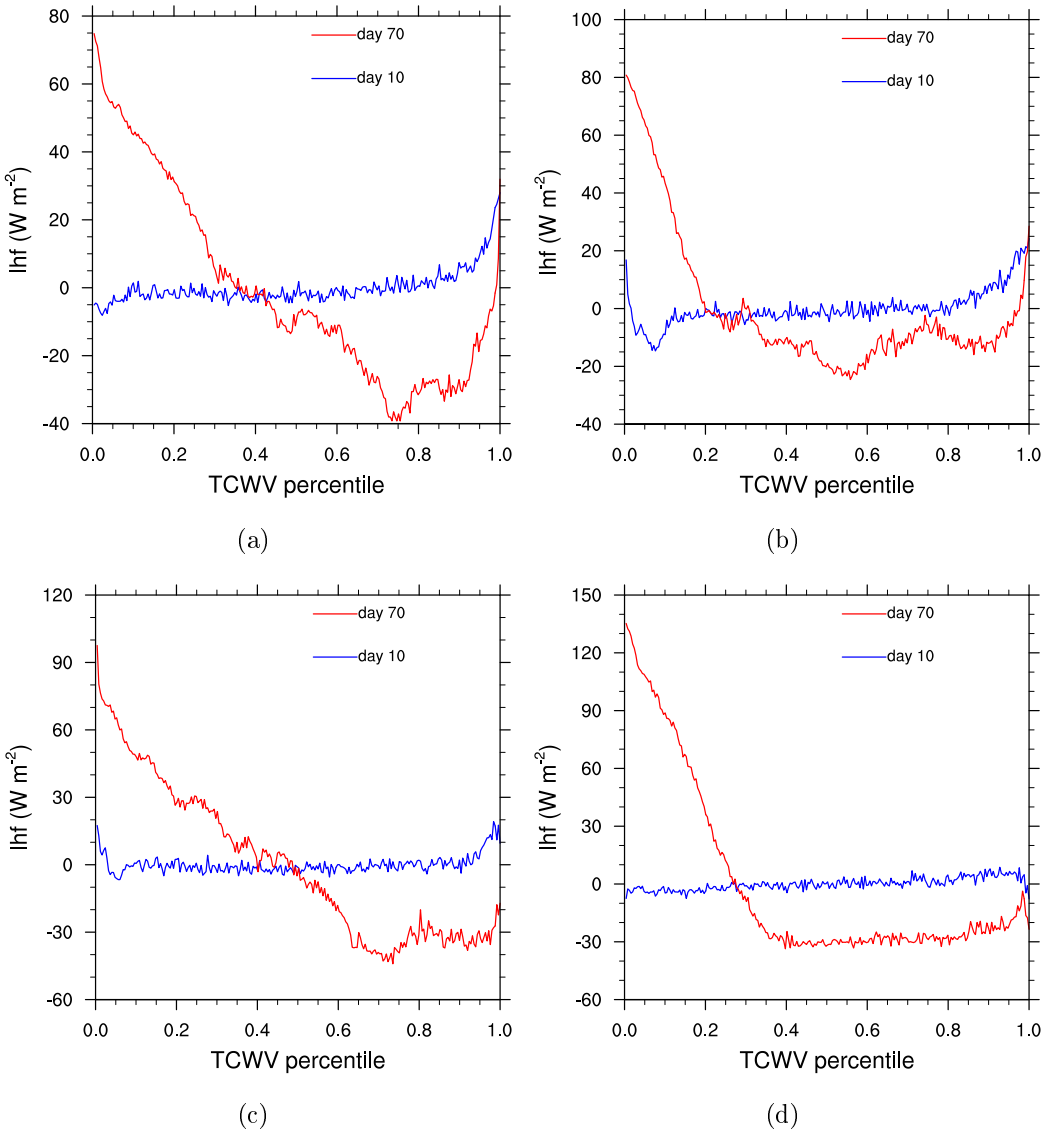

Figure 5.5: The departure from domain mean of latent heat flux arranged based on TCWV on day 10 and 70 for experiments with horizontal wind speed of a) control experiment 0 m s^{-1} b) 1 m s^{-1} c) 5 m s^{-1} d) 10 m s^{-1}.

Figure 5.5 also shows the latent heat flux distribution on the last day of the simulation. All experiments display higher values of latent heat fluxes in the dry region. This is due to the difference in moisture value of surface and the underlying air, and it is shown in the control experiment that the air-sea enthalpy disequilibrium enforces a negative feedback for the organisation of

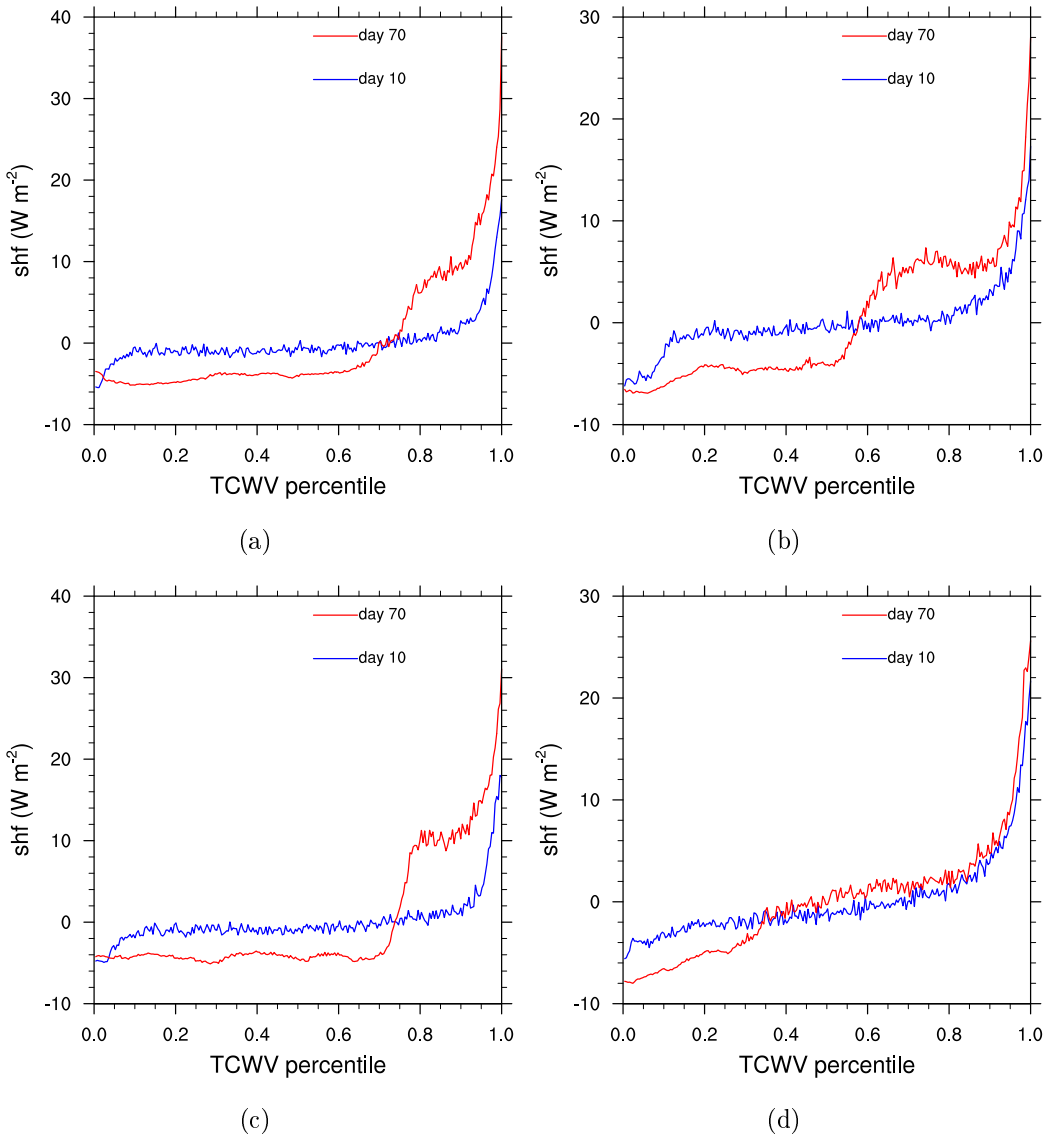

Figure 5.6: The departure from domain mean of sensible heat flux arranged based on TCWV on day 10 and 70 for experiments with horizontal wind speed of a) control experiment 0 m s^{-1} b) 1 m s^{-1} c) 5 m s^{-1} d) 10 m s^{-1}.

convection (Wing and Emanuel, 2014).

It is recalled that in the control experiment the sensible heat flux was found to be a positive feedback in the moistest regions during the matured state of self-aggregation. This effect is related to cold pools and gustiness of winds that facilitate the enhancement of sensible heat flux and localization of convection in this region (Tompkins, 2001b; Wing and Emanuel, 2014). A similar enhancement in sensible heat flux is found in all experiments as shown in figure 5.6. During day 10, the enhancement of sensible heat flux is observed

in the moistest 8% (approximately) of the bins (rightmost). It indicates that the organisation process is not yet intensified and there is a small indication for the enhancement of the sensible heat flux by the cold pools. However, in the later stage of the simulation the distinction between dry and moist regions is apparent (Fig. 5.3). As a result, the role of cold pools in enhancing the sensible heat flux is clearly visible as shown in experiment wind1 and wind5 (Fig. 5.6). This effect is not so clear in the wind10 experiment where the enhancement rate of sensible heat flux is almost the same during the beginning and latter stages of the simulation. This effect can be related to a slow expansion of the dry region that is caused by a delayed onset of self-organisation.

The sensitivity experiments highlighted the role of the background mean wind and suggest that, if the imposed wind is larger than the magnitude of the surface wind gust associated with convective downdraughts and cold pool formation, then the wind gust enhancement of surface fluxes is negated and the onset of organisation is strongly suppressed. Many previous idealized studies have either imposed zero mean winds, or low wind speeds develop during the course of the simulation (Held et al., 1993; Tompkins and Craig, 1998a; Wing and Timothy, 2015). Does this mean that these idealized setups exaggerate the effect of wind feedback on organisation? Examining the statistics of surface winds at the meteorological station in Darwin, Australia which is situated at 12S as an example, most months the mean wind speeds lies in the 2.7 to 8.3 m s^{-1} range the majority (roughly 70 to 90%, depending on the calendar month) of the time. At the upper end of this range the wind feedback is likely to be subdued, while at the lower end, gustiness is still important. Further experiments with the WRF model in realistic situations would help to put the wind feedback into context.

5.2 Interactive SST

The control experiment which displays the characteristics of self-organisation used a fixed SST value of 301.5 K. However, it is possible that the introduction of an interactive SST that can respond to changes in surface flux forcing (both latent/sensible and radiative) may result in additional feedback mechanisms that could either amplify or counter the organisation of convection. For example, the enhanced downwelling shortwave radiation in the convectively sup-

pressed area should lead to enhanced SST (sometime termed SST hot spots Waliser, 1996; Tompkins, 2001c). This will act as a negative feedback that may slow the development of organisation or perhaps even ultimately lead to convection if the atmosphere moistens sufficiently to permit it. For instance, Grabowski (2006*a*) used a slab ocean model with a fixed oceanic mixed layer depth of 5 to 45 m and showed the restriction of large scale organisation during an interactive SST experiments due to negative convective-SST feedback. In addition, positive feedbacks such as the gustiness effect discussed above may be weakened if the surface is allowed to cool in response to enhanced latent heat fluxes.

Several previous authors have examined the impact of an interactive surface. Bretherton et al. (2005) implement a slab ocean of 2 m depth and briefly describe that the effect is to slow down the organisation onset in their experiments. The mean SST was not constrained in their set up and the models start to drift toward the end of the experiment. This raises the issue of the adjustment time scale when the surface is allowed to interact with surface fluxes and Cronin and Emanuel (2013) point out that the adjustment to equilibrium is much slower with an interactive surface, on the order of 100 days or more, slower than the radiative-subsidence overturning time scale of 30-40 days identified in Tompkins and Craig (1998b). Romps (2011) and Khairoutdinov and Yang (2013) also used an interactive ocean but did not focus on the issue of organisation. Neither of those integrations constrained the SST, with the former paper applying a fixed energy sink of 120 W m^{-2} as a proxy for the combined atmospheric-ocean heat transport to higher latitudes, thus preventing unrealistically high SSTs. Both these latter experiments required O(year) long integrations and the experiments of Khairoutdinov and Yang (2013) still had not reached equilibrium by the experiment end.

We therefore extend the numerical idealized experiment framework by including the effect of an interactive lower boundary condition. Two model types are employed. Firstly we use a simple slab ocean similar to previous work, with a fixed depth, and driven by surface latent, sensible and radiative fluxes. This is then followed by a preliminary investigation that uses a more complex surface ocean model that also represents mixing of heat to a deeper ocean layer. With both of these experiments, we employ a modification to the experimental framework that has been previously employed. Similar to the

wind experiments above, a Newtonian relaxation tendency is employed to the ocean surface layer to ensure that the domain-mean SST remains close to a specified target value of 301.5 K. This relaxation term is effectively extracting the net energy imbalance and plays the same role as the fixed energy extraction applied in e.g. Romps (2011). However, by using a relaxation, we ensure that there is no adjustment process and the model reaches equilibrium on the same 30-40 day time scale. It is strongly emphasized that spatial heterogeneities in surface fluxes are free to set up SST inhomogeities in this framework, allowing spatial feedbacks involving SST to be represented; the relaxation term is identical spatially and only changes as a function of time. The timescale is set to be 1 hour which effectively extract the correct amount of heat from the domain to prevent domain-mean SST drift.

5.2.1 Slab model with fixed mixed layer depth

In order to investigate the role of interactive SST on the organisation of convection, a slab model with a fixed mixed layer depth is introduced. All the other model settings are identical to the control run. Three simulations are conducted for the duration of 60 days using a mixed layer depth of 50, 10 and 2 m, respectively. Here, these experiments are referred as dmixed50, dmixed10 and dmixed2 for the corresponding mixed layer depth of 50, 10 and 2 m simulations, respectively.

Figure 5.7 shows the horizontal distribution of TCWV on day 60 of the simulations. An organized structure is observed in control and dmixed50 experiments, where a moist convective band is stretched in south-north/west-east direction in the control/dmixed50 experiments (Fig. 5.7 a and b). In contrast, an organised structure is not observed in experiments dmixed10 and dmixed2 (Fig. 5.7 c and d), instead, these simulations display a uniformly distributed high moisture value throughout their domain.

In figure 5.8, the domain of each of the experiments is partitioned based on TCWV into four quartile regions (moistest, moist, dry and driest) to investigate the evolution of each of these regions as the simulations progress. The control experiment exhibits a large variation between the quartiles in terms of equilibrium values of TCWV due to the self-organisation process as already discussed in chapter 3 (Fig. 5.8 a). Similarly, experiment dmixed50 displays

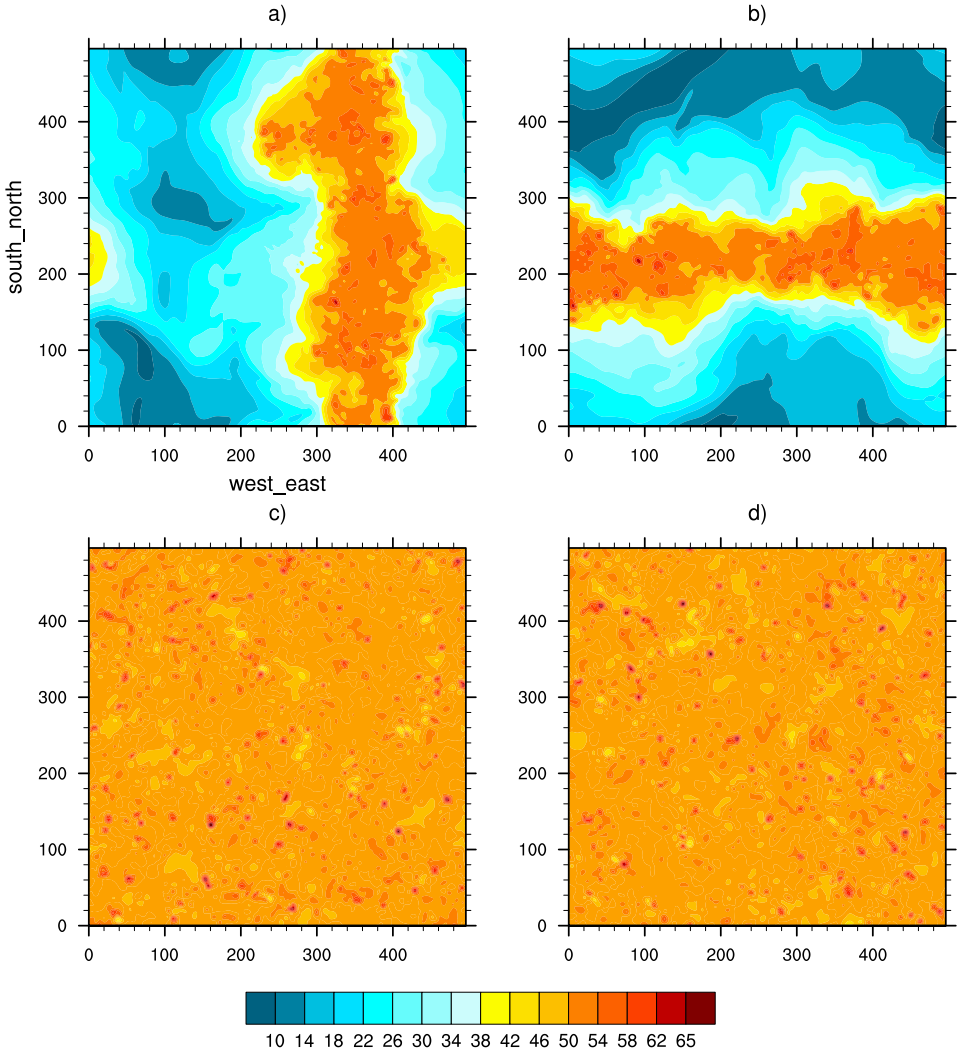

Figure 5.7: Column integrated water vapor (kg m s^{-1}) on day 60 for experiments with mixed layer depth a) fixed (no mixed layer) b) 50 m c) 10 m d) 2 m.

a wide difference among the quartiles but with a slower adjustment time scale of the quartiles when they are compared to their respective regions of the control experiment (Fig. 5.8 b). The driest quartile of experiment dmixed50 reaches equilibrium on day 42, while the control run reached on day 35 of the simulation. Additional simulation time is required to observe the equilibrium state of the intermediate (moist and dry) quartiles, while in control run, the equilibrium state of these quartiles are observed within the duration of the experiment. This indicates a possibility of further expansion of dry patch in the experiment dmixed50, if the simulation were allowed to run further. In contrast, the moistest quartile reached 52 kg m^{-2} during the first 4 days and remains close to this value as observed for the control experiment. Experi-

ments dmixed10 and dmixed2 are characterized by higher values of TCWV for all quartiles in equilibrium state with a maximum variation of 4 kg m^{-2} (Fig. 5.8 c and d). The presence of variation between the quartiles for the control and dmixed50 experiments is a diagnostic of the organised state (Bretherton et al., 2005).

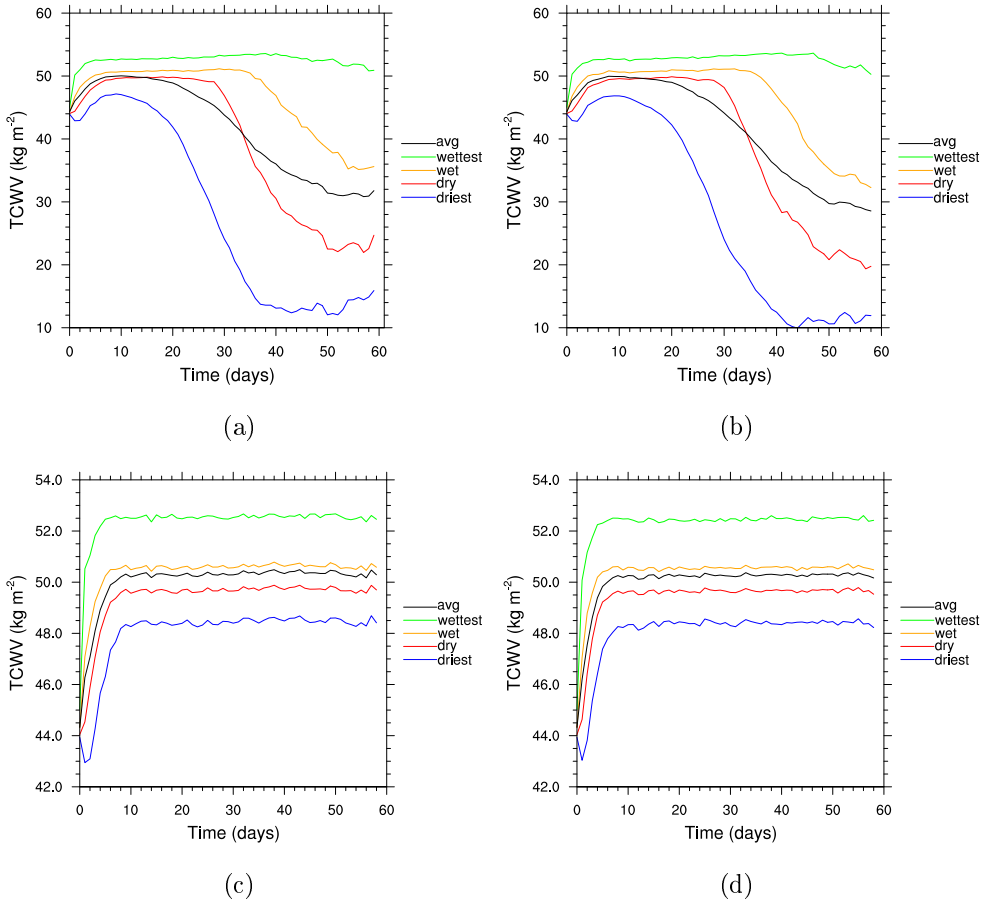

Figure 5.8: Time series of domain average total column water vapor (TCWV) for the entire integration. The black lines are domain means and the other curves are means of sub domain regions partitioned into four quartiles on the basis of their daily mean of column integrated water vapor content a) control experiment (no mixed layer) b) 50 m c) 10 m d) 2 m mixed layer depth.

The level of the observed organised structures are quantified by the organisation index (Fig. 5.9). The experiment dmixed50 reached self-organized state (with I_{org} greater than 0.5) starting from day 29, while dmixed10 and dmixed2 experiments reveal a random distribution of convection throughout their simulation with I_{org} close to 0.5. The control run reaches a self-organized state

earlier (by about 8 days) than dmixed50 experiment since the interactive SST experiment needs some more time for the dry patch to expand significantly, this can be observed by comparing the decreasing rate of the driest quartiles of the control and dmixed50 experiments (Fig. 5.8 a and b).

The following discussion focuses on the energy budget at the surface to investigate the role of an interactive SST layer on the level of organisation. It should be noted that the result obtained for experiments with mixed layer depth of 2 and 10 m are similar, hence in the following analysis only the 2 m experiment is considered for brevity.

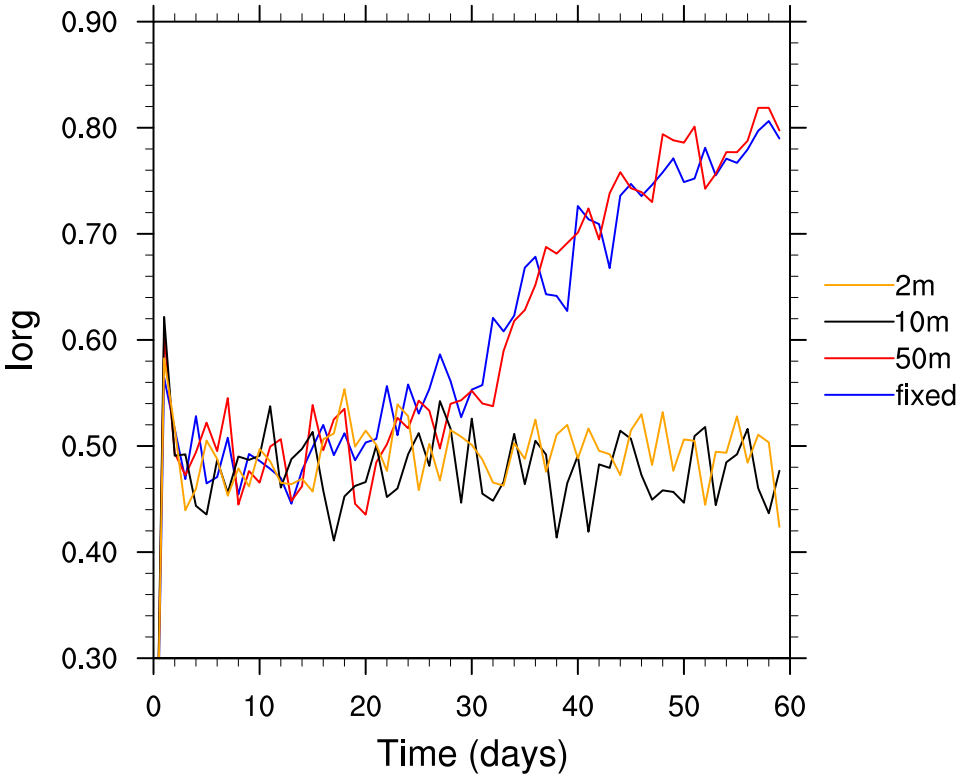

Figure 5.9: Time series of organisation index (I_{org}) for experiments with mixed layer depth of fixed (no mixed layer), 50 m, 10 m and 2 m.

Figure 5.10 a and b show the departures from domain mean of SST values for experiments dmixed50 and dmixed2, respectively, in the moisture-time field, where the variation terms are sorted based on the values of total column water vapor. The corresponding net infrared radiation from the surface are also presented in figure 5.10 c and d for the respective mixed layer depths. The dmixed50 experiment displays warming in the driest region (leftmost) and cooling in the moistest columns (rightmost) for the first 20 days of the

simulation. The SST anomalies are in the range of -0.2 to 0.2 k relative to the specified domain mean during this period of the simulation. The corresponding infrared radiation from the surface is in transition during this period and shows an increase from the value of 10 to 30 W m^{-2}. This indicates the onset of the self-organisation process initialized as a small dry patch which continues to expand as the organisation process evolves. As a result a strong SST cooling with a range of 1 K is observed on the driest columns, while an enhancement of SST is shown in the moistest part of the domain. This pattern of SST in the moisture-time field is similar to the net longwave radiation at the surface, where there is higher net outgoing infrared radiation in the driest region and SST is lower than the domain average. The opposite is true for moistest regions (5.10 a and c).

In contrast, there is no clear pattern that relates the SST anomalies of experiment dmixed2 with its net surface emitted infrared radiation (Fig. 5.10 b and d). This can be related to higher value of TCWV and insignificant difference in the moisture content of dry and moist regions, that increases the infrared opacity and limits the positive feedback of longwave radiation observed in experiment dmixed50. As a result (in experiment dmixed2), a limited variation both in the infrared radiation and SST is observed.

Figure 5.11 shows the time series of diabatic values at the surface for the experiment dmixed2 and is used to explain how the organisation/disorganisation is affected by these processes. The upward direction is considered to have a positive value and the fluxes are partitioned into four quartiles based on their TCWV values. All the diabatic terms show limited differences between the quartiles as a result of similar TCWV values (Fig. 5.8 d). Latent and sensible heat fluxes slightly enhanced in the moistest region as result of relatively higher value of convective gustiness (Fig. 5.11 a and b).

Similarly, shortwave radiation is dominated by higher values of TCWV, as a result the quartiles have similar values throughout the simulation (Fig. 5.11 c). The total amount of energy at the surface considers the shortwave radiation as input energy while longwave radiation and surface flux are extracting energy from the surface. Throughout the simulation there is no significant difference among the quartiles and all the quartiles show a net absorption (Fig. 5.11 d). Organisation does not occur as shown by the organisation index (Fig. 5.9) for this experiment.

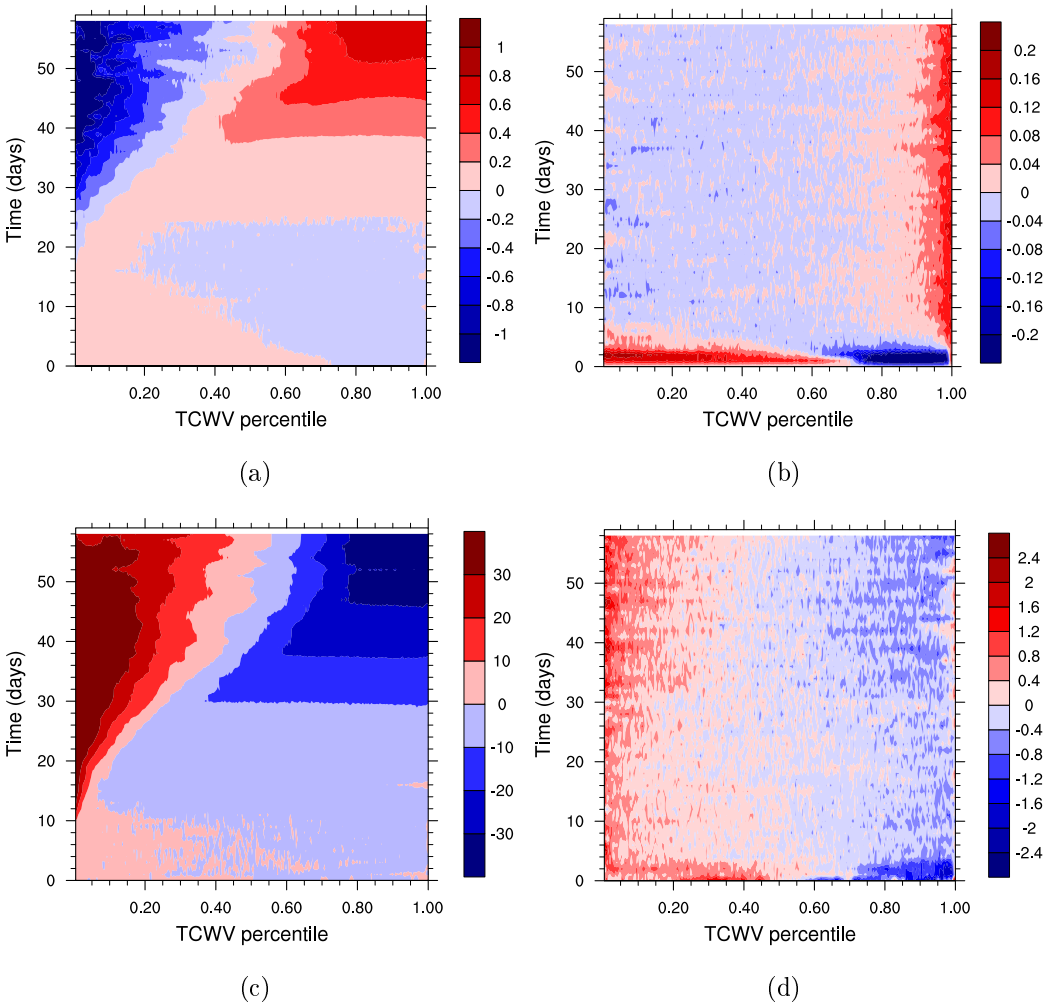

Figure 5.10: Departure from domain mean of SST values calculated for each day a) 50 m mixed layer experiment b) 2 m mixed layer experiment. Departure from domain mean of longwave radiation at the surface c) 50 m mixed layer experiment d) 2 m mixed layer experiment.

In contrast, surface terms of the dmixed50 experiment vary widely between the quartiles (Fig. 5.12). The longwave radiation emitted from the surface of the driest region started to intensify after 10 days of simulation and are doubled by day 42 as organisation establishes (Fig. 5.12 a). After this period the driest quartile remains close to the values of 125 W m^{-2} until the end of the simulation. This indicates longwave cooling is playing a significant role in the dry cool SST region by efficiently radiating to space; the radiator fins of Pierrehumbert (1995). In contrast, there is insignificant variation (2 W m^{-2}) of longwave radiation at the surface in the wettest quartile throughout

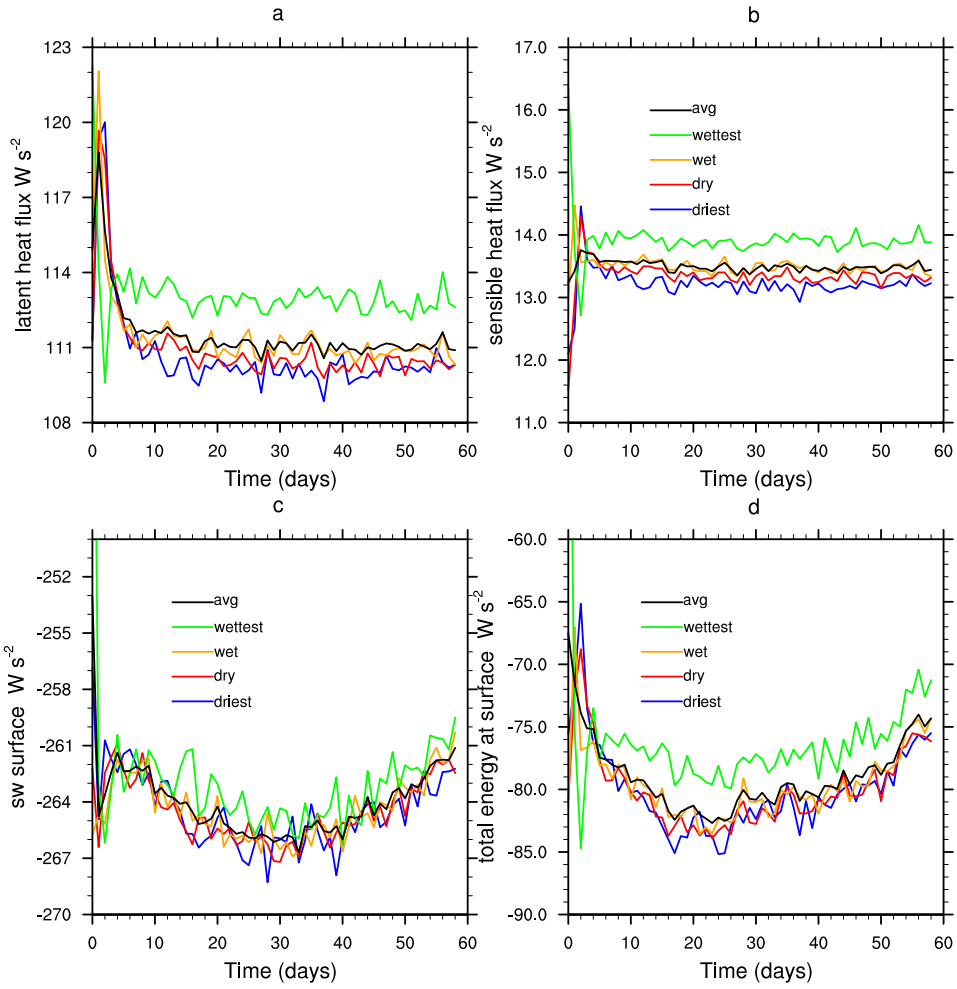

Figure 5.11: Time series of surface energy budget a) latent heat flux b) sensible heat flux c) shortwave radiation and d) net total energy at the surface for domain average and 4 quartiles. The black lines are domain means and the other curves are means of sub domain regions partitioned into four quartiles on the basis of their daily mean of column integrated water vapor content for experiment with mixed layer depth of 2 m.

the simulation period. The behavior of longwave radiation in moistest region compares well with the corresponding TCWV (Fig. 5.8 b).

The difference between the driest and moistest quartiles of shortwave radiation flux arriving at the surface increases as the organisation process matures (Fig. 5.12 b). The shortwave radiation started to intensify following the on-set of self-organisation around day 16 from the value of 270 to 315 W m^{-2} within 26 days and then remains close to this value until the end of the simulation. On the other hand, the shortwave radiation in the moistest region drops by

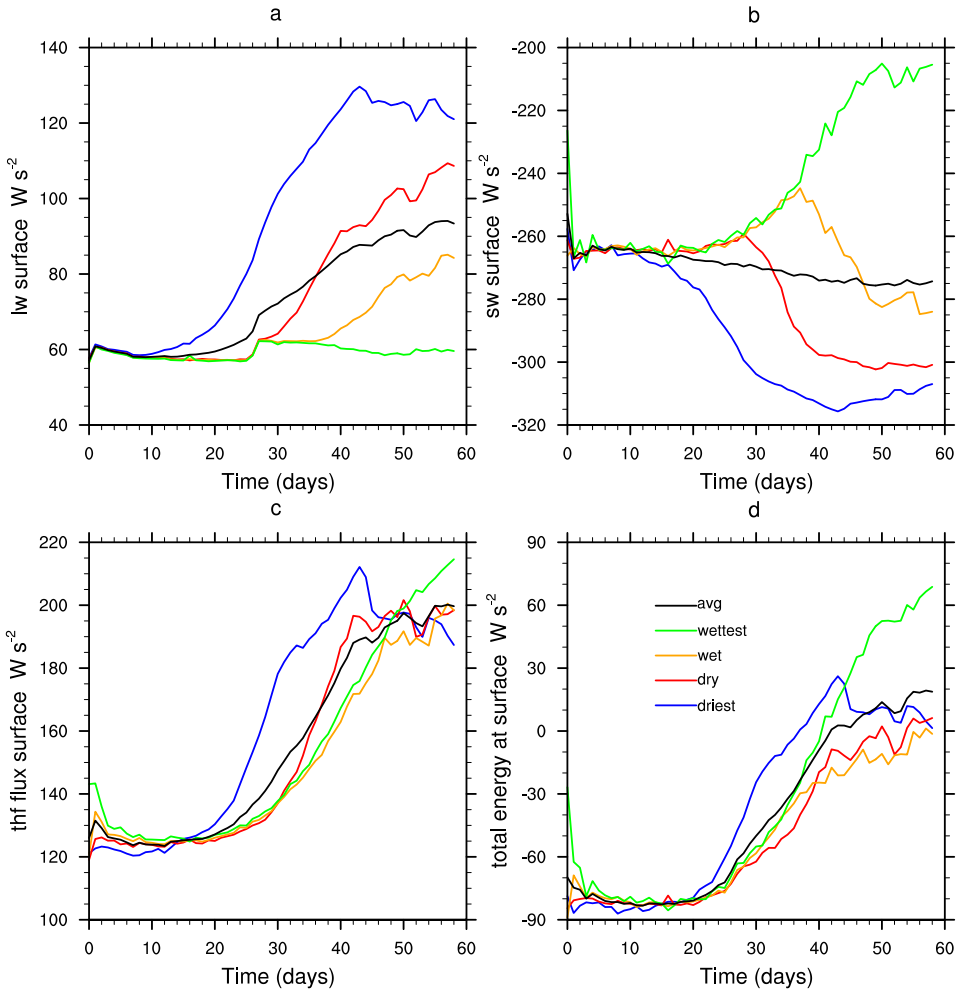

Figure 5.12: Time series of surface energy budget a) longwave radiation b) shortwave radiation c) total heat flux and d) net total energy at the surface for domain average and 4 quartiles. The black lines are domain means and the other curves are means of sub domain regions partitioned into four quartiles on the basis of their daily mean of column integrated water vapor content for experiment with mixed layer depth of 50 m.

60 W m^{-2} within the first 50 days and after that it stays close to this equilibrium value. This is due to increasing absorption of shortwave radiation by water vapor and cloud anvils reducing insolation over precipitating regions (e.g Bretherton et al., 2005; Wing and Emanuel, 2014).

The surface fluxes in the driest quartile increases substantially as the the atmosphere gets drier (Fig. 5.12 c). The increasing pattern of surface flux is similar to the latent heat flux (Fig. 5.13 a), since sensible heat flux is dominated by latent heat flux over the ocean surfaces as described in chapter

3. As a result, the contribution of the decreasing pattern of sensible heat flux in the driest region due to the influence of subsidence is barely discernible in the plot of surface fluxes (Fig. 5.12 c).

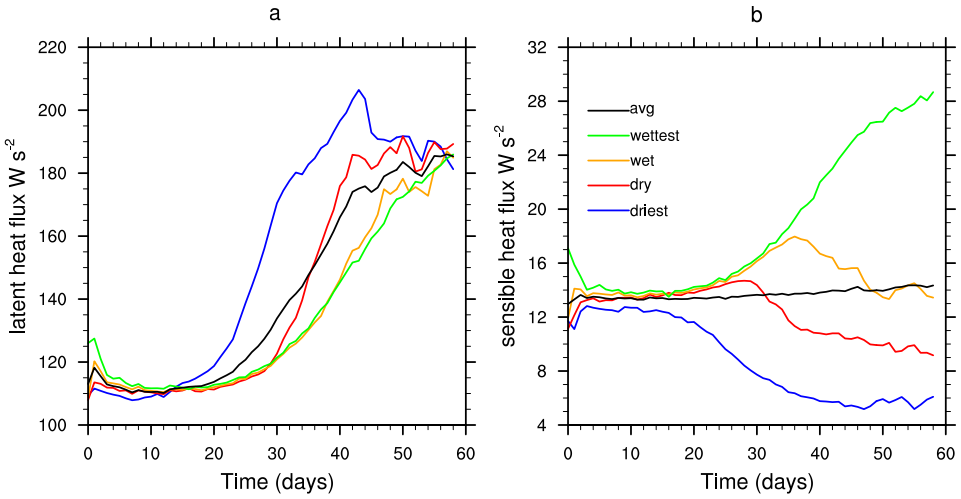

Figure 5.13: Time series of surface energy budget a) latent heat flux b) sensible heat flux. The black lines are domain means and the other curves are means of sub domain regions partitioned into four quartiles on the basis of their daily mean of column integrated water vapor content for experiment with mixed layer depth of 50 m.

However, the effect of sensible heat flux significantly increases in the moistest quartile as the self-organisation process matures (Fig. 5.13 b). This is caused by the effect of cold pools and convective gustiness, which are a key positive mechanisms for self-organisation processes (e.g Tompkins, 2001b; Bretherton et al., 2005). Convective gustiness also enhances latent heat flux in this region (Fig. 5.13 a). The combined effect of these fluxes remarkably enhance the total surface heat flux as well as the net total energy at the surface during the matured state of the organisation process in the moistest region (Fig. 5.12 d). This is an important positive feedback for self-organisation process, which was not observed to play a critical role for the control run 3.11 a.

The dmixed10 and dmixed2 experiments are characterized by insignificant difference in the content of moisture across the domain. This is observed to highly affect the feedback from the radiation and surface fluxes. This supports the hypothesis that states enhancement of shortwave radiation in non-convective region will allow convection if the atmosphere is moist enough. This result is not consistent with Bretherton et al. (2005), who found a significant

delay in the self-organisation of convection in the presence of mixed layer layer depth (2 m). In their simulation, the shortwave radiation which was initially a negative feedback in convective region by reducing the solar radiation is dominated in the latter stages by the dry regions that start to efficiently radiate infrared radiation to space. However, this radiative cooling in the dry region is not observed to be strong in these experiments as observed for experiment dmixed50. Surface flux feedback is also limited, which was observed to be a positive feedback for the onset of self-organisation in the control and dmixed50 run (Tompkins and Craig, 1998a).

5.2.2 A slab model with varying mixed layer depth

An additional preliminary experiment is conducted using a slab model that allows the evolution of the mixed layer according to an imposed wind stress, in addition to mixing of heat between the surface mixed layer and a deeper 200 m layer. The model is outlined in Pollard et al. (1973). Similar to the fixed mixed layer experiments, a Newtonian relaxation towards a temperature value of 301.5 K is applied on the time scale of an hour. The initial mixed layer depth is 2 m throughout the domain and the simulation is conducted for the duration of 100 days in order to observe the longer adjustment time scale. Thus, in areas subject to gustiness the ocean mixed layer depth will deepen rapidly, reducing flux feedbacks, while the deep can reduce in the dry regions subject to low wind speeds.

The departure from the domain mean of SST sorted based on their TCWV is displayed in figure 5.14. A strong cooling of SST is observed in the dry columns while the moist columns indicate an increase in SST. The spatial variation is on the order of 1.5 K which is much higher than dmixed10 and dmixed2 experiments. An oscillating behavior between higher and lower cooling is observed with approximate time scale of 40 days, the cause of which is not certain and requires further investigation. Randall et al. (1994) suggested that radiative-convective states can undergo such oscillations. The moistest columns are characterized by enhancement of SST in the range of 0.3 K to 1 K throughout the integration period and equilibrium is not fully reached within the hundred days, in accordance with Cronin and Emanuel (2013)

The general behavior of interactive SST that allows deepening of mixed

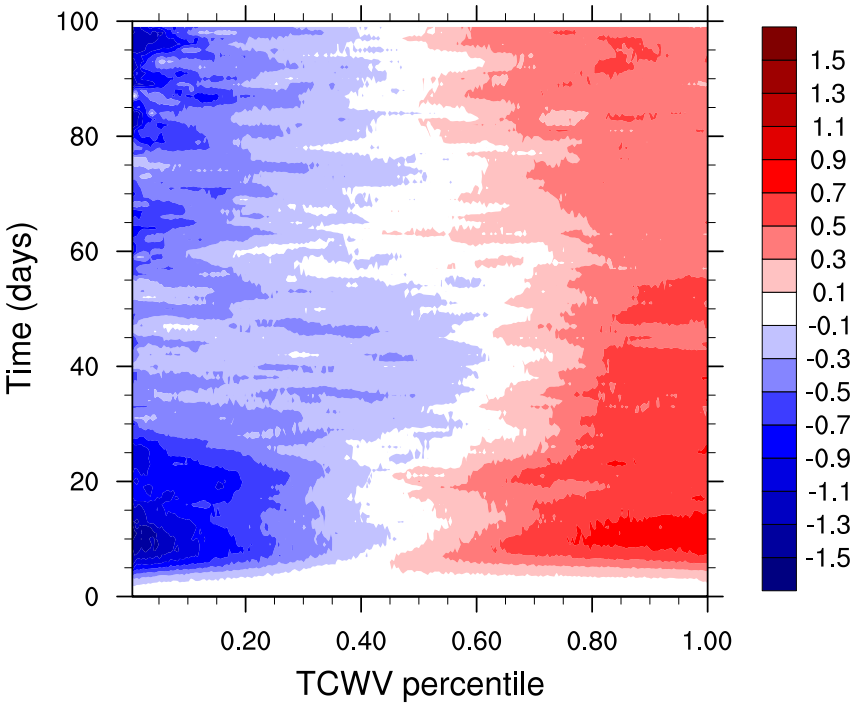

Figure 5.14: Departure from domain mean of SST values calculated for each day and arranged based on TCWV on the Hovmuller plot of 100 days for the experiment with varying mixed layer depth.

layer can be analyzed by considering the radiation and surface fluxes at the surface. These fluxes are partitioned into four quartiles (moistest, moist, dry and driest) based on their TCWV value at each time step. The surface fluxes do not demonstrate significant differences between the quartiles (Fig. 5.15 c) especially towards the end of the simulations. In contrast, the longwave and shortwave radiations display a significant spatial variations between the quartiles (Fig. 5.15 a and b).

The shortwave radiation arriving at the surface decreases as the simulation progress (Fig. 5.15 b). This is due to increasing absorption of shortwave radiation by water vapor and cloud anvils reducing insolation over precipitating regions (e.g Bretherton et al., 2005; Wing and Emanuel, 2014). The decreasing rate of shortwave radiation reached to equilibrium around day 50 for the fixed SST and dmixed50 experiments but in this experiment the shortwave radiation doesn't reach to equilibrium even after 100 days of simulation. By day 100 the amount of shortwave radiation arriving at the surface in the moistest column is 200 W m^{-2} which represents a reduction of 80 W m^{-2} from the initial period. In contrast, the driest quartile receives about 260 W m^{-2}, which represents the

highest incoming shortwave radiation during the last day of the simulation.

The longwave radiation emitted from the surface displays a variation 60 - 70 W m^{-2} (Fig. 5.15 a). The driest quartile increases by 70 W m^{-2} within the first 10 days of the simulation and remains close to this value until the end of the simulation, while insignificant variation is observed for the moistest quartile. This indicates longwave cooling is playing a significant role in the dry cool SST region by efficiently radiating to space. As a result the dry region is associated to cold SST despite an increase of incoming shortwave radiation. This is also observed in the total energy flux at the surface where higher release of energy is observed in the dry region which can be a possible reason to observe lower SST in the dry region (Fig. 5.15 d).

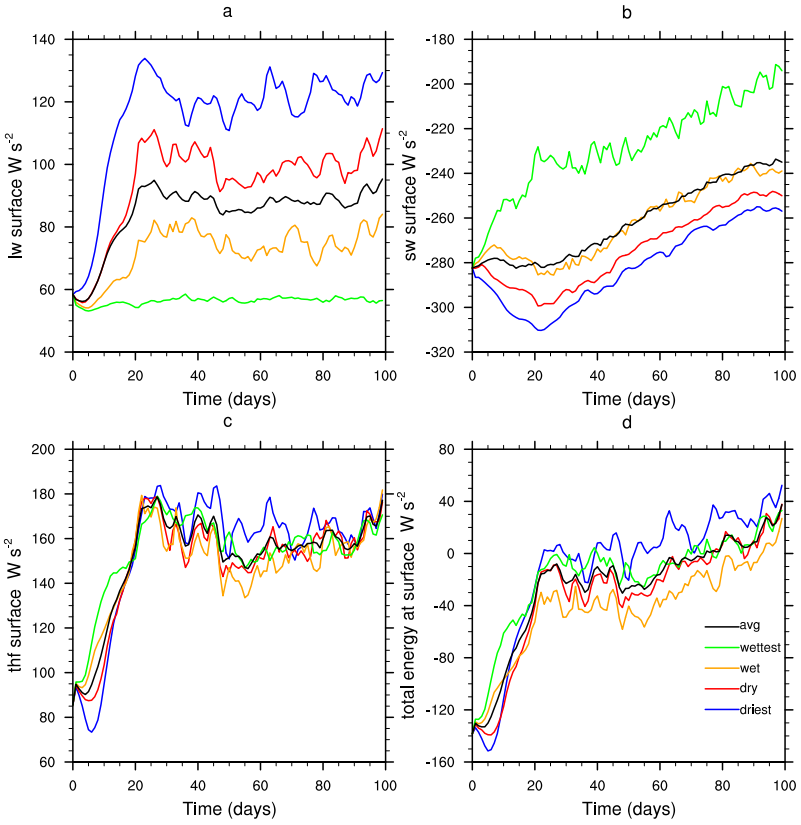

Figure 5.15: Time series of surface energy budget a) longwave radiation b) shortwave radiation c) total heat flux and d) net total energy at the surface for domain average and 4 quartiles.

Figure 5.16 shows the time series of TCWV partitioned into four quartiles (moistest, moist, dry and driest). The moistest quartile reach to the maximum value of 59 kg m^{-2} within the first 6 days of the simulation. This value

is higher by about 7 kg m^{-2} than the control and dmixed50 experiments. The other quartiles require at least 20 days to reach to their minimum values, corresponding to the subsidence time scale (Tompkins and Craig, 1998b). Despite higher values of the moistest quartile, the driest quartile and the domain average TCWV values are similar to the control experiment. This highlights the presence of strong organisation in the interactive SST experiment with varying mixing layer depth.

As stated above, the simulations with the interactive mixing layer depth are very preliminary, and further analysis needs to be conducted to additional diagnostics to quantify the magnitude of the heat fluxes to the deep ocean and to ascertain why the reactive mixing layer depth may act to maintain the ability to evolve to organised states.

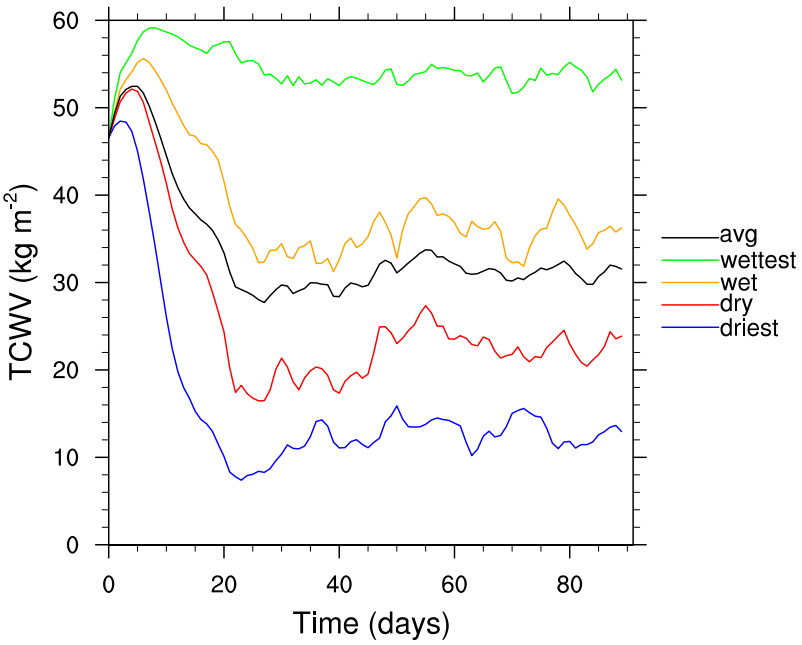

Figure 5.16: Time series of domain average Total column water vapor (TCWV) for the entire integration. The black lines are domain means and the other curves are means of sub domain regions partitioned into four quartiles on the basis of their daily mean of column integrated water vapor content.

5.2.3 Summary

Two types of slab ocean models are considered for the interactive SST experiments. The first set of experiments are conducted using a fixed mixed layer

depth of 50, 10 and 2 m. These sensitivity tests exhibit different organisation behavior based on their mixed layer depths. The experiments with a shallow mixed layer depth (dmixed10 and dmixed2) don't undergo self-organisation. In these experiments, a uniformly distributed high moisture value is observed to suppress the expected positive feedback from infrared radiation. The initial hypothesis is that self-organisation could potentially be prevented by short-wave feedback with an interactive SST which is partly confirmed by these fixed mixed layer depth experiments. Experiment (dmixed50) with deeper mixed layer doesn't respond much to perturbations similar to the fixed SST experiment, as a result it displays organisation behavior with a strong positive feedback of longwave radiation and surface fluxes.

A second preliminary experiment allows the deepening of mixed layer depth and heat transfer to the deeper ocean and is found to display the characteristics of self-organisation and an intriguing 40 day oscillation in the equilibrium state. This experiment requires further investigation to understand the long adjustment time scale observed in SST. In general, the interactive SST experiments suggest additional mechanisms that can possibly affect the organisation process, if the surface layer is shallow enough to respond significantly to perturbations in surface fluxes. Such a situation may arise in the tropics in low wind conditions. These experiments can be considered as an initial attempt to understand organisation processes observed in more realistic situations by introducing more realistic lower boundary conditions.

Chapter 6

Conclusions

Clusters of convective clouds are an important phenomena in the tropics that occur over a wide range of spatial and temporal scales. Convection manifested in organised systems is responsible for the majority of tropical rainfall and the process of organisation has also been recently suggested as a potential regulator of climate, hence understanding how and why tropical convection organizes is important to improve our insight on the tropical and global climate variability. An in-depth understanding of the mechanisms that lead to organisation will pave the way to the inclusion of the effect of self-organisation in parameterizations of convection in global circulation models.

Towards this goal, three dimensional idealized modelling of convective organisation in radiative-convective equilibrium (RCE) was employed. The tool for this experimentation was a model that employed convection-permitting horizontal resolutions (CRM). The general setup of the model uses a domain size of 500 by 500 km as suggested by Muller and Held (2012), who found self-aggregation on domain size larger than 200 km. The general set up was idealized, with periodic lateral conditions implying no interaction with the larger-scale flow, no topography, and an underlying ocean surface. The model was used to conduct a number of long term simulations ranging from 15 to 100 days in order to address the research questions set out in the introduction of this thesis:

- Using a fixed-SST, convection permitting CRM experiment, can we reproduce the results of previous research regarding the spontaneous organisation and its key drivers?

This question is addressed in chapter 3, which discusses in detail the control experiment conducted using fixed SST with no mean wind and Coriolis force for the duration of 70 days. The system displays a small dry patch in the early stage of the simulation and this dry patch eventually expands and dominates most of the domain. This is indicated by a significant difference in TCWV between dry and moist quartiles as the simulation evolves to equilibrium states. The variation between dry and moist region is also manifested in the vertical profiles of RH and hydrometers, where the profiles of the dry quartiles were increasingly get drier while the moist quartiles become moister as the self-organisation process intensifies. As a result, the domain is divided into a moist region where all convection occurs and a dry region where all convection is suppressed.

To better quantify the state of organisation, a simple organisation index, I_{org}, is introduced in the thesis based on the comparison of nearest neighbour distances between updraft cores to the expected distribution if the convection were randomly organised. I_{org} provides precise information on the level of clustering (greater than 0.5), randomness (equal to 0.5) and regularity (less than 0.5) of convective fields at equilibrium, and potentially allowed the clustering to be determined as a function of spatial scale, and also for the statistical testing to be conducted on the organisational state classification. For the control run, the I_{org} index also confirms the onset and intensification of self-organisation with higher values (greater than 0.5) starting from around day 20 of the simulation.

The mechanisms responsible for the organisation of convection are investigated using frozen moist static energy budget and the diabatic correlation terms, using Wing and Emanuel (2014) approach. Horizontal convergence of vertically integrated FMSE and diabatic processes are demonstrated in the context of their impact on the evolution of self-organisation process. The diabatic processes include the involvement of shortwave, longwave, latent heat and sensible heat fluxes are found to vary their feedback roles at different stages of the organisational process. For instance, longwave radiative feedback is positive during the first 20 days of the simulation both in dry and moist regions of the domain but later on the longwave radiative feedback in dry regions is changed to a negative feedback. The reason for change of sign in the feedback of longwave radiation is related to the response of longwave cooling to

the dry perturbation that is found to vary in space and time of the simulation. Similar to the recent analysis by Emanuel et al. (2014), at the outset of the experiment, the dry patches form first in the upper troposphere. This reduces the emissivity of the upper troposphere and thus increases net IR cooling from the lower troposphere in the driest regions. The result is a diabatic forcing of the lower tropospheric circulation, driving convergence towards the moistest regions (note that this is shown to be dependent on the sensitivity of convection to the moisture through entrainment mixing in chapter 4). However, as the simulation and the organisation of convection progresses, the moisture perturbation develops in the vertical and impacts the humidity in the lower troposphere in the dry regions. The result is that the emissivity also reduces in these regions and the IR feedback reverses between the moderately dry and driest regions.

In contrast, the shortwave radiation flux is a positive feedback in all stages of the self-organisation process in almost all part of the domain since the amount of shortwave radiation absorbed by atmosphere increases with increasing water vapor content. The surface flux feedback is a positive feedback during the initial stage of the simulation since the gustiness of the wind offsets the air-sea enthalpy disequilibrium value found in the driest quartile. However, in the later stages of the simulation negative surface flux feedback is indicated due to the dominance of air-sea enthalpy disequilibrium.

All the feedback mechanisms in the moisture-time field demonstrate a strong link between the organisation processes and the way the diabatic forces responds. Furthermore, the upgradient transport of FMSE is a positive advection feedback which is observed in the intermediate stages of the simulation. The interchanging roles of different mechanisms at different stages of the simulation for the control run are found to be generally consistent with the experiment of Wing and Emanuel (2014), who provided evidence for a distinction between the feedbacks that initialize and maintain the self-aggregation of convection. This is encouraging since it indicates that the general role of these feedbacks may not be overly dependent on the model physics employed, since the modelling system employed here is distinct from the one used by Wing and Emanuel (2014). That said, it is noted that anvil feedback in the shortwave appear to be possibly understated in both models, and suggests that, the formation of organised states is highly sensitive to the choice of the subgrid-scale

turbulence scheme employed.

- How does the basic experimental framework such as imposed wind affect the organisation?

In order to investigate the role of imposed winds on self-organisation, additional experiments are conducted using an imposed wind of 1 ms^{-1}, 5 ms^{-1} and 10 ms^{-1} in the model west-east direction. The experiments indicate the presence of self-organisation in all the experiments, however the experiment with 10 ms^{-1} imposed wind has indicated a delay on the onset of self-organisation. This effect is related to the influence of imposed wind in affecting gust fronts of cold pools. Hence, it is suggested that if the imposed wind is strong enough to halt the spread of the gust front, it can slow down the organisation process.

- How does the updraught entrainment process and its representation in the subgrid parameterization affect the equilibrium state?

Similar to previous studies in this field, the experiments in this thesis employed 2 km horizontal resolution. Since this grid spacing resolves deep convective cores marginally, all entrainment into updraught cores is represented by the subgrid-scale turbulence scheme and thus a number of sensitivity tests to the mixing scheme choice are conducted to identify how the sub-grid mixing determined entrainment affects the self-organisation. The role of updraught entrainment process on the organisation of convection is investigated in chapter 4. The representation of sub-plume turbulence and entrainment processes depend on sub-grid scale parameterizations such as first order Smagorinski approach applied in 2 or 3 dimensions and a 1.5 order TKE closure. A number of experiments are conducted by varying the sub-grid mixing schemes and it is found that self-organisation is sensitive to the choice of these schemes.

Two experiments use the 3D Smagorinski approach to calculate their horizontal sub-grid mixing coefficient (xkmh), which accounts for the full 3D wind shear tensor (most critically regarding convective entrainment, including the horizontal shear of the vertical wind component) and the vertical buoyancy gradient. In one experiment the calculation of the vertical mixing coefficient (xkmv) uses the YSU PBL scheme which can also account for non-local mass transport; while in the second, the 3D Smagorinski also handles vertical mixing with the local approach. Both schemes lead to the strong organisation of

convection, although the strength of the organisation is slightly greater with the non-local vertical mixing, which apparently increased the rate at which the growing dry perturbation was mixed vertical throughout the troposphere.

Experiments that use the same YSU PBL scheme for the vertical subgrid mixing but vary the calculation of horizontal mixing by replacing the 3D Smagorinski approach with either the 2D version of the scheme (that pointedly does not include the vertical wind shear term) or the 1.5 order TKE scheme showed drastic differences, in that convection organisation was absent when the 3D Smagorinki scheme was not employed. This indicates that horizontal mixing had a very strong influence on the establishment of organisation, stronger than the vertical mixing.

Horizontal mixing can potentially play two roles in the organisation of convection, acting as both a positive and negative feedback. For example, horizontal mixing between the dry and moist regions would tend to remove large scale gradients of moisture and destroy organisation, as in the experiments of Grabowski and Moncrieff (2004) who employed a horizontal Newtonian relaxation term as an artificial strong mixing between moist and dry regions and destroyed convective organisation as a result. It is likely that mixing on the mesoscale is underrepresented in these idealized modelling frameworks where periodic boundary conditions are employed with zero shear at the domain scale. Eddies at the scales approaching the domain size are likely underrepresented as evidenced by the spectra of Wing and Timothy (2015) which show less activity than expected on wavelengths exceeding one tenth of the domain length. However, this lack of mesoscale eddies is an issue of the experimental set up (which is being investigated with further experiments not reported in this thesis) and is not an artifact of the turbulence scheme, since away from the convective updrafts in the free troposphere, flow is approximately laminar and all three turbulence closure approaches simply diagnose the minimum or close to the minimum diffusion mixing.

The second way in which mixing is important, is the entrainment in updrafts. Entrainment is still poorly understood and the subject of active research with high resolution models (Romps, 2010; Romps and Kuang, 2010b; Sherwood et al., 2013) but it is clear that with a 2 km resolution that results in updrafts of one or a few grid points that the turbulence scheme is responsible for all entrainment mixing. In contrast to mesoscale mixing in the

horizontal, entrainment mixing is a strong positive feedback on organisation. This is because entrainment of dry air causes much evaporative cooling and reduces updraught buoyancy. Thus strong entrainment mixing only allows the survival of deep convection and its ability to reach the radiative tropopause in moist regions; a positive feedback on organisation. Without the vertical wind shear source term, the 2D Smagorinski scheme produced very weak entrainment mixing, meaning deep convection can occur in regions with a developing upper tropospheric dry patch, detraining water there and negating the dry patch as a result, preventing the onset of convective organisation.

The 1.5 order TKE scheme does include a vertical wind shear term, but possibly as a result of the prognostic nature of the scheme and the scheme's parameter setting choices, horizontal mixing, while enhanced near updraft cores, was nevertheless considerably weaker than with the use of the 3D Smagorinski scheme and convection organisation did not occur. If the above hypothesis that entrainment mixing is key for organisation is correct, the theory predicts that increasing the mixing strength of the TKE scheme should lead to convective organisation. A series of experiments were therefore conducted increasing the eddy transport coefficient, which would act to scale the turbulence field without changing the spatial distribution. These experiments demonstrated that increasing the mixing by approximately a factor of three was sufficient to reestablish convective organisation in the experiments. The results of chapter 4 thus show that the entrainment mixing process appears to be a necessary but non-sufficient condition for the onset of self-organisation.

- How does the boundary conditions such as employing an interactive SST affect the self-aggregation state?

This question is the topic of section 5.2, which introduce two different slab ocean models to investigate the role of interactive SST in self-organisation process. The first slab model imposes a fixed mixed layer depth. Three experiments are conducted using a fixed mixed layer depth of 50, 10 and 2 m, and exhibited different organisation behavior based on their mixed layer depths. The experiments with shall mixed layer depth (10 and 2 m) prevent organisation, while the 50 m experiment display organisation structure. The former two experiments indicate the possibility of restricting self-organisation through the action of interactive SST that can be influenced by negative feedback of

shortwave radiation in convective regions. In contrast, the deep fixed mixed layer experiment (50 m) is accompanied by strong positive feedback of longwave radiation and surface fluxes that enables it to overcome the negative feedback of shortwave radiation.

The second slab model allows deepening of the mixed layer according to an imposed wind stress and heat transfer to a deeper ocean layer. This experiment displays a characteristics of self-organisation with a significant difference between the quartiles of column water vapor. The mixing of heat to the deeper ocean layer apparently weakens the negative feedbacks that acts with the simple slab ocean model, having shallow mixed layer depths, and allow organisation to proceed, but further analysis of these preliminary experiments is required. Nevertheless, it is apparent that caution must be applied when interpreting the results of very simple modelling frameworks. For example, the simple addition of a subduction heat flux and deeper mixed layers are already adequate to negate the impact of the slab ocean in this case.

6.1 Recommendations

In this thesis, the mechanisms that controls the spontaneous organisation of convection is investigated in an idealized environment and subsequently with the introduction of lower boundary conditions in sensitivity tests that showed the important role of imposed wind and interactive SST for self-organisation of convection. A natural extension is to continue the investigation of interactive SST runs and determine origin of longer time scale oscillations. Furthermore, the interactive SST experiments that use an ocean slab with fixed mixed layer depth require further investigation to understand if there is correlation between mixed layer depth and level of the organisation.

A sharp gradient between moist and dry regions was observed in all the experiments that demonstrate organisation of convection. However, this gradient can be weaken in a more realistic setting that imposes mesoscale lateral mixing. It would be interesting to study the impact of this lateral mixing on the level of convection clustering as an additional step towards understanding the self-organisation process in less idealized situations.

Finally, the research in the thesis relied heavily on the moist static energy anomaly budgets that were introduced by Wing and Emanuel (2014). While

informative, these budgets do not account for the impact of diabatic tendencies on the local moist convective stability. For example, one can consider the alternative impact of applying an atmospheric temperature anomaly in either the upper or lower troposphere that are equivalent in terms of their change in the column integrated moist static energy. The diagnostical approach of Wing and Emanuel (2014) used here, does not differentiate between the two imposes anomalies; their moist static energy change is equivalent. However, a cooling in the lower troposphere locally increases the convective inhibition energy and decreases CAPE, and is likely to decrease the possibility of convection in the vicinity of the perturbation. In contrast, an upper tropospheric temperature anomaly increase CAPE, and may increase convective mass flux in the region of the anomaly. Thus, it is crucial that further metrics are added to the diagnostic armory in order to further improve our understanding of convective organisation.

Bibliography

Addis, R. P., Garstang, M. and Emmitt, G. D. (1984), 'Downdrafts from tropical oceanic cumuli.', *Bound.-Layer Meteor.* **28**, 23–49.

Arakawa, A. and Shubert, W. H. (1974), 'Interaction of a cumulus ensemble with the large- scale environment. Part 1', *J. Atmos. Sci.* **31**, 674–701.

Bergman, J. W. and Hendon, H. (2000), 'The impact of clouds on the seasonal cycle of radiative heating over the Pacific.', *J. Climate* **57**, 545–566.

Betts, A. K. (1984), 'Boundary layer thermodynamics of a High Plains severe storm.', *Mon. Wea. Rev.* **112**, 2199–2211.

Betts, A. K. (1990), 'Greenhouse warming and the tropical water budget.', *Bull. Am. Met. Soc.* **71**, 1464–1465.

Boing, S. J., Jonker, H. J. J., Siebesma, A. P. and W.Grabowski, W. (2012), 'Influence of the subcloud layer on the development of a deep convective ensemble.', *J. Atmos. Sci.* **69**(9), 2682–2698.

Bony, S. and Dufresne, J.-L. (2005), 'Marine boundary layer clouds at the heart of tropical cloud feedback uncertainties in climate models', *Geophysical Research Letters* **32**(20).

Bony, S., Lau, K.-M. and Sud, Y. C. (1997), 'Sea surface temperature and large-scale circulation influences on tropical greenhouse effect and cloud radiative forcing', *J. Climate* **10**, 2055–2076.

Bretherton, C., Blossey, P. and Khairoutdinov, M. (2005), 'An energy-balance

analysis of deep convective self-aggregation above uniform SST.', *J. Atmos. Sci.* **62**, 4237–4292.

Bretherton, C. S. (2015), 'Insights into low-latitude cloud feedbacks from high-resolution models.', *Phil.Trans.R.Soc.A* **373: 20140415**, doi:10.1098/rsta.2014.0415.

Bretherton, C. S. and Khairoutdinov, M. F. (2015), 'Convective self-aggregation feedbacks in near-global cloud-resolving simulations of an aquaplanet', *Journal of Advances in Modeling Earth Systems* .

Bretherton, C. S., Peters, M. E. and Back, L. E. (2004), 'Relationships between water vapor path and precipitation over the tropical oceans', *Journal of climate* **17**(7), 1517–1528.

Bretherton, C. and Smolarkiewicz, P. K. (1989), 'Gravity waves, compensating subsidence and detrainment around cumulus clouds.', *J. Atmos. Sci.* **46**, 740–759.

Bryan, G. H. (2005), 'Spurious convective organization in simulated squall lines owing to moist absolutely unstable layers.', *Mon. Wea. Rev.* **133**, 1978–1997.

Bryan, G. H., Wyngaard, J. C. and Fritsch, J. M. (2003), 'Resolution requirements for the simulation of deep moist convection', *Monthly Weather Review* **131**(10), 2394–2416.

Chou, C. and Neelin, J. D. (1999), 'Cirrus-detrainment temperature feedback.', *Geophys. Res. Lett.* **26**, 1295âĂŞ1298.

Chuda, T., Niino, H., Yoneyama, K., Katsumata, M., Ushiyama, T. and Tsukamoto, O. (2008), 'A statistical analysis of surface turbulent heat flux enhancements due to precipitating clouds observed in the tropical Western Pacific.', *Meteorol. Soc. Jpn.* **86**(3), 439–457.

Clough, S. A. and Iacono, M, J. (1995), 'Line-by-Line Calculations of Atmospheric Fluxes and Cooling Rates II: Application to Carbon Dioxide, Ozone, Methane, Nitrous Oxide, and the Halocarbons', *J. Geophys. Res.* **100**(16), 519–535.

Craig, G. C. (1996), 'Dimensional analysis of a convecting atmosphere in equilibrium with external forcing', *Q. J. R. Meteorol. Soc.* **122**, 1963–1967.

Craig, G. and Mack, J. (2013), 'A coarsening model for self-organization of tropical convection', *J. Geophys. Res.* **118**(16), 8761–8769.

Cronin, T. W. and Emanuel, K. A. (2013), 'The climate time scale in the approach to radiative-convective equilibrium', *J. Adv. Model. Earth Syst.* **5**(4), 843–849.

de Garidel-Thoron, T., Rosenthal, Y., Bassinot, F. and Beaufort, L. (2005), 'Stable sea surface temperatures in the western pacific warm pool over the past 1.75 million years', *Nature* **433**(7023), 294–298.

Derbyshire, S. H., Beau, I., Bechtold, P., Y.Grandpeix, J., Piriou, J. M., Redelsperger, J. L. and Soares, P. M. M. (2004), 'Sensitivity of moist convection to environmental humidity.', *Q. J. R. Meteorol. Soc.* **130**, 3055–3079.

Dodd, J. P. and James, I. N. (1996), 'Diagnosing the global hydrological cycle from routine atmospheric analyses.', *Quart. J. Roy. Meteor. Soc.* **122**, 1475–1499.

Dyer, A. J. and Hicks, B. B. (1970), 'Flux-gradient relationships in the constant flux layer', *Quart. J. Roy. Meteor. Soc.* **96**, 715–721.

Emanuel, K. A. (1987), 'An air-sea interaction model of intraseasonal oscillations in the Tropics.', *J. Atmos. Sci.* **44**, 2324–2340.

Emanuel, K. A. (1991), 'A scheme for representing cumulus convection in large-scale models', *J. Atmos. Sci.* **48**, 2313–2335.

Emanuel, K. A., Wing, A. A. and Vincent, E. M. (2014), 'Radiative-convective instability.', *J. Adv. Model. Earth Syst.* **6**, 75–90.

Emanuel, K. A. and Zivkovic-Rothman, M. (1999), 'Development and evaluation of a convective scheme for use in climate models', *J. Atmos. Sci.* **56**, 1766–1782.

Esbensen, S. (1978), 'Bulk thermodynamic effects and properties of small tropical cumuli.', *J. Atmos. Sci.* **35**, 826–831.

Feng, Z., Hagos, S., Rowe, A. K., Burleyson, C. D., Martini, M. N. and Szoeke, S. P. (2015), 'Mechanisms of convective cloud organization by cold pools over tropical warm ocean during the AMIE/DYNAMO field campaign.', *J. Adv. Model. Earth Syst.* **7**, 357–381.

Fritsch, J. M. and Forbes, G. S. (1997), MESOSCALE CONVECTIVE SYSTEMS, Technical report, Penn State University, available at http://www.ems.psu.edu/.

Grabowski, W. (2003*a*), 'MJO-like coherent structures: Sensitivity simulations using the cloud-resolving convection parameterization (CRCP).', *J. Atmos. Sci.* **60**, 847–864.

Grabowski, W., Bechtold, P., Cheng, A., Forbes, R., Halliwell, C., Khairoutdinov, M., Lang, S., Nasuno, T., Petch, J., Tao, W.-K. et al. (2006), 'Daytime convective development over land: A model intercomparison based on lba observations', *Quarterly Journal of the Royal Meteorological Society* **132**(615), 317–344.

Grabowski, W. W. (2003*b*), 'Impact of cloud microphysics on convective-radiative quasi equilibrium revealed by cloud-resolving convection parameterization', *Journal of climate* **16**(21), 3463–3475.

Grabowski, W. W. (2006*a*), 'Impact of explicit atmosphere-ocean coupling on mjo-like coherent structures in idealized aquaplanet simulations', *Journal of the atmospheric sciences* **63**(9), 2289–2306.

Grabowski, W. W. (2006*b*), 'Indirect impact of atmospheric aerosols in idealized simulations of convective-radiative quasi equilibrium', *Journal of climate* **19**(18), 4664–4682.

Grabowski, W., W. and Moncrieff, M, W. (2001), 'Large-scale organization of tropical convection in two-dimensional explicit numerical simulations.', *Quart. J. Roy. Meteor. Soc.* **127**, 445–468.

Grabowski, W. W. and Moncrieff, M. W. (2002), 'Large-scale organization of tropical convection in two-dimensional explicit numerical simulations: Effects of interactive radiation', *Quarterly Journal of the Royal Meteorological Society* **128**(585), 2349–2375.

Grabowski, W., W. and Moncrieff, M, W. (2004), 'Moisture-convection feedback in the tropics.', *Quart. J. Roy. Meteor. Soc.* **130**, 3081–3104.

Gray, W. M. (1973), 'Cumulus convection and large-scale circulations. I. Broadscale and mesoscale circulations.', *Mon. Wea. Rev.* **101**, 839–855.

Gray, W. M. and Jacobson Jr, R. W. (1977), 'Diurnal-variation of deep cumulus convection', *Mon. Wea. Rev.* **105**, 1171–1188.

Gray, W. M., Ruprecht, E. and Phelps, R. (1975), 'Relative humidity in tropical weather systems.', *Mon. Wea. Rev.* **103**, 685–690.

Hanley, K. E., Plant, R. S., Stein, T. H., Hogan, R. J., Nicol, J. C., Lean, H. W., Halliwell, C. and Clark, P. A. (2015), 'Mixing-length controls on high-resolution simulations of convective storms', *Quarterly Journal of the Royal Meteorological Society* **141**(686), 272–284.

Held, A. M., Hemler, R. S. and Ramaswamy, V. (1993), 'Radiative convective equilibrium with explicit two-dimensional moist convection', *J. Atmos. Sci.* **50**, 3909–3927.

Hong, S. Y., Noh, Y. and Dudhia, J. (2006), 'A new vertical diffusion package with an explicit treatment of entrainment processes.', *Mon. Wea. Rev.* **134**, 2318–2341.

Houze Jr, R. A. (2014), *Cloud dynamics*, Vol. 104, Academic press.

Houze, R. A., Jr. and Betts, A. K. (1981), 'Convection in GATE', *Rev. Geophys.* **19**, 541–576.

Jeevanjee, N. and Romps, D. M. (2013), 'Convective self-aggregation, cold pools, and domain size.', *Geophys. Res. Lett.* **40**, 994–998.

Jeevanjee, N. and Romps, D. M. (2015), 'Effective buoyancy, inertial pressure, and the mechanical generation of boundary layer mass flux by cold pools', *Journal of the Atmospheric Sciences* **72**(8), 3199–3213.

Johnson, R. H. (1978), 'Cumulus transports in a tropical wave composite for phase-III of GATE.', *J. Atmos. Sci.* **35**, 484–494.

Johnson, R. H., Rickenbach, T. M., Rutledge, S. A., Ciesielski, P. E. and Schubert, W. H. (1999), 'Trimodal characteristics of tropical convection', *Journal of climate* **12**(8), 2397–2418.

Jordan, C. L. (1958), 'Mean soundings for the West Indies area.', *J. Meteorology* **15**, 91–97.

Khairoutdinov, M. F., Krueger, S. K., Moeng, C.-H., Bogenschutz, P. A. and Randall, D. A. (2009), 'Large-eddy simulation of maritime deep tropical convection', *Journal of Advances in Modeling Earth Systems* **1**(4).

Khairoutdinov, M. F. and Randall, D. (2003), 'Cloud resolving modeling of the ARM summer 1997 IOP: Model formulation, results, uncertainties,and sensitivities.', *J. Atmos. Sci.* **60**, 607–625.

Khairoutdinov, M. F. and Randall, D. (2006), 'High-resolution simulation of shallow-to-deep convection transition over land.', *J. Atmos. Sci.* **63**(12), 3421–3436.

Khairoutdinov, M. and Yang, C.-E. (2013), 'Cloud-resolving modelling of aerosol indirect effects in idealised radiative-convective equilibrium with interactive and fixed sea surface temperature', *Atmospheric Chemistry and Physics* **13**(8), 4133–4144.

Kiladis, G. N., Wheeler, M. C., Haertel, P. T., Straub, K. H. and Roundy, P. E. (2009), 'Convectively coupled equatorial waves', *Reviews of Geophysics* **47**(2).

Klemp, J. B. and Skamarock, W. C.and Dudhia, J. (2007), 'Conservative split-explicit time integration methods for the compressible nonhydrostatic equations', *Mon. Wea. Rev.* **135**, 2897âĂŞ2913.

Knievel, J. C., Bryan, G. H. and Hacker, J. P. (2007), 'Explicit numerical diffusion in the WRF Model.', *Mon. Wea. Rev.* **135**, 3808–3824.

Krüger, S. K. (1988), 'Numerical simulation of tropical cumulus clouds and their interaction with the subcloud layer', *J. Atmos. Sci.* **45**(16), 2221–2250.

Küpper, C., Thuburn, J., Craig, G. C. and Birner, T. (2004), 'Mass and water transport into the tropical stratosphere: A cloud-resolving simulation', *Journal of Geophysical Research: Atmospheres* **109**(D10).

Laprise, R. (1992), 'The Euler Equations of motion with hydrostatic pressure as independent variable.', *Mon. Wea. Rev.* **120**, 197–207.

LeMone, M. A. and Zipser, E. J. (1980), 'Cumulonimbus vertical velocity events in GATE. Part I: Diameter, intensity and mass flux.', *J. Atmos. Sci.* **37**, 2444–2457.

LeMone, M. A., Zipser, E. J. and Trier, S. B. (1998), 'The role of environmental shear and thermodynamic conditions in determining the structure and evolution of mesoscale convective systems during TOGA COARE.', *J. Appl. Meteor.* **55**, 3493–3518.

Lilly, D. K. and Gal-Chen, T. (2013), *Mesoscale meteorology-theories, observations and models*, Vol. 114, Springer Science & Business Media.

Lima, M. A. and Wilson, J. W. (2008), 'Convective storm initiation in a moist tropical environment.', *Mon. Weather Rev.* **136**(6), 1847–1864.

Lin, Y. L., Farley, R., D. and Orville, H. D. (1983), 'Bulk parameterization of the snow field in a cloud model', *J. Climate Appl. Meteor.,* **22**, 1065–1092.

Lindzen, R. S., Chou, M. D. and Hou, A. Y. (2001), 'Does the earth have an adaptive infrared iris?', *Bull. Am. Met. Soc.* **82**, 417–432.

Machado, L. A. and Chaboureau, J.-P. (2015), 'Effect of turbulence parameterization on assessment of cloud organization', *Monthly Weather Review* **143**(8), 3246–3262.

Madden, R. A. and Julian, P. R. (1971), 'Detection of a 40-50 day oscillation in the zonal wind in the tropical pacific', *J. Atmos. Sci.* **5**, 702–708.

Maloney, E. D. and Hartmann, D. L. (1998), 'Frictional moisture convergence in a composite life cycle of the Madden-Julian oscillation', *J. Climate* **11**, 2387–2403.

Manabe, S. and Strickler, R, F. (1964), 'On the thermal equilibrium of the atmosphere with convective adjustment.', *J. Atmos.* **21**, 361–385.

Mapes, B. E. and Zuidema, P. (1996), 'Radiative-dynamical consequences of dry tongues in the tropical troposphere.', *J. Atmos. Sci.* **53**, 620–638.

Mathon, V., Laurent, H. and Lebel, T. (2002), 'Mesoscale convective system rainfall in Sahel', *J. Appl. Meteor.* **41**, 1081–1092.

Mauritsen, T. and Stevens, B. (2015), 'Missing iris effect as a possible cause of muted hydrological change and high climate sensitivity in models', *Nature Geoscience* **8**(5), 346–351.

Medeiros, B., Stevens, B., Held, I. M., Zhao, M., Williamson, D. L., Olson, J. G. and Bretherton, C. S. (2008), 'Aquaplanets, climate sensitivity, and low clouds', *Journal of Climate* **21**(19), 4974–4991.

Mlawer, E. J. and Clough, S. (1997), Shortwave and longwave enhancements in the Rapid Radiative Transfer Model, *in* 'Proc. of the 7th Atmospheric Radiation Measurement (ARM) Science Team Meeting', ARM, U.S. Department of Energy, available at http://www.arm.gov/publications, pp. CONF–9603149.

Mlawer, E. J., Taubman, S. J., Brown, P. D., Iacono, M. J. and Clough, S. A. (1997), 'Radiative transfer for inhomogeneous atmospheres: RRTM, a validated correlated-k model for the longwave', *J. Geophys. Res.* **102**, 16663–16682.

Moncrieff, M. W. and Liu, C. (1999), 'Convection initiation by density currents: Role of convergence, shear, and dynamical organization', *Monthly weather review* **127**(10), 2455–2464.

Muller, C. and Held, I. (2012), 'Detailed investigation of the self-aggregation of convection in cloud resovling simulations.', *J. Atmos. Sci.* **69**, 2551–2565.

Muller, C. J. and Bony, S. (2015), 'What favors convective aggregation and why?', *J. Geophys. Res.* **42**(13), 5626–5634.

Neelin, J. D., Held, I. M. and Cook, K. H. (1987), 'Evaporation-wind feedback and low-frequency variability in the tropical atmosphere', *J. Atmos. Sci.* **44**, 2341–2348.

Nicholls, S. and Lemone, A. M. (1980), 'The fair weather boundary layer in gate-The relationship of sub-cloud fluxes and structure to the distribution and enhancement of cumulus clouds.', *J. Atmos. Sci.* **37**, 2051–2067.

Numaguti, A., Oki, R., Nakamura, K., Tsuboki, K., Misawa, N. and Asai, T. (1995), '4-5 Day-Period Variation and Low-Level Dry Air Observed in the Equatorial Western Pacific during the TOGA-COARE IOP ', *J. Meteor. Soc. Japan* **73**, 267–290.

Paulson, C. A. (1970), 'The mathematical representation of wind speed and temperature profiles in the unstable atmospheric surface layer', *J. Appl. Meteor.* **9**, 857–861.

Pauluis, O. and Garner, S. (2006), 'Sensitivity of radiative-convective equilibrium simulations to horizontal resolution', *J. Atmos. Sci.* **63**(7), 1910–1923.

Pierrehumbert, R. (1995), 'Thermostats, radiator fins, and the local runaway greenhouse.', *J. Atmos. Sci.* **52**, 1784–1806.

Pierrehumbert, R. T. and Yang, H. (1993), 'Global chaotic mixing on isentropic surfaces', *J. Atmos. Sci.* **50**, 2462–2480.

Plant, R. S. and Craig, G. C. (2008), 'A stochastic parameterization for deep convection based on equilibrium statistics.', *J. Atmos. Sci.* **65**, 87–105.

Pollard, R. T., Rhines, P. B. and Thompson, R. O. (1973), 'The deepening of the wind-mixed layer.', *Geophysical Fluid Dynamics* **3**, 381–404.

Ramanathan, V. and Collins, W. D. (1991), 'Thermodynamic regulation of the ocean warming by cirrus clouds deduced from observations of the 1987 El NiÃśo.', *Nature* **351**, 27–32.

Randall, D. A. (1980), 'Conditional instability of the first kind upside-down.', *J. Atmos. Sci.* **37**, 125–130.

Randall, D. A., Hu, Q., Xu, K.-M. and Krueger, S. K. (1994), 'Radiative-convective disequilibrium', *Atmospheric research* **31**(4), 315–327.

Raymond, D. J. (2000), 'Thermodynamic control of tropical rainfall.', *Q. J. R. Meteorol. Soc.* **126**, 889–898.

Raymond, D. J. and Blyth, A. M. (1986), 'A stochastic mixing model for nonprecipitating cumulus clouds', *J. Atmos. Sci.* **43**, 2708–2718.

Redelsperger, J. L., Guichard, F. and Mondon, S. (2000), 'A parameterization of mesoscale enhancement of surface fluxes for large-scale models.', *J. Clim.* **13**(2), 402–421.

Redelsperger, J. L., Parsons, D. B. and Guichard, F. (2002), 'Recovery processes and factors limiting cloud-top height following the arrival of a dry intrusion observed during TOGA COARE.', *J. Atmos. Sci.* **59**, 2438–2457.

Rio, C., Hourdin, F., Grandpeix, J. Y. and Lafore, J. P. (2009), 'Shifting the diurnal cycle of parameterized deep convection over land.', *Geophys. Res. Lett.* **36**.

Robe, F. R. and Emanuel, K. A. (1996), 'Dependence of tropical convection on radiative forcing', *J. Atmos. Sci.* **53**, 3265–3275.

Robe, F. R. and Emanuel, K. A. (2001), 'The effect of vertical wind shear on radiative-convective equilibrium states', *Journal of the atmospheric sciences* **58**(11), 1427–1445.

Romps, D. (2010), 'A direct measurement of entrainment', *J. Atmos. Sci.* **67**, 1908–1927.

Romps, D. (2011), 'Response of Tropical Precipitation to Global Warming', *J. Atmos. Sci.* **68**, 123–138.

Romps, D. M. and Kuang, Z. (2010b), 'Do undiluted convective plumes exist in the upper tropical troposphere?', *Journal of the Atmospheric Sciences* **67**(2), 468–484.

Rotunno, R. and Emanuel, K. A. (1987), 'An air-sea interaction theory for tropical cyclones:Part II.', *J. Atmos. Sci.* **44**, 542–561.

Rotunno, R., Klemp, J. B. and Weisman, M. L. (1988), 'A theory for long-lived squall lines.', *J. Atmos. Sci.* **45**, 463–485.

Rutledge, S. A., Hobbs, P., V. and Orville, H. D. (1984), 'The mesoscale and microscale structure and organization of clouds and precipitation in midlatitude cyclones. XII: A diagnostic modeling study of precipitation development in narrow cloud-frontal rainbands', *J. Atmos. Sci.* **20**, 2949–2972.

Schmetz, J., Tjemkes, S., Gube, M. and Van de Berg, L. (1997), 'Monitoring deep convection and convective overshooting with meteosat', *Advances in Space Research* **19**(3), 433–441.

Sherwood, S. C. (1999), 'Convective precursors and predictability in the tropical western Pacific.', *Mon. Wea. Rev.* **127**, 2977–2991.

Sherwood, S. C., Hernández-Deckers, D., Colin, M. and Robinson, F. (2013), 'Slippery thermals and the cumulus entrainment paradox*', *Journal of the Atmospheric Sciences* **70**(8), 2426–2442.

Simpson, J. (1980), 'Downdrafts as linkages in dynamic cumulus seeding effects', *J. Appl. Meteor.* **19**, 477–487.

Skamarock, W. C., Klemp, J. B., Dudhia, J., Gill, D., O., Barker, D. M., Duda, M. G., Huang, X., Wang, W. and Powers, J. G. (2008), 'A Description of the Advanced Research WRF version 3', *NCAR* **NCAR Technical Note**.

Slingo, A. and Slingo, J. M. (1988), 'The response of a general-circulation model to cloud longwave radiative forcing .1. Introduction and initial experiments', *Q. J. R. Meteorol. Soc.* **114**, 1027–1062.

Slingo, J. M. and Slingo, A. (1991), 'The response of a general-circulation model to cloud longwave radiative forcing .2. Further-studies', *Q. J. R. Meteorol. Soc.* **117**, 333–364.

Sobel, A. H., Nilsson, J. and Polvani, L. M. (2001), 'The weak temperature gradient approximation and balanced tropical moisture waves', *J. Atmos. Sci.* **58**, 3650âĂŞ3665.

Stephens, G. L., van den Heever, S. and Pakula, L. (2008), 'Radiative convective feedbacks in idealized states of radiative-convective equilibrium.', *J. Atmos. Sci.* **65**, 3899–3916.

Stoyan, D., Kendalla, W. S. and Mecke, J. (1987), *Stochastic Geometry and Its Applications.*, John Wiley,New York.

Sui, C., Lau, K., Tao, W. and Simpson, J. (1994), 'The tropical water and energy cycles in a cumulus ensemble model. part i: Equilibrium climate', *Journal of the atmospheric sciences* **51**(5), 711–728.

Takemi, T. and Rotunno, R. (2003), 'The effects of subgrid model mixing and numerical filtering in simulations of mesoscale cloud systems.', *Mon. Wea. Rev.* **131**, 2085–2101.

Tao, W. K., Simpson, J. and McCumbe, M. (1989), 'An ice-water saturation adjustment', *Mon. Wea. Rev.* **117**, 231–235.

Thorpe, A. J., Miller, M. J. and Moncrieff, M. W. (1982), 'Two-dimensional convection in non-constant shear: A model of mid-latitude squall lines', *Quart. J. Roy. Meteor. Soc.* **108**, 739–762.

Tiedtke, M. (1989), 'A comprehensive mass flux scheme for cumulus parameterization in large-scale models.', *Mon. Wea. Rev.* **117**, 1779–1800.

Tompkins, A. (2000*a*), 'The impact of dimensionality on long-term cloud-resolving model simulations', *Monthly Weather Review* **128**(5), 1521–1535.

Tompkins, A. M. (2000*b*), 'The impact of dimensionality on long-term cloud resolving model simulations', *Mon. Wea. Rev.* **128**, 1521–1535.

Tompkins, A. M. (2001a), 'Organization of tropical convection in low vertical wind shears: The role of water vapor', *J. Atmos. Sci.* **58**, 529–545.

Tompkins, A. M. (2001b), 'Organization of tropical convection in low vertical wind shears: The role of cold pools', *J. Atmos. Sci.* **58**, 1650–1672.

Tompkins, A. M. (2001c), 'On the relationship between tropical convection and sea surface temperature', *Journal of climate* **14**(5), 633–637.

Tompkins, A. M. and Craig, G, C. (1998a), 'Radiative-convective equilibrium in a three-dimensional cloud ensemble model.', *Quart. J. Roy. Meteor. Soc.* **124**, 2073–2097.

Tompkins, A. M. and Craig, G, C. (1998b), 'Timescales of adjustment to radiative-convective equilibrium in the tropical atmosphere.', *Quart. J. Roy. Meteor. Soc.* **124**, 2693–2713.

Tompkins, A. M. and Craig, G. C. (1999), 'Sensitivity of tropical convection to sea surface temperature in the absence of large-scale flow', *J. Climate* **12**, 462–476.

Trenberth, K. E., Yongxin, Z., John, F. T. and Shoichi, T. (2015), 'Climate variability and relationships between topâĂŘofâĂŘatmosphere radiation and temperatures on earth.', *Journal of Geophysical Research: Atmospheres* **120**(9).

Verrelle, A., Ricard, D. and Lac, C. (2015), 'Sensitivity of high-resolution idealized simulations of thunderstorms to horizontal resolution and turbulence parametrization', *Quarterly Journal of the Royal Meteorological Society* **141**(687), 433–448.

Waliser, D. E. (1996), 'Formation and limiting mechanisms for very high sea surface temperature: Linking the dynamics and the thermodynamics', *J. Climate* **9**, 161–188.

Warner, J. (1955), 'The water content of cumuliform cloud', *Tellus* **7**, 449–457.

Warner, J. (1970), 'On steady state one-dimensional models of cumulus convection', *J. Atmos. Sci.* **27**, 1035–1040.

WARNER, J. and Newnham, T. D. (1952), 'new method of measurement of cloud water content', *Q. J. R. Meteorol. Soc.* **78**, 46–52.

Weaver, C. P., Collins, W. D. and Grassl, H. (1994), 'Relationship between clear-sky atmospheric greenhouse effect and deep convection during the Central Equatorial Pacific Experiment: Model calculations and satellite observations', *J. Geophys. Res.* **99**, 25891–25901.

Webb, E. K. (1970), 'Profile relationships: The log-linear range, and extension to strong stability', *Quart. J. Roy. Meteor. Soc.* **96**, 67–90.

Weger, R. C., Lee, J., Zhu, T. and Welch, R. M. (1992), 'Clustering, Randomness and Regularity in Cloud Fields: 1. Theoretical Considerations.', *J. Geophys. Res.* **97(D18)**(20), 537–558.

Wheeler, M. and Kiladis, G. N. (1999), 'Convectively coupled equatorial waves: Analysis of clouds and temperature in the wavenumber-frequency domain', *Journal of the Atmospheric Sciences* **56**(3), 374–399.

Wheeler, M., Kiladis, G. N. and Webster, P. J. (2000), 'Large-scale dynamical fields associated with convectively coupled equatorial waves', *Journal of the Atmospheric Sciences* **57**(5), 613–640.

Wing, A. A. and Emanuel, K. A. (2014), 'Physical mechanisms controlling self aggregation of convection in idealized numerical modeling simulations.', *J. Adv. Model. Earth Syst.* **6**, 59–74.

Wing, A. A. and Timothy, W. C. (2015), 'SelfâĂŘaggregation of convection in long channel geometry.', *Quart. J. Roy. Meteor. Soc.* **142**, 1–15.

Yang, H. and Pierrehumbert, R. T. (1994), 'Production of dry air by isentropic mixing', *J. Atmos. Sci.* **51**, 3437–3454.

Yoneyama, K. and Fujitani, T. (1995), 'The behavior of dry westerly air associated with convection observed during the TOGA-COARE R/V Natsushima cruise ', *J. Meteor. Soc. Japan* **73**, 291–290.

Zeng, X., Zhang, Q., Johnson, D. and Tao, W. K. (2002), 'Parameterization of wind gustiness for the computation of ocean surface fluxes at different spatial scales.', *Mon. Wea. Rev.* **130**(8), 2125–2133.

Zhang, C. (2005), 'Madden-Julian oscillation', *Rev. Geophys* **43**(2).

Zhang, C., Mapes, B. E. and Soden, B. J. (2003), 'Bimodality in tropical water vapour.', *Q. J. R. Meteorol. Soc.* **129**, 2847–2866.

Zhang, D. L. and Anthes, R. A. (1982), 'A high-resolution model of the planetary boundary layer sensitivity tests and comparisons with SESAMEâĂŞ79 data.', *J. Appl. Meteor.* **21**, 1594âĂŞ1609.

Zhang, G. J., Wu, X., Zeng, X. and Mitovski, T. (2015), 'Estimation of convective entrainment properties from a cloud-resolving model simulation during TWP-ICE', *Climate Dynamics* pp. 1–16.

Zipser, E. J. (1977), 'Mesoscale and convective-scale downdraughts as distinct components of squall-line circulation', *Mon. Wea. Rev.* **105**, 1568–1589.